ない．しかし，患者はリスクを納得のうえで自分の体を術者に預けてくれたという，人間と人間の信頼関係や感情がある．麻痺を引き起こした術者の精神的負担が大きいことはいうまでもないが，患者・家族への説明は，可能なかぎり術者自身が行うべきである．そして，術者は毎日（できれば1日に数回）患者のところに顔を出して，患者・家族を少しでも励ますように心がけるべきであるし，可能なかぎり頻回に患者・家族への説明を行うことも大切である．

文　献

1) 冨士武史，細野　昇，向井克容：脊椎手術後硬膜外血腫．in 冨士武史（編）：整形外科 治療と手術の合併症―起こさない対応・起きた時の対応．金原出版，2011，pp 231-236
2) Kimura A, Seichi A, Hoshino Y, et al：Perioperative complications of anterior cervical decompression with fusion in patients with ossification of the posterior longitudinal ligament：a retrospective, multi-institutional study. *J Orthop Sci* **17**：667-672, 2012
3) Matsumoto M, Chiba K, Toyama Y, et al：Surgical results and related factors for ossification of posterior longitudinal ligament of the thoracic spine：a multi-institutional retrospective study. *Spine (Phila Pa 1976)* **33**：1034-1041, 2008
4) Seichi A, Hoshino Y, Kimura A, et al：Neurological complications of cervical laminoplasty for patients with ossification of the posterior longitudinal ligament—a multi-institutional retrospective study. *Spine (Phila Pa 1976)* **36**：E998-E1003, 2011
5) Yamazaki M, Koda M, Okawa A, et al：Transient paraparesis after laminectomy for thoracic ossification of the posterior longitudinal ligament and ossification of the ligamentum flavum. *Spinal Cord* **44**：130-134, 2006
6) Yamazaki M, Mochizuki M, Ikeda Y, et al：Clinical results of surgery for thoracic myelopathy caused by ossification of the posterior longitudinal ligament：operative indication of posterior decompression with instrumented fusion. *Spine (Phila Pa 1976)* **31**：1452-1460, 2006
7) Yamazaki M, Okawa A, Fujiyoshi T, et al：Posterior decompression with instrumented fusion for thoracic myelopathy caused by ossification of the posterior longitudinal ligament. *Eur Spine J* **19**：691-698, 2010
8) Yamazaki M, Okawa A, Koda M, et al：Transient paraparesis after laminectomy for thoracic myelopathy due to ossification of the posterior longitudinal ligament：a case report. *Spine (Phila Pa 1976)* **30**：E343-E346, 2005
9) Yamazaki M, Okawa A, Mannoji C, et al：Postoperative paralysis after posterior decompression with instrumented fusion for thoracic myelopathy due to ossification of the posterior longitudinal ligament. *J Clin Neurosci* **18**：294-296, 2011
10) 山崎正志：上位頸椎手術．in 冨士武史（編）：整形外科治療と手術の合併症―起こさない対応・起きた時の対応．金原出版，2011，pp 144-149

J Orthop Sci (2014) 19:530–536
DOI 10.1007/s00776-014-0577-4

ORIGINAL ARTICLE

New classification system for ossification of the posterior longitudinal ligament using CT images

Yoshiharu Kawaguchi · Morio Matsumoto · Motoki Iwasaki · Tomohiro Izumi · Atsushi Okawa · Shunji Matsunaga · Kazuhiro Chiba · Takashi Tsuji · Masashi Yamazaki · Takahito Fujimori · Toshitaka Yoshii · Yoshiaki Toyama

Received: 17 December 2013 / Accepted: 2 March 2014 / Published online: 10 May 2014

Abstract
Background Ossification of the posterior longitudinal ligament (OPLL) is most frequently seen in the cervical spine. The types of cervical OPLL are classified into continuous, mixed, segmental, and other based on plain lateral X-ray. Computed tomography (CT) imaging is often used in clinical practice for evaluating ossified lesions as it can detect their precise location, size, and shape. However, to date, no CT classification of OPLL lesions has been proposed.
Methods One hundred and forty-four patients diagnosed with cervical OPLL by plain radiograph were included in this study. Sagittal and axial CT images of the cervical spine were obtained. We propose three classification systems: A, B, and axial. Classification A comprises two lesion types: bridge and nonbridge. Classification B requires examiners to describe all vertebral and intervertebral levels where OPLL exits in the cervical spine. Axial classification comprises central and lateral lesions identified on axial CT images. Seven observers evaluated CT images using this classification system, and intra- and interrater reliability were examined.
Results Averaged Fleiss' kappa coefficient of interrater agreement was 0.43 ± 0.26 among the seven observers, averaged intrarater reliability for the existence of OPLL was 72.4 ± 8.8 % [95 % confidence interval (CI) 67.5–76.8]. Fifty-four patients (37.5 %) had the bridge type and 90 the nonbridge type according to Classification A; 102 (70.8 %) had central and 42 (29.2 %) lateral OPLL in the axial classification. Four representative cases defined according to the three classification types are reported here.
Conclusion Subcommittee members of the Investigation Committee on the Ossification of the Spinal Ligaments of the Japanese Ministry of Public Health and Welfare propose three new classification systems of cervical OPLL based on CT imaging: A, B, and axial.

Study group of subcommittee members of the Investigation Committee on the Ossification of the Spinal Ligaments of the Japanese Ministry of Public Health and Welfare.

Y. Kawaguchi (✉)
Department of Orthopaedic Surgery, Faculty of Medicine, University of Toyama, 2630 Sugitani, Toyama, Toyama 930-0194, Japan
e-mail: zenji@med.u-toyama.ac.jp

M. Matsumoto · Y. Toyama
Department of Orthopaedic Surgery, Keio University, Tokyo, Japan

M. Iwasaki · T. Fujimori
Department of Orthopaedic Surgery, Osaka University, Osaka, Japan

T. Izumi
Department of Orthopaedic Surgery, Niigata Central Hospital, Niigata, Japan

A. Okawa · T. Yoshii
Department of Orthopaedic Surgery, Tokyo Medical and Dental University, Tokyo, Japan

S. Matsunaga
Division of Orthopaedic Surgery, Imakiire Sougou Hospital, Kagoshima, Japan

K. Chiba · T. Tsuji
Spine Center, Kitasato University Kitasato Institute Hospital, Tokyo, Japan

M. Yamazaki
Department of Orthopaedic Surgery, Tsukuba University, Ibaraki, Japan

Introduction

Ossification of the posterior longitudinal ligament (OPLL) is characterized by the replacement of ligamentous tissue by ectopic new bone [1]. OPLL often causes narrowing of the spinal canal and has been recognized as one of the causes of myelopathy and/or radiculopathy [2]. The disease was first reported in Japan in 1960 [1]. Since then, numerous cases of OPLL have been reported, and its existence in the general Japanese population is reported to be 1.9–4.3 % among people >30 years [3]. Although the pathogenesis of OPLL has not been fully elucidated, a genetic background factor related to systemic ossification could be involved [4].

A radiological study revealed that OPLL is frequently observed in the cervical spine [5] and are classified as continuous, mixed, segmental, and other types based on plain lateral X-ray of the cervical spine according to the classification established by the Investigation Committee on the Ossification of Spinal Ligaments of the Japanese Ministry of Public Health and Welfare in 1981 [6]. This classification [6] is very simple and easy to use; however, X-ray-based classification has the following potential limitations:

1. Explicit definition of each type is unclear
2. Agreement ratio between examiners has not been confirmed
3. Precise evaluation of the ossified lesion at each vertebral and intervertebral level is not sufficiently expressed
4. Data collection regarding lesion location might be difficult using X-ray classification

Computed tomography (CT) imaging is often used in clinical practice to evaluate OPLL lesions and can detect the precise location, size, and shape of ossified lesions. Thus, several members of the investigation committee were selected to develop new classifications for cervical OPLL using CT imaging. The purpose of this study was to introduce the new classification system and assess its classification adequacy.

Materials and methods

One hundred and forty-four patients diagnosed with cervical OPLL by plain radiograph were entered into this study. All patients were treated and followed in one university hospital. There were 90 men and 54 women, with an average age of 67.5 years (range 36–86 years). Informed consent was obtained from each patient before enrollment, and the study was approved by the Institutional Review Board of the university hospital. Forty-six patients had a history of cervical laminoplasty, which is a posterior decompression surgery in the cervical spine. Patients who had anterior decompression surgery (ADS) for OPLL treatment were excluded, because ADS might affect OPLL configuration. Lateral radiographs [6] were obtained in all patients; accordingly, 35 were classified with continuous, 66 with mixed, 41 with segmental, and two with other OPLL types. Sagittal and axial multidetector CT images (SOMATOME Sensation 64 Cardiac, SIEMENS Co., Erlangen, Germany) were also obtained. Specific CT parameters were 1 tube rotation/s, 17.28 mm/s table-feed speed, 160 mA, and 120 kV. Image reconstructions were made using a CT console (Wizard, SIEMENS, Co.) at a 1-mm interval from the 0.75-mm scan-slice data. A technique was used to determine the threshold for bone-density measurement. Images were constructed using the bone-window setting (width 1,500, center 200); OPLL lesion classifications were established and then evaluated. Classification analysis was independently performed by seven senior spine surgeons. Classification system details are described below.

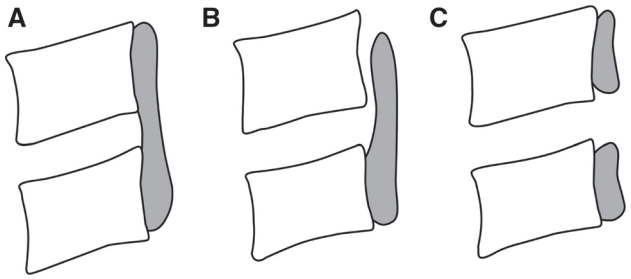

Fig. 1 Typical bridge (**a**) and nonbridge (**b**, **c**) lesions. *Gray areas* ossification of the posterior longitudinal ligament (OPLL) lesions

Classification A

In classification A, ossified lesions were divided into two types: bridge and nonbridge, based on presence or absence of a bony bridge between vertebral bodies on sagittal CT images (Fig. 1). Bony bridge is defined as an OPLL connection to the adjacent posterior margins of vertebral bodies at two or more levels. The observers evaluated the ossification using all of the sagittal CT images. When an ossified lesion connected to the adjacent posterior margin of a vertebral body, even if a small ossification and not necessarily the most extended ossification, it was classified as a bridge type. The number of connected vertebral bodies is included in the classification.

Classification B

This classification requires the examiners to describe all vertebral and intervertebral levels where OPLL >2 mm in

width exist in the cervical spine. Then, connection or disconnection of OPLL is expressed as follows:

① A dot (".") is applied when the OPLL lesion is disconnected, similar to the segmental type in the X-ray classification.
② A slash ("/") is applied when the OPLL lesion is beyond the intervertebral level, without any bridge formation to the adjacent vertebral body.
③ A bar ("-") is applied when the OPLL lesion is beyond the intervertebral level, with bridge formation to the adjacent vertebral body.
④ A circle ("○") is applied at the level of the vertebral body when the OPLL lesion is not attached to the vertebral body (level number is circled). This means that if the OPLL lesion is fused with the vertebral body, the circle is not applied at the level of the vertebral body.

Axial classification

The ossified lesion is divided into two types, central and lateral, on axial CT images at the level where the ossification most significantly occupies the spinal canal. If the posterior prominence of the OPLL is located in the middle third of the spinal canal, it is defined as central; the lateral type is subdivided into left- and right-side types.

Interrater and intrarater reliability and agreement

To evaluate the adequacy of classification A, inter- and intrarater reliability measures were determined with Fleiss' kappa coefficient using a dedicated MATLAB (Mathworks, Paris, France) program. Kappa values of 0.00–0.20 were considered as being slight agreement, 0.21–0.40 as fair, 0.41–0.60 as moderate, 0.61–0.80 as substantial, and 0.81–1.00 as almost perfect [7, 8]. As classification B is a complex process, we did not calculate its inter- and intrarater agreement ratio. Likewise, we did not calculate the agreement ratio of the axial image classification.

Results

Interrater and intrarater reliability and agreement in classification A

Averaged Fleiss' kappa coefficient of interrater agreement was 0.43 ± 0.26 among the seven observers. The averaged intrarater reliability for the existence of OPLL was 72.4 ± 8.8 % [95 % confidence interval (CI) 67.5–76.8].

Table 1 Classification A

Ossification of posterior longitudinal ligament (OPLL) lesions	No. of patients
Bridge type	54
2-level	28
3-level	4
4-level	5
4 continuous levels	2
2 + 2 levels	3
>5-level	17
5 continuous levels	3
2 + 3 levels	5
3 + 2 levels	2
7 continuous levels	4
2 + 5 levels	1
8 continuous levels	1
4 + 4 levels	1
Nonbridge type	90

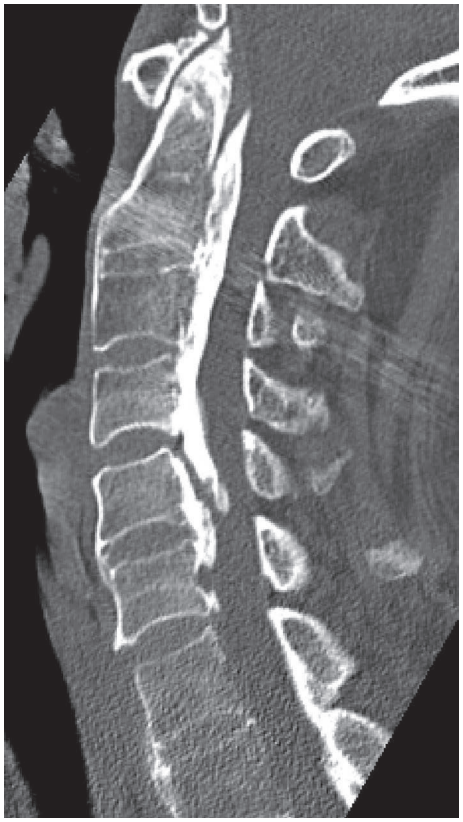

Fig. 2 Typical case with bridge formation in two separate areas. 63-year-old man with three-level bridge at C2–4 and two-level bridge at C5–6 (3 + 2)

Analysis of OPLL type according to classification A and axial classification in 144 patients

Classification A

Fifty-four patients (37.5 %) had a bridge formation between vertebral bodies on the sagittal plane. Bridge formation occurred from vertebral bodies 2–8: in 28 patients at two levels, four patients at three levels, five patients at four levels, and 17 patients at more than five levels (Table 1). Twelve patients had bridge formation in two separate areas, shown as 2 + 2 (2-level bridge + 2-level bridge), 2 + 3, 4 + 4 and 2 + 5 (Table 1 and Fig. 2). Ninety patients had nonbridge OPLL.

Axial classification

One hundred and two patients (70.8 %) had central-type OPLL, and 42 (29.2 %) had the lateral type.

Case presentation

Case 1

The patient, a 59-year-old man, had mixed type OPLL according to X-ray of the cervical spine (Fig. 3a). He had the bridge type according to classification A, as OPLL was seen from C5–7 and was connected to vertebral bodies (Fig. 3b). In classification B, the OPLL lesion was expressed as "C③/4, 5–7". The spinal canal was the narrowest at C4. Ossification was classified as the central type on axial image at C4 (Fig. 3c).

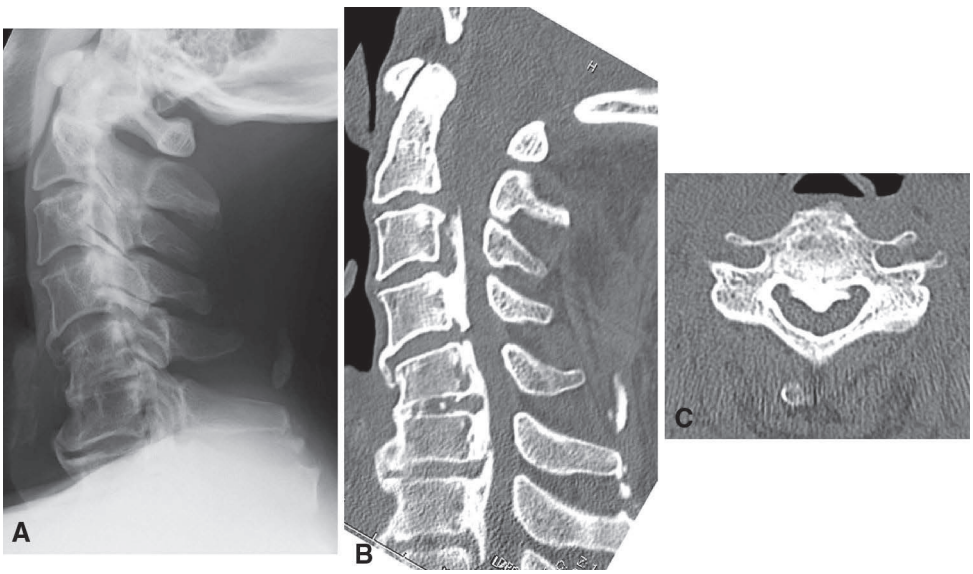

Fig. 3 A 59-year-old man. Lateral cervical X-ray (**a**), midsagittal computed tomography (CT) image (**b**), and axial CT image at C4 (**c**)

Case 2

A 74-year-old had a C3–7 laminoplasty 5 years earlier. His OPLL was classified as continuous based on cervical X-ray (Fig. 4a). According to classification A, he had bridge type OPLL from C3 to T2 (Fig. 4b). OPLL lesions were expressed as "C3–7" according to classification B and left lateral type at C5–6 according to axial classification (Fig. 4c).

Case 3

A 69-year-old woman with OPLL considered as the segmental type according to X-ray (Fig. 5a). She had the nonbridge type at C4 and C5 and was classified as "C4.5.6" according to classification B (Fig. 5b). She had the central type in axial classification at C5, where the OPLL was the most pronounced (Fig. 5c).

Case 4

A 66-year-old man had mixed OPLL according to cervical X-ray (Fig. 6a), bridge type in classification A, expressed as "C②/3–4/5/6" in classification B (Fig. 6b) and as central type in axial classification at C3 level (Fig. 6c).

Discussion

Lateral X-ray examination is the gold standard by which to determine the existence of OPLL in the cervical spine and by which most physicians establish the diagnosis. OPLL classification by lateral X-ray, proposed by the Investigation Committee on OPLL of the Japanese Ministry of Public Health and Welfare in 1981, has widely been used

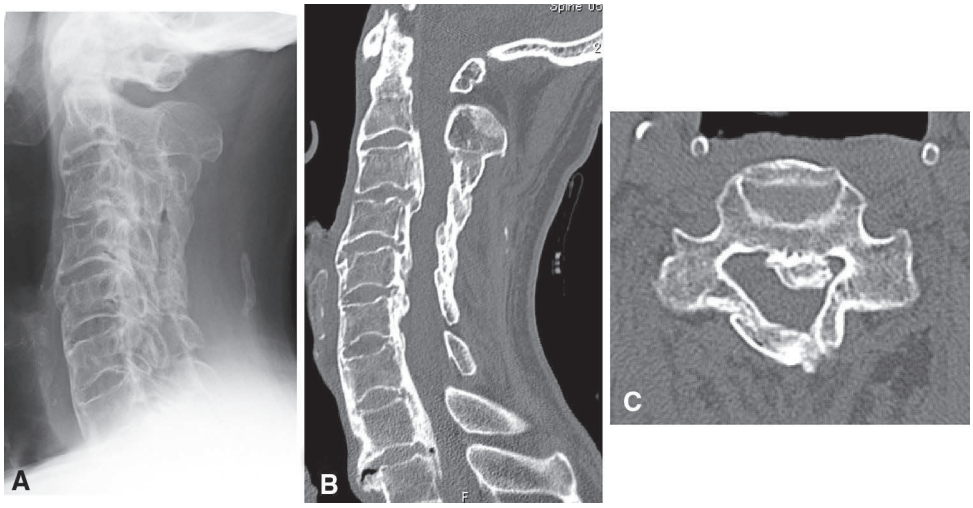

Fig. 4 A 74-year-old man. Lateral cervical X-ray (**a**), midsagittal computed tomography (CT) image (**b**), and axial CT image at C5–6 level (**c**)

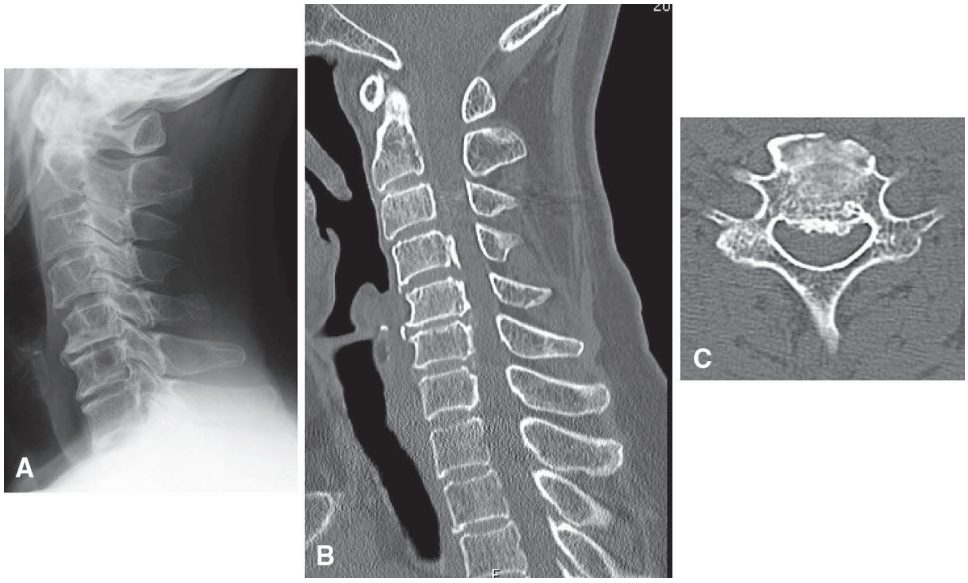

Fig. 5 A 69-year-old woman. Lateral cervical X-ray (**a**), midsagittal computed tomography (CT) (**b**), and axial CT at C5 level (**c**)

[6] and is useful for assessing OPLL characteristics because it is easy to identify ossified lesions and is beneficial for predicting OPLL progression and the occurrence of cervical myelopathy. However, the lateral X-ray does not provide details of lesions themselves. A recent study has shown that CT imaging is necessary for precise detection of such lesions [9]. In fact, CT has become a standard tool for evaluating such ossified lesions, and most spine surgeons obtain CT imaging before surgical intervention in patients with OPLL. Therefore, we decided to develop a new classification system of OPLL based on CT imaging.

In classification A, we noted bridge formation of ossified lesions to the vertebral body for the following two reasons: (1) The absence of bridge formation is directly related to segmental motion of vertebrae, which is lost at the level where the bridge is formed [10]. On the other hand, the segment adjacent to the bridge formation might have greater motion, which results in adjacent segmental instability. It has been reported that segmental motion is a factor causing neurological impairment, such as cervical myelopathy [11]. In their long-term follow-up study, Matsunaga et al. [11] stated that range of motion (ROM) was significantly larger in patients with than those without myelopathy. They emphasized the importance of cervical motion that might lead to the development of neurological compromise. (2) Bridge formation may be related to the extension of ossified lesions along the entire spine. Matsunaga et al. also demonstrated that bridge formation in OPLL in the cervical spine is strongly related to multiple OPLL in the entire spine [9] and might represent the characteristics of diffuse ossification in PLL in the entire spine. Bridge formation can be precisely evaluated by CT imaging, but it is difficult to assess the finding using lateral

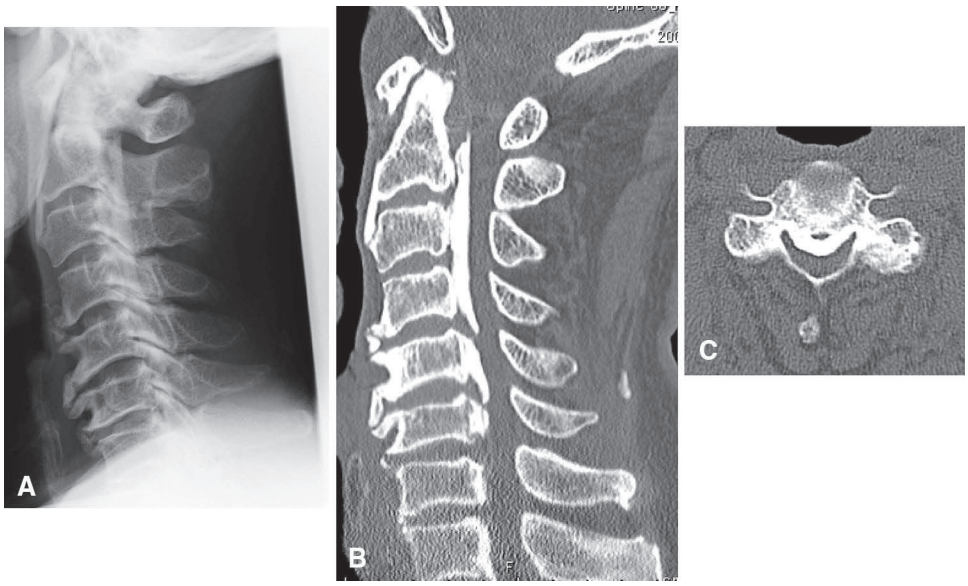

Fig. 6 A 66-year-old man. Lateral cervical X-ray (**a**), midsagittal computed tomography (CT) image (**b**), and axial CT image at C3 (**c**)

X-ray alone. In classification A, the interrater agreement ratio was 0.43 among the seven examiners, indicating moderate agreement. Interrater agreement ratio was not high but seems to be acceptable according to evaluation among the seven examiners. This low ratio might be due to examiners' unfamiliarity with evaluating ossified lesions on CT images. In particular, it is difficult to judge the bony bridge on a CT image if the small ossification connects to the adjacent vertebrae. It might be important to check segmental motion in order to evaluate connection or disconnection between adjacent vertebrae. When the examiners become familiar with the evaluation technique using CT images, the agreement ratio might increase. The averaged intrarater reliability was 72.4 %, which indicates substantial agreement. Therefore, we believe that this classification system is very easy to use and has the potential benefit for evaluating characteristics of cervical OPLL lesions.

CT provides an excellent axial view of the spinal canal, yielding valuable information on the area and median or paramedian location of ossification. In axial-image classification, we selected the level where OPLL most frequently occurs in the spinal canal. Information regarding the ratio of ossified lesions to the spinal canal is very important, because previous report indicate that patients with $\geq$60 % of the cervical spinal canal/stenosis by OPLL had cervical myelopathy [12, 13]. Laterality of the ossified lesion can be evaluated using this classification. Patients with cervical myelopathy due to OPLL sometimes have a predominant side of neurological impairment [12]. However, data of patients' clinical symptoms were not included in the study reported here. The relationship between the axial classification and clinical symptoms will be an important research theme for future studies.

For classification B, we evaluated ossified lesions at all vertebral and intervertebral levels and checked for and described their connection or disconnection and whether or not lesions are attached to the upper or lower border of the vertebral body. This classification provides a precise means of identifying the existence of OPLL lesions and, if they are present, describes their characteristics. However, this classification is somewhat complex, and we believe it may not be appropriate for daily clinical use but, rather, may be useful for precise data collection in future studies.

This study has several limitations. First, we did not check the dynamic factor or cervical spine alignment using CT images. CT was taken with the patient in a supine position without performing flexion and extension analysis. Thus, segmental motion could not be detected. Second, we did not evaluate the relationship between OPLL types and clinical symptoms. In the axial image, the occupied ratio against the spinal canal can be easily detected. It might be interesting to determine how laterality is related to the predominant side of the neurological deficit; however, we have no MRI information regarding spinal cord compression due to OPLL. The relationship of OPLL lesions and/or dynamic factors to clinical symptoms is a theme for future study. Thirdl, the agreement ratio for both types of classification A is moderate, although we consider it acceptable for use. Classification B is a highly complicated procedure, and we thus did not analyze intra- or interobserver agreement ratio. Despite these several study limitations, CT classification provides precise evaluation of OPLL lesions and might also be useful to help determine the appropriate operative procedure. For example, fusion surgery is not necessary at a level where there is bridge formation, because there is no segment motion at that level. This might be the advantage of CT classification over X-ray classification.

In conclusion, we, the subcommittee members of the Investigation Committee on the Ossification of the Spinal Ligaments of the Japanese Ministry of Public Health and Welfare, propose three new classification systems for cervical OPLL based on CT imaging: classification A, classification B, and the axial image classification. It is our hope that these classifications will be recognized as useful clinical assessment tools for evaluating OPLL lesions.

Acknowledgments This work was supported by Health Labour Sciences Research Grant, Research on intractable diseases, Committee for Study of Ossification of Spinal Ligament. The authors thank Mika Kigawa, assistant professor, Department of Public Health, Toyama University, for statistical assistance.

Conflict of interest The authors declare that they have no conflict of interest.

References

1. Tsukimoto H. On an autopsied case of compression myelopathy with a callus formation in the cervical spinal canal. Nihon Geka Hokan. 1960;29:1003–7 (in Japanese).
2. Onji Y, Akiyama H, Shimomura Y, Ono K, Hukuda S, Mizuno S. Posterior paravertebral ossification causing cervical myelopathy. J Bone Jt Surg Am. 1967;49:1314–28.
3. Matsunaga S, Sakou T. OPLL: disease entity, incidence, literature search and prognosis. In: Yonenobu K, Nakamura K, Toyama Y, editors. Ossification of the posterior longitudinal ligament. 2nd ed. Tokyo: Springer; 2006. p. 11–7.
4. Inoue I. Genetic susceptibility to OPLL. In: Yonenobu K, Nakamura K, Toyama Y, editors. Ossification of the posterior longitudinal ligament. 2nd ed. Tokyo: Springer; 2006. p. 19–25.
5. Matsunaga S, Sakou T. Ossification of the posterior longitudinal ligament. In: Clark CR, editor. The cervical spine. 4th ed. Philadelphia: Lippincott Williams & Wilkins; 2005. p. 1091–8.
6. Tsuyama N. The investigation committee on OPLL of the Japanese Ministry of Public Health and Welfare. the ossification of the posterior longitudinal ligament of the spine (OPLL). J Jpn Orthop Assoc. 1981;55:425–40.
7. Sim J, Wright CC. The kappa statistic in reliability studies: use, interpretation, and sample size requirements. Phys Ther. 2005;85:257–68.
8. Karanicolas PJ, Bhandari M, Kreder H, Moroni A, Richardson M, Walter SD, Norman GR, Guyatt GH, Collaboration for outcome assessment in surgical trials (COAST) musculoskeletal group. Evaluating agreement: conducting a reliability study. J Bone Jt Surg Am. 2009;91(3 Suppl):99–106.
9. Kawaguchi Y, Nakano M, Yasuda T, Seki S, Hori T, Kimura T. Ossification of the posterior longitudinal ligament in not only cervical spine, but also other spinal regions: analysis using multidetector CT of the whole spine. Spine. 2013;38:E1477–82.
10. Fujimori T, Iwasaki M, Nagamoto Y, Kashii M, Ishii T, Sakaura H, Sugamoto K, Yoshikawa H. Three-dimensional measurement of intervertebral range of motion in ossification of the posterior longitudinal ligament: are there mobile segments in the continuous type? J Neurosurg Spine. 2012;17:74–81.
11. Matsunaga S, Kukita M, Hayashi K, Shinkura R, Koriyama C, Sakou T, Komiya S. Pathogenesis of myelopathy of patients with ossification of the posterior longitudinal ligament. J Neurosurg Spine. 2002;96(2 Suppl):168–72.
12. Matsunaga S, Nakamura K, Seichi A, Yokoyama T, Toh S, Ichimura S, Satomi K, Endo K, Yamamoto K, Kato Y, Ito T, Tokuhashi Y, Uchida K, Baba H, Kawahara N, Tomita K, Matsuyama Y, Ishiguro N, Iwasaki M, Yoshikawa H, Yonenobu K, Kawakami M, Yoshida M, Inoue S, Tani T, Kaneko K, Taguchi T, Imakiire T, Komiya S. Radiographic predictors for the development of myelopathy in patients with ossification of the posterior longitudinal ligament: a multicenter cohort study. Spine. 2008;33:2648–50.
13. Nagata K, Sato K. Diagnostic imaging of cervical ossification of the posterior longitudinal ligament. In: Yonenobu K, Nakamura K, Toyama Y, editors. Ossification of the posterior longitudinal ligament. 2nd ed. Tokyo: Springer; 2006. p. 127–43.

Journal of Clinical Neuroscience 21 (2014) 2175–2178

Contents lists available at ScienceDirect

Journal of Clinical Neuroscience

journal homepage: www.elsevier.com/locate/jocn

Clinical Study

Phosphorylated neurofilament subunit NF-H becomes elevated in the cerebrospinal fluid of patients with acutely worsening symptoms of compression myelopathy

Hiroshi Takahashi [a,*], Yasuchika Aoki [a], Arata Nakajima [a], Masato Sonobe [a], Fumiaki Terajima [a], Masahiko Saito [a], Shinji Taniguchi [a], Manabu Yamada [a], Fusako Watanabe [a], Takeo Furuya [b], Masao Koda [b], Masashi Yamazaki [c], Kazuhisa Takahashi [b], Koichi Nakagawa [a]

[a] Department of Orthopaedic Surgery, Toho University Sakura Medical Center, 564-1, Shimoshizu, Sakura City, Chiba 285-8741, Japan
[b] Department of Orthopedic Surgery, Chiba University Graduate School of Medicine, Japan
[c] Department of Orthopedic Surgery, Faculty of Medicine, University of Tsukuba, Japan

ARTICLE INFO

Article history:
Received 24 February 2014
Accepted 22 April 2014

Keywords:
Biomarker
Cerebrospinal fluid
Compression myelopathy
pNF-H

ABSTRACT

It is known that the severity of compression myelopathy sometimes worsens rapidly and results in poor functional recovery because of limited axonal regeneration. Levels of phosphorylated neurofilament subunit NF-H (pNF-H), which indicate axonal degeneration, are elevated in other neurological disorders. To our knowledge, there has been no examination of pNF-H levels in compression myelopathy. Therefore, we conducted a pilot cross-sectional study to evaluate pNF-H levels in the cerebrospinal fluid (CSF) of patients with worsening symptoms of cervical compression myelopathy. From January 2011 to March 2013, 51 samples of CSF were collected from patients at the time of myelography before spinal surgery. The indications for surgery were acutely worsening compression myelopathy (AM) in eight, chronic compression myelopathy (CM) in six, and lumbar canal stenosis (LCS) in 37 patients. The pNF-H levels were measured using a standard enzyme-linked immunosorbent assay. The mean ± standard deviation pNF-H value was 2127.1 ± 556.8 pg/ml in AM patients, 175.8 ± 67.38 pg/ml in CM patients and 518.7 ± 665.7 pg/ml in LCS patients. A significant increase in pNF-H levels was detected in the CSF of patients with AM compared with those with either CM or LCS. The clinical outcome of surgical treatment for patients with cervical myelopathy was satisfactory in both AM and CM patients. Despite the limitations of small sample size and lack of healthy CSF control data due to ethical considerations, our results suggest that pNF-H in CSF can act as a biomarker that reflects the severity of AM.

1. Introduction

Cervical compression myelopathy is one of the most common spinal cord disorders affecting the elderly. It is well known that the mechanism of compression myelopathy is chronic compression of the spinal cord by osteophytes, degenerated discs, thickened ligamenta flava, and ossification of the posterior longitudinal ligament [1]. Usually, a slow and stepwise decline in function is observed after compression myelopathy. However, a rapid progression of motor paralysis and paresthesia with mild or no trauma is occasionally observed. The severity of compression myelopathy has been reported to worsen rapidly in almost 5% of patients [2]. Rapid worsening of compression myelopathy results in severe neurological deficits with poor functional recovery because of limited axonal regeneration [1,3]. To date, the only effective therapy for compression myelopathy is early surgical treatment [4]. Generally, the recovery rate of neurological function after surgical treatment is about 50–70% [5]. However, in some patients, sufficient improvement of neurological function is not achieved. At present we cannot accurately predict the recovery rate before surgical treatment. Moreover, the only indicators to assess the severity of neurological status are subjective, including the Japanese Orthopaedic Association (JOA) score [6]. Therefore, biomarkers that reflect the degree of damage to the spinal cord and the severity of neurological symptoms would be useful.

Phosphorylated neurofilament subunit NF-H (pNF-H) is a structural protein of axon fibers and is not detected in the cerebrospinal

* Corresponding author. Tel.: +81 43 462 8811; fax: +81 43 462 8820.
E-mail address: hirochann@syd.odn.ne.jp (H. Takahashi).

http://dx.doi.org/10.1016/j.jocn.2014.04.021
0967-5868/

fluid (CSF) or blood of healthy subjects. However, axonal breakdown increases the level of pNF-H in plasma and CSF [7]. A recent report has indicated that the level of pNF-H in the plasma and CSF is elevated in various neurological disorders such as subarachnoid hemorrhage, traumatic brain injury, amyotrophic lateral sclerosis, and acute spinal cord injury [8–12]. Therefore, pNF-H may be useful to evaluate the severity of progression and the effect of treatment in such disorders.

However, there are no studies examining the level of pNF-H in the CSF or plasma of patients with compression myelopathy to our knowledge. Therefore, we conducted a pilot cross-sectional study to determine the level of pNF-H in the CSF of patients with compression myelopathy.

2. Methods

2.1. Patients and samples

This study was given approval by our University Human Ethics Committee. From January 2011 to March 2013, 51 CSF samples were obtained from patients at the time of myelography before spinal surgery at the Toho University Sakura Medical Center. Informed consent was obtained from all patients. The indications for surgery were cervical compression myelopathy in 15 patients and lumbar canal stenosis (LCS), which was used as a control disorder, in 37 patients. Furthermore, we divided compression myelopathy samples into patients with acutely worsening symptoms (AM) and patients with chronic symptoms (CM). We defined acutely worsening compression myelopathy as that in which the JOA score of patients with cervical myelopathy decreased by 2 points or more during a recent 1 month period [13]. Ultimately, eight patients were allocated to the AM group and six patients to the CM group. Patients who were diagnosed as having cervical spondylotic radiculopathy and cervical spondylotic amyotrophy were excluded from this study. Patients with double lesions (cervical compression myelopathy and LCS) were also excluded.

2.2. Clinical outcome of patients with compression myelopathy

In all patients with compression myelopathy (AM and CM groups), neurological evaluation using a JOA score for cervical myelopathy (scores range from 0 to 17) was performed [6]. The scores were evaluated at the time of myelography before surgery and 6 months after surgery by two orthopedic spine surgeons.

2.3. pNF-H assay

The pNF-H assay was performed using a commercially available enzyme-linked immunosorbent assay kit (ELISA; BioVendor, Brno, Czech Republic). Frozen CSF samples were allowed to thaw, and diluted 1/2 in a buffer. The samples were then loaded onto an ELISA plate. The assay was performed according to the manufacturer's protocol. To standardize the pNF-H value, all samples were tested in duplicate, and the average value for each sample was calculated.

2.4. Statistical analyses

Results are presented as mean ± standard deviation. A one factor analysis of variance with a *post hoc* Tukey–Kramer test was used to evaluate the difference in the pNF-H levels between AM, CM, and LCS patients. Spearman's correlation coefficient by rank test was used to evaluate the correlation between pNF-H and JOA score. $p < 0.05$ was considered statistically significant.

Table 1
Patient characteristics in each group

	AM	CM	LCS
Patients, n	8	6	37
Sex			
Male	4	5	14
Female	4	1	23
Age, years*			
	64.9 ± 10.2 (45–79)	65.0 ± 13.2 (39–75)	70.3 ± 7.9 (55–86)
Preop JOA*	9.25 ± 2.43 (6–14)	10.6 ± 0.80 (10–12)	
Surgical procedure			
Laminoplasty	4	2	
Laminoplasty with posterior fusion	1	2	
Anterior corpectomy and fusion	3	2	

AM = acutely worsening compression myelopathy, CM = chronic compression myelopathy, JOA = Japanese Orthopaedic Association, LCS = lumbar canal stenosis, preop = preoperative.
* Data presented as mean ± standard deviation (range).

3. Results

3.1. Patient characteristics

Table 1 shows the characteristics of each group of patients. The mean age was 64.9 ± 10.2 (range 45–79 years) in the AM group, 65.0 ± 13.2 (range 39–75 years) in the CM group, and 70.3 ± 7.9 (range 55–86 years) in the LCS group. The mean JOA score at the time of CSF sampling in the AM group was 9.5 ± 2.51 (range 6–14), and 10.6 ± 0.80 (range 10–12) in the CM group. The surgical procedure in the AM group was laminoplasty in four patients, laminoplasty with posterior fusion in one patient, and anterior corpectomy and fusion in three patients. The surgical procedure in the CM group was laminoplasty in two patients, laminoplasty with posterior fusion in two patients, and anterior corpectomy and fusion in two patients.

3.2. Levels of pNF-H

Figure 1 shows the level of pNF-H in the CSF of patients from each group. The level of pNF-H was 2127.1 ± 556.8 pg/ml in the AM group, 175.8 ± 27.5 pg/ml in the CM group, and 518.7 ± 665.7 pg/ml in the LCS group. Our findings show that a significant increase in the level of pNF-H was detected in patients in the AM group compared with that in the CM and LCS group ($p < 0.01$). A slightly increased level of pNF-H was detected in CSF from patients in the LCS group compared with levels in the CM group. However, there was no significant difference in the levels between these two groups.

3.3. Evaluation of clinical outcome

Table 2 shows the change of JOA scores after surgery. JOA scores at the time of CSF collection were 9.5 ± 2.51 (range 6–14) in the AM group and 10.6 ± 0.80 (range 10–12) in the CM group. After surgery, neurological improvement was seen in all patients. JOA scores 6 months after surgery were 14.3 ± 1.82 (range 13.5–16.5) in the AM group and 13.9 ± 0.58 (range 13.5–15) in the CM group. The recovery rate of JOA score was 66.0 ± 16.9 (range 46.2–86.7) in the AM group and 51.2 ± 12.5 (range 30–66.7) in the CM group. Although a slightly higher recovery rate of JOA score was seen in the AM group, no statistical difference in recovery rate of JOA score was observed between patients in the AM and CM groups ($p = 0.096$).

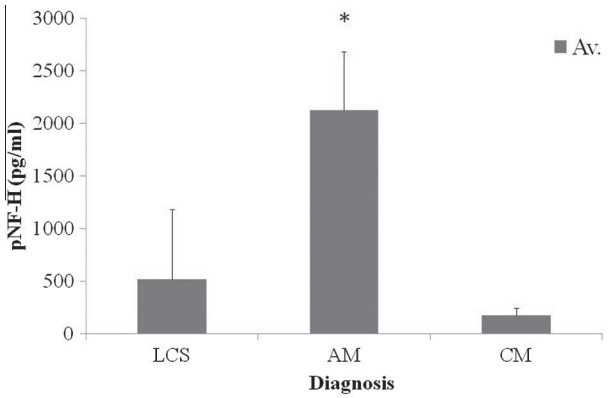

Fig. 1. Levels of phosphorylated neurofilament subunit NF-H. AM = acutely worsening compression myelopathy, Av. = average, CM = chronic compression myelopathy, LCS = lumbar canal stenosis. *$p < 0.01$ compared to lumbar canal stenosis and chronic compression myelopathy group.

Table 2
Recovery of Japanese Orthopaedic Association score

	AM	CM	*p* value
JOA score at the time of CSF collection	9.5 ± 2.51 (6–14)	10.6 ± 0.80 (10–12)	0.146
JOA score at 6 months after surgery	14.3 ± 1.82 (13.5–16.5)	13.9 ± 0.58 (13.5–15)	0.377
Recovery rate of JOA score	66.0 ± 16.9 (46.2–86.7)	51.2 ± 12.5 (30–66.7)	0.096

AM = acutely worsening compression myelopathy, CM = chronic compression myelopathy, CSF = cerebrospinal fluid, JOA = Japanese Orthopaedic Association.

No statistical correlation was found between the level of pNF-H and the recovery rate of JOA score ($p = 0.128$).

4. Discussion

To our knowledge, the present cross-sectional study is the first to determine the level of pNF-H in CSF samples from patients with cervical compression myelopathy and LCS. Our results showed a significant increase in the level of pNF-H of up to 2000 pg/ml in patients with AM. Elevated levels of pNF-H have suggested axonal breakdown in studies of other neurological disorders [7–9,11]. Furthermore, plasma pNF-H was found to be elevated proportional to the severity of acute spinal cord injury (SCI) and to reflect a greater extent of axonal damage because of the secondary damage to the injured spinal cord [10,12]. Increased levels of plasma pNF-H were seen in patients with complete SCI, but not in patients suffering incomplete paralysis [10]. In the present study, we hypothesized that increased levels of plasma pNF-H are not seen in compression myelopathy because of minor injury to the spinal cord compared with SCI. Therefore, we determined the levels of pNF-H in CSF rather than plasma. Although the pathogenesis and prognosis of compression myelopathy remain unclear, inflammation, hypoxia, and excitotoxicity are likely to cause secondary damage in SCI. An increase in the concentration of interleukin-6 has been detected in the CSF of patients with cervical compression myelopathy [14]. An increase in the concentration of interleukin-8 has been detected in the CSF of patients with cervical spondylotic myelopathy [15]. The increased level of pNF-H in the present study suggests that pNF-H reflects the severity of AM, and the pathogenesis in AM may be acute axonal damage followed by secondary damage, as seen in SCI.

In the present study, although a slightly higher recovery rate of JOA score was seen in the AM group, no statistical difference was observed between AM and CM patients. The surgical outcome was satisfactory in patients from both the AM and CM groups. There was no correlation between the level of pNF-H and the recovery rate of JOA score. Although surgical procedures for compression myelopathy are not standardized, our study suggests that early surgical treatment of AM results in sufficient neurological improvement, even in patients with CM.

The present study has several limitations. First, because CSF samples were only collected from patients at the time of myelography before surgery, the sample size was small and there is bias toward more severe disease. We found no statistical correlation between pNF-H and JOA recovery rate. However, a slightly higher JOA recovery rate was seen in AM patients. Further investigation with long-term follow-up after surgery and standardization of both the severity of the myelopathy and the surgical procedure performed are required to support our findings. Second, the collection method for CSF precludes the collection of CSF samples from healthy control subjects because of ethical issues. A slightly increased level of pNF-H was found in the CSF from LCS patients. A rodent study indicated that the level of pNF-is up-regulated in rat dorsal root ganglions [16]. In humans, increased interleukin-6 levels were detected in the CSF of patients with lumbar radiculopathy [14]. The present finding of slightly increased pNF-H levels in the CSF of patients with LCS may reflect axonal damage to the nerve roots or the cauda equina. The average level of pNF-H in the CSF of patients with LCS was about 500 pg/ml. The present findings suggest that pNF-H may be useful in the differential diagnosis of double lesions (cervical myelopathy and LCS). Further investigation using comparison samples from healthy control subjects is required. Third, the detailed pathogenesis of increased pNF-H levels in the CSF of patients with AM or CM remains unclear. Further research using animal models of compression myelopathy may clarify the pathogenesis.

In conclusion, despite the limitations indicated above, a significantly increased level of pNF-H was detected in the CSF of patients with AM. Clinical outcome after surgical treatment for cervical myelopathy was satisfactory in patients with both AM and CM. The present results suggest that pNF-H in CSF may be a biomarker that reflects the severity of AM.

Conflicts of Interest/Disclosures

The authors declare that they have no financial or other conflicts of interest in relation to this research and its publication.

Acknowledgements

This study was supported in part by JSPS KAKENHI Grant Number 25861346.

References

[1] Baba H, Maezawa Y, Imura S, et al. Quantitative analysis of the spinal cord motor neuron under chronic compression: an experimental observation. J Neurol 1996;243:109–16.
[2] Schmidt MH, Quinones-Hinojosa A, Rosenberg WS. Cervical myelopathy associated with degenerative spine disease and ossification of the posterior longitudinal ligament. Semin Neurol 2002;22:143–8.
[3] Fehlings MG, Skaf G. A review of the pathophysiology of cervical spondylotic myelopathy with insights for potential novel mechanisms drawn from traumatic spinal cord injury. Spine (Phila Pa 1976) 1998;23:2730–7.
[4] Sampath P, Benbebba M, Davis JD, et al. Outcome of patients treated for cervical myelopathy. A prospective multicenter study with independent clinical review. Spine (Phila Pa 1976) 2000;25:670–6.
[5] Zhu B, Xu Y, Liu X, et al. Anterior approach versus posterior approach for the treatment of multilevel cervical spondylotic myelopathy: a systemic review and meta-analysis. Eur Spine J 2013;22:1583–93.
[6] Masaki Y, Yamazaki M, Okawa A, et al. An analysis of factors causing poor surgical outcome in patients with cervical myelopathy due to ossification of

the posterior longitudinal ligament: anterior decompression with spinal fusion versus laminoplasty. J Spinal Disord Tech 2007;20:7–13.
[7] Shaw G, Yang C, Ellis R, et al. Hyperphosphorylated neurofilament NF-H is a serum biomarker of axonal injury. Biochem Biophys Res Commun 2005;336:1268–77.
[8] Anderson KJ, Scheff SW, Miller KM, et al. The phosphorylated axonal form of the neurofilament subunit NF-H (pNF-H) as a blood biomarker of traumatic brain injury. J Neurotrauma 2008;25:1079–85.
[9] Boylan K, Yang C, Crock J, et al. Immunoreactivity of the phosphorylated axonal neurofilament H subunit (pNF-H) in blood of ALS model rodents and ALS patients: evaluation of blood pNF-H as a potential ALS biomarker. J Neurochem 2009;111:1182–91.
[10] Hayakawa K, Okazaki R, Ishii K, et al. Phosphorylated neurofilament subunit NF-H as a biomarker for evaluating the severity of spinal cord injury patients, a pilot study. Spinal Cord 2012;50:493–6.
[11] Lewis SB, Wolper RA, Miralia L, et al. Detection of phosphorylated NF-H in the cerebrospinal fluid and blood of aneurysmal subarachnoid hemorrhage patients. J Cereb Blood Flow Metab 2008;28:1261–71.
[12] Ueno T, Ohori Y, Ito J, et al. Hyperphosphorylated neurofilament NF-H as a biomarker of the efficacy of minocycline therapy for spinal cord injury. Spinal Cord 2011;49:333–6.
[13] Sakuma T, Yamazaki M, Okawa A, et al. Neuroprotective therapy using granulocyte colony-stimulating factor for patients with worsening symptoms of compression myelopathy, part 1: a phase I and IIa clinical trial. Eur Spine J 2012;21:482–9.
[14] Nagashima H, Morio Y, Yamane K, et al. Tumor necrosis factor-alpha, interleukin-1beta, and interleukin-6 in the cerebrospinal fluid of patients with cervical myelopathy and lumbar radiculopathy. Eur Spine J 2009;18:1946–50.
[15] Ito K, Matsuyama Y, Yukawa Y, et al. Analysis of interleukin-8, interleukin-10, and tumor necrosis factor-alpha in the cerebrospinal fluid of patients with cervical spondylotic myelopathy. J Spinal Disord Tech 2008;21:145–7.
[16] Jamieson SM, Jubramanian J, Liu JJ, et al. Oxaliplatin-induced loss of phosphorylated heavy neurofilament subunit neuronal immunoreactivity in rat DRG tissue. Mol Pain 2009;5:66.

Eur Spine J (2015) 24:963–967
DOI 10.1007/s00586-014-3373-0

ORIGINAL ARTICLE

Neuroprotective therapy with granulocyte colony-stimulating factor in acute spinal cord injury: a comparison with high-dose methylprednisolone as a historical control

Koshiro Kamiya · Masao Koda · Takeo Furuya · Kei Kato · Hiroshi Takahashi · Tsuyoshi Sakuma · Taigo Inada · Mitsutoshi Ota · Satoshi Maki · Akihiko Okawa · Yasuo Ito · Kazuhisa Takahashi · Masashi Yamazaki

Received: 5 November 2013 / Revised: 4 May 2014 / Accepted: 4 May 2014 / Published online: 25 June 2014

Abstract
Purpose We performed a phase I/IIa clinical trial and confirmed the safety and feasibility of granulocyte colony-stimulating factor (G-CSF) as neuroprotective therapy in patients with acute spinal cord injury (SCI). In this study, we retrospectively analyzed the clinical outcome in SCI patients treated with G-CSF and compared these results to a historical cohort of SCI patients treated with high-dose methylprednisolone sodium succinate (MPSS).
Methods In the G-CSF group ($n = 28$), patients were treated from August 2009 to July 2012 within 48 h of the injury, and G-CSF (10 μg/kg/day) was administered intravenously for five consecutive days. In the MPSS group ($n = 34$), patients underwent high-dose MPSS therapy from August 2003 to July 2005 following the NASCIS II protocol. We evaluated the ASIA motor score and the AIS grade elevation between the time of treatment and 3-month follow-up and adverse events.
Results The ΔASIA motor score was significantly higher in the G-CSF group than in the MPSS group ($p < 0.01$). When we compared AIS grade elevation in patients with AIS grades B/C incomplete paralysis, 17.9 % of patients in the G-CSF group had an AIS grade elevation of two steps compared to 0 % of patients in the MPSS group ($p < 0.05$), and the incidence of pneumonia was significantly higher in the MPSS group (42.9 %) compared to the G-CSF group (8.3 %) ($p < 0.05$).
Conclusions These results suggest that G-CSF administration is safe and effective, but a prospective randomized controlled clinical trial is needed to compare the efficacy of MPSS versus G-CSF treatment in patients with SCI.

Keywords Spinal cord injury · Neuroprotective therapy · G-CSF · High-dose methylprednisolone · Clinical trial

K. Kamiya · M. Koda (✉) · T. Furuya · K. Kato · T. Inada · M. Ota · S. Maki · A. Okawa · K. Takahashi
Department of Orthopedic Surgery, Chiba University Graduate School of Medicine, 1-8-1 Inohana, Chuo-Ku, Chiba 2608670, Japan
e-mail: masaokod@gmail.com

H. Takahashi
Department of Orthopaedic Science, Toho University Sakura Medical Center, Chiba, Japan

T. Sakuma
Seirei Sakura Citizen Hospital, Chiba, Japan

Y. Ito
Japanese Red Cross Kobe Hospital, Kobe, Japan

M. Yamazaki
Department of Medicine, University of Tsukuba, Tsukuba, Japan

Introduction

Acute spinal cord injury (SCI) is characterized by two pathological phases known as primary and secondary injury [1]. Primary injury occurs when the tissue is destroyed by direct mechanical trauma. Secondary injury occurs when the spinal cord reacts to the primary injury. Neurons and glial cells that were left intact by the initial trauma undergo apoptosis during the secondary phase of injury. Multiple factors exacerbate the secondary phase of injury, including vascular changes, increased concentrations of free radicals and free fatty acids, ionic mechanisms of axonal injury, glutamate excitotoxicity and immune and inflammatory reactions [2]. Secondary injury is, therefore, a rich target for drug therapy [3]. According to the NASCIS II protocol, high-dose methylprednisolone sodium succinate (MPSS) is the standard treatment for attenuation of

secondary injury after acute SCI [4]. In recent years, MPSS therapy for acute SCI became controversial. Cochran review shows the efficacy of MPSS therapy for SCI [5]. In contrast, the updated guidelines for the management of acute cervical spine and spinal cord injury released by American Association of Neurological Surgeons and Congress of Neurological Surgeons Guidelines Committee described MPSS therapy for SCI as "not recommend" [6]. Hence, new drug therapies for the treatment of secondary injury after acute SCI are needed.

Granulocyte colony-stimulating factor (G-CSF) is a clinically important cytokine that is commonly used to treat neutropenia [7]. Granulocyte colony-stimulating factor also has non-hematopoietic functions and has been suggested as a treatment for neuronal injury [8]. We have previously reported that G-CSF promotes functional recovery in a rodent model of SCI [9–12]. Based on these results, we performed a preliminary phase I/IIa clinical trial and confirmed the safety and feasibility of G-CSF as neuroprotective therapy in patients with acute SCI [13]. The next step is to verify the efficacy of G-CSF compared to standard high-dose MPSS therapy. Toward this end, we retrospectively analyzed the clinical outcome and the incidence of drug-related adverse events in SCI patients treated with G-CSF and compared these results to a historical cohort of SCI patients treated with MPSS.

Methods

Study design

The study was designed as a retrospective comparative analysis using an historical cohort control.

Patient population

Between August 2009 and July 2012, all patients with complete or incomplete C3-C7 cervical SCI who presented to Chiba University Hospital within 48 h of injury were recruited into the study. Exclusion criteria included the following: (1) age younger than 16 years or greater than 85 years, (2) treatment with high-dose MPSS therapy after the SCI event, (3) splenomegaly or altered mental status, (4) history of leukemia, thrombosis or embolism, (5) current treatment of myocardial infarction or angina, and (6) evidence of malignant disease within the last 5 years. Pregnant patients were also excluded. Written informed consent was obtained from all patients prior to G-CSF treatment (G-CSF group).

Patients with acute cervical SCI who received high-dose MPSS therapy following the NASCIS II protocol between August 2003 and July 2005 served as an historical control (MPSS group). Patients were selected based on the same exclusion criteria outlined above. A larger number of patients with complete paralysis (American Spinal Injury Association impairment scale: AIS grade A) were observed in the MPSS group compared to the G-CSF group. No other significant differences in patient background were observed between the two groups, including patient age, sex, injury level and AIS grade (Chi square test).

Standard protocol approvals, registrations, and patient consents

This study was approved by the Institutional Review Boards of both participating institutions. The study was conducted in compliance with the Declaration of Helsinki and the International Conference on harmonization good clinical practice guidelines.

Treatment

G-CSF group

Patients were treated with i.v. Granulocyte colony-stimulating factor (dissolved in normal saline) at a dose of 10 μg/kg/day (administered over 1 h) for five consecutive days. Granulocyte colony-stimulating factor dose regimen was determined by the previous preliminary clinical trial of G-CSF neuroprotective therapy for acute SCI, of which study design was single armed with dose escalation [13].

MPSS group

Methylprednisolone sodium succinate was administered according to the NASCIS II protocol within 8 h after injury. Methylprednisolone sodium succinate was first administered as a bolus dose of 30 mg/kg MPSS. After a 45-min withdrawal period, 5.4 mg/kg was administered intravenously over the next 23 h.

Patients in each group received similar surgical, rehabilitation and nursing care.

Efficacy assessments

Neurologic function was assessed with the American spinal injury association (ASIA) motor and sensory scores immediately upon study entry and after 3 months of follow-up. The primary outcome was the change in ASIA motor score between the time of treatment and 3 months following treatment. The initial analysis included all patients, including those with AIS grade A paralysis. However, because these patients have complete paralysis and typically demonstrate little significant neurological

recovery, a second comparison was performed in which patients with AIS grade A were excluded.

Assessment of adverse events

Adverse events were evaluated retrospectively by review of patient records and compared between treatment groups. Pneumonia was defined as respiratory distress accompanied by an infiltrating shadow on plain radiogram, positive sputum cultures and an elevated white blood cell count (WBC) or C-reactive protein. Urinary tract infection was defined as fever and elevated WBC in the context of positive urinary cultures. Notably, G-CSF treatment alone increases WBC, hence these criteria were excluded from the diagnosis of pneumonia and urinary tract infection in the G-CSF group. Gastric ulcers were defined as obvious ulcers of any stage observed by upper gastrointestinal fiber examination. Other adverse events were determined by review of patient records. The severity of each adverse event was assessed according to the Japanese version of the common terminology criteria for adverse events (CTCAE), version 4.0. The initial analysis of adverse events was performed on all patients, including those with AIS grade A. However, because these patients have complete paralysis which might increase the incidence of pneumonia and urinary tract infections, a second analysis was performed in which patients with severe incomplete paresis AIS grades B and C.

Statistical analysis

The ASIA motor score and the ΔASIA motor score were analyzed by the Mann–Whitney's *U* test. The extent of AIS grade elevation between the time of treatment and 3-month follow-up and the number of adverse events were compared between treatment groups using Fisher's exact test. A $p < 0.05$ was considered significant.

Results

Patient background data are shown in Table 1. No statistically significant differences in age, sex, mechanism of injury or injured vertebral level were observed between the groups. No statistically significant difference was observed in the baseline ASIA motor scores between the G-CSF and control groups (59.0 ± 29.6 and 50.3 ± 33.0, respectively). The ΔASIA motor score was significantly higher in the G-CSF group than in the MPSS group (27.7 ± 19.8 and 12.0 ± 11.0, respectively, $p < 0.01$) when all patients were included in the analysis.

The difference in patient background data between the groups, the MPSS group contained significantly larger number of AIS A patients who generally show poor neurological recovery, must influence the neurological outcome. Therefore, we excluded patients with AIS A complete paralysis and compared ΔASIA motor score in patients with severe incomplete paresis AIS grades B and C between both groups (12 patients in the G-CSF group and 14 patients in the MPSS group). Repeatedly, the ΔASIA motor score was also significantly higher in the G-CSF compared to the MPSS group (44.4 ± 17.2 and 17.4 ± 13.6, respectively, Fig. 1a, $p \leq 0.01$).

Next, the change in the AIS grade between the time of treatment and 3 months after treatment was compared between groups (Fig. 1b). We found that 67.9 % of patients in the G-CSF group had an AIS grade elevation of more than one step compared to 50.0 % of patients in the MPSS group, a difference that was not statistically significant. It is widely known that patients with AIS grade A complete paralysis demonstrate very little AIS grade elevation following injury. The MPSS group included more patients with AIS grade A paralysis, hence these results might underestimate the grade elevation in this group. To exclude the bias of patient background difference, we compared AIS grade change between both groups in AIS B/C patients, excluding AIS A complete paralysis patients and AIS D minor injury patients. We found that 91.7 % of patients in the G-CSF group had an

Table 1 Patient background data

	G-CSF	MPSS
Number	28	34
Male	21	27
Female	7	7
Age cause of injury	57.5 (38–72)	60.5 (18–85)
Over-turning	11	11
Falling	7	11
Road trauma	6	11
Falling Object	1	0
Sports	3	1
AIS		
A	2	9
B	4	3
C	8	11
D	14	11
Level of injury		
C2/3	0	3
C3/4	10	13
C4/5	9	5
C5/6	7	8
C6/7	2	4
Unclear case		1

The MPSS group contained significantly larger number of AIS A patients, whereas no statistically significant differences in age, sex, mechanism of injury, injured vertebral level or baseline ASIA motor score were observed between the groups

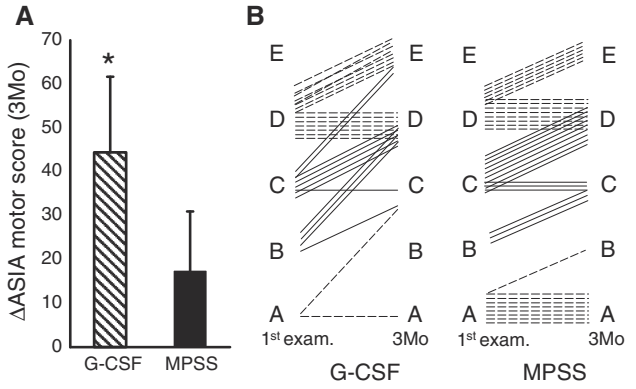

Fig. 1 Neurological recovery. The difference in patient background data between the groups, the MPSS group contained significantly larger number of AIS A patients who generally show poor neurological recovery, must influence the neurological outcome. Therefore, we excluded patients with AIS A complete paralysis and compared ΔASIA motor score in patients with severe incomplete paresis AIS grades B and C between both groups [12 patients in the G-CSF group and 14 patients in the MPSS group, (**a**)]. The ΔASIA motor score was also significantly higher in the G-CSF compared to the MPSS group [44.4 ± 17.2 and 17.4 ± 13.6, respectively, (**a**), $p < 0.01$]. Next, the change in the AIS grade between the baseline and 3 months after treatment was compared between groups (**b**). To exclude the bias of patient background difference, we compared AIS grade change between both groups in AIS B/C patients (*solid lines*), excluding AIS A complete paralysis patients and AIS D minor injury patients (*dashed line*). We found that 91.7 % of patients in the G-CSF group had an AIS grade elevation of more than one step compared to 78.6 % of patients in the MPSS group, a difference that was not statistically significant. However, we observed that 17.9 % of patients in the G-CSF group had an AIS grade elevation of two steps compared to 0 % of patients in the MPSS group ($p < 0.05$)

AIS grade elevation of more than one step compared to 78.6 % of patients in the MPSS group, a difference that was not statistically significant. However, we observed that 17.9 % of patients in the G-CSF group had an AIS grade elevation of two steps compared to 0 % of patients in the MPSS group ($p \leq 0.05$).

Finally, we compared the incidence of adverse events between treatment groups. The incidence of pneumonia was significantly higher in the MPSS group (44.1 %) compared to the G-CSF group (3.6 %). It has been shown that the severity of paralysis positively correlates with the incidence of pneumonia in patients with SCI. Hence, the fact that the MPSS group contained more patients with AIS grade A complete paralysis might have contributed to the higher incidence of pneumonia observed in the MPSS group. To exclude this bias, we analyzed the incidence of pneumonia in patients with AIS grades B/C incomplete paralysis. Again, we observed a significant difference in the incidence of pneumonia between treatment groups (42.9 % in the MPSS group and 8.3 % in the G-CSF group, Table 2, $p < 0.05$).

No significant difference in the incidence of urinary tract infections was observed between groups (35.7 % in the MPSS group and 16.7 % in the G-CSF group).

Table 2 Incidence of adverse events in AIS B/C incomplete paralysis patients

	G-CSF ($n = 12$)	MPSS ($n = 14$)	p-value
Pneumonia	1 (8.3 %)	6 (42.9 %)	$p < 0.05$
Urinary tract infection	2 (16.7 %)	5 (35.7 %)	$p = 0.17$
Gastric ulcer	0 (0 %)	2 (14.3 %)	$p = 0.27$

The difference in patient background data between the groups, the MPSS group contained significantly larger number of AIS A patients who can be easily affected with pneumonia, must influence the incidence of pneumonia. Therefore, we compared the incidence of pneumonia in incomplete paralysis patients of both groups, the result showed significant difference between G-CSF and MPSS groups

The incidence of gastric ulcers tended to be higher in the MPSS group compared to the G-CSF group (14.7 and 0 %, respectively, $p = 0.051$). When patients with AIS grade A and D were excluded from the analysis, no significant difference was observed between treatment groups.

Discussion

In the present study, the G-CSF group showed better neurological recovery compared to the MPSS group. Moreover, the incidence of severe adverse events is less frequent in patients treated with G-CSF than in patients treated with MPSS.

The MPSS group contained significantly larger number of AIS A patients who generally show poor neurological recovery, must influence the neurological outcome. Therefore, we assessed neurological outcome in severe incomplete paralysis patients (excluding AIS A and D patients) between both groups. Repeatedly, the G-CSF group showed better neurological recovery compared to the MPSS group, suggesting the superior neuroprotective potential of G-CSF treatment in SCI.

We observed that the incidence of pneumonia was significantly higher in patients treated with MPSS than in patients treated with G-CSF. The difference in patient background data between the groups, the MPSS group contained significantly larger number of AIS A patients who can be easily affected with pneumonia, must influence the incidence of pneumonia. Therefore, we compared the incidence of pneumonia in severe incomplete paralysis patients of both groups, the result repeatedly showed significant difference between G-CSF and MPSS groups (Table 2).

Methylprednisolone sodium succinate is a widely recognized immunosuppressant. In addition, spinal cord injury itself can induce systemic immunosuppression [14]. Hence, the immunosuppressive effects of SCI and MPSS may function in an additive or synergistic manner, increasing

the incidence of infections. In contrast, G-CSF increases the number of white blood cells in the peripheral blood. This feature of G-CSF is used clinically to treat neutropenia and prevent infectious complications. In this manner, G-CSF treatment might decrease the incidence of infections in SCI patients. Previous studies have reported a 31.4 % incidence of pneumonia in SCI patients with a Frankel Grade of A, B, or C [15]. Matsumoto reported a 30.4 % incidence of pneumonia and a 4.3 % incidence of urinary tract infections in SCI patients who received MPSS [16]. We cannot directly compare the incidence of infections between the present study and previous reports, and the anti-infection properties of G-CSF remain to be clarified, but our findings suggest that the incidence of pneumonia might be reduced in patients treated with G-CSF compared to those treated with MPSS.

We observed a lower incidence of gastric ulcers in patients treated with G-CSF than in patients treated MPSS. When we analyzed the incidence of ulcers among patients with severe incomplete paralysis (AIS grades B and C) to exclude the bias introduced by the difference in paralysis severity between the groups, no significant difference was observed. Treatment of gastric ulcers has been dramatically improved by the increased use of proton pump inhibitors. Our results might thus reflect this change in ulcer prophylaxis and treatment.

Those findings suggest that G-CSF treatment has a lower risk of severe adverse events than MPSS treatment. Hence, G-CSF may be a reasonable alternative to MPSS, but a direct comparison of the efficacy of each drug is needed.

As for the cost, the price of G-CSF (300 μg) in Japan is 24,926 yen (175.2 Euro in the rate of Jan. 26, 2014).We employed the G-CSF dose regimen of 10 μg/kg/d × 5 days. Therefore, the total cost of G-CSF therapy in patient with 60 kg body weight is 249,260 yen (1,752.05 Euro). MPSS (500 mg) costs 3,536 yen (24.85 Euro). The dose regimen of MPSS in NASCIS 2 is 5.4 mg/kg as a bolus injection followed by 5.4 mg/kg/h for 23 h. Therefore, the total cost of MPSS therapy protocol in patient with 60 kg body weight is 67,184 yen (472.17 Euro). The cost of G-CSF therapy is higher than that in the MPSS therapy, of which difference in total cost is 182,816 yen (1,284.83 Euro).

The present study has several major limitations. First, the patients were not randomly allocated to the treatment groups. Second, the control group was historical. Third, the number of patients was too small to prove the efficacy of G-CSF treatment with sufficient statistical power. Finally, the timing of treatment initiation differed between treatment groups (within 8 h after injury in the MPSS group and within 48 h after injury in the G-CSF group).

The results of the current study suggest that G-CSF administration is both safe and effective. Although we cannot draw conclusions about the efficacy of G-CSF without prospective randomized controlled trial, the present results encourage us to make step forward to perform next phase of clinical trial.

Conflict of interest None.

References

1. Bauchet L, Lonjon N, Perrin FE et al (2009) Strategies for spinal cord repair after injury: a review of the literature and information. Ann Phys Rehabil Med 52:330–351
2. Park E, Velumian A, Fehlings MG (2004) The role of excitotoxicity in secondary mechanisms of spinal cord injury: a review with an emphasis on the implications for white matter degeneration. J Neurotrauma 21:754–774
3. Varma AK, Das A, Wallace G 4th et al (2013) Spinal Cord Injury: a review of current therapy, future treatments, and basic science frontiers. Neurochem Res 38:895–905
4. Bracken MB, Shepard MJ, Collins WF et al (1990) A randomized, controlled trial of methylprednisolone or naloxone in the treatment of acute spinal-cord injury: results of the second national acute spinal cord injury study. N Engl J Med 322:1405–1411
5. Bracken MB (2012) Steroids for acute spinal cord injury. Cochrane Database Syst Rev. doi:10.1002/14651858
6. Hurlbert RJ, Hadley MN, Walters BC et al (2013) Pharmacological therapy for acute spinal cord injury. Neurosurgery 72(Suppl 2):93–105. doi:10.1227/NEU.0b013e31827765c6
7. Nicola NA, Metcalf D, Matsumoto M et al (1983) Purification of a factor inducing differentiation in murine myelomonocytic leukemia cells. Identification as granulocyte colony-stimulating factor. J Biol Chem 258:9017–9023
8. Roberts AW (2005) G-CSF: a key regulator of neutrophil production, but that's no all! Growth Factors 23:33–41
9. Kawabe J, Koda M, Hashimoto M et al (2011) Neuroprotective effects of granulocyte colony-stimulating factor and relationship to promotion of angiogenesis after spinal cord injury in rats. J Neurosurg Spine 15:414–421. doi:10.3171/2011.5.SPINE10421
10. Koda M, Nishio Y, Kamada T et al (2007) Granulocyte colony-stimulating factor (G-CSF) mobilizes bone marrow-derived cells into injured spinal cord and promotes functional recovery after compression-induced spinal cord injury in mice. Brain Res 1149:223–231
11. Nishio Y, Koda M, Kamada T et al (2007) Granulocyte colony-stimulating factor (G-CSF) attenuates neuronal death and promotes functional recovery after spinal cord injury in mice. J Neuropathol Exp Neurol 66:724–731
12. Kadota R, Koda M, Kawabe J et al (2012) Granulocyte Colony-Stimulating Factor (G-CSF) Protects Oligpdendrocyte and promotes hindlimb functional recovery after spinal cord injury in rats. PLoS One 7:e50391. doi:10.1371/journal.pone.0050391
13. Takahashi H, Yamazaki M, Okawa A et al (2012) Neuroprotective therapy using granulocyte colony-stimulating factor for acute spinal cord injury: a phase I/IIa clinical trial. Eur Spine J 21:2580–2587. doi:10.1007/s00586-012-2213-3
14. Kliesch WF, Cruse JM, Lewis RE et al (1996) Restoration of depressed immune function in spinal cord injury patients receiving rehabilitation therapy. Paraplegia 34:82–90
15. Jackson AB, Groomes TE (1994) Incidence of respiratory complications following spinal cord injury. Arch Phys Med Rehabil 75:270–275
16. Matsumoto T, Tamaki T, Kawakami M et al (2001) Early complications of high-dose methyl-prednisolone sodium succinate treatment in the follow-up of acute cervical spinal cord injury. Spine 26:426–430

Spine

SPINE Volume 39, Number 3, pp 192-197

BASIC SCIENCE

Delayed Granulocyte Colony-Stimulating Factor Treatment in Rats Attenuates Mechanical Allodynia Induced by Chronic Constriction Injury of the Sciatic Nerve

Masao Koda, MD, PhD,* Takeo Furuya, MD, PhD,* Kei Kato, MD, PhD,* Chikato Mannoji, MD, PhD,† Masayuki Hashimoto, MD, PhD,‡ Taigo Inada, MD,* Koshiro Kamiya, MD,* Mitsutoshi Ota, MD,* Satoshi Maki, MD,* Akihiko Okawa, MD, PhD,* Kazuhisa Takahashi, MD, PhD,* Tetsuhiro Ishikawa, MD, PhD,* and Masashi Yamazaki, MD, PhD§

Study Design. Animal experimental study with intervention.

Objective. The aim of this study was to elucidate therapeutic effects of delayed granulocyte colony-stimulating factor treatment for mechanical allodynia induced by chronic constriction injury (CCI) of the sciatic nerve in rats.

Summary of Background Data. Granulocyte colony-stimulating factor (G-CSF) is used clinically for patients with hematological disorders. Previous reports showed that immediate G-CSF attenuates neuropathic pain in CCI of the sciatic nerve. However, the acute treatment for neuropathic pain prior to accurate diagnosis is not realistic in clinical settings.

Methods. Adult, female Sprague-Dawley rats were subjected to the CCI model. This model induces mechanical allodynia on the ipsilateral hind paw within the first week after the injury. One week after CCI, rats received intraperitoneal G-CSF (15.0 μg/kg) for 5 consecutive days. Mechanical allodynia was assessed using the von Frey hair test. Immunohistochemistry for phosphorylated p38 mitogen-activated kinase (p-p38MAPK) and OX-42 (a marker for activated microglia) on tissue slides from a subset of rats 2 weeks after surgery. Western blot analyses were carried out to determine protein expression level of p-p38MAPK and interleukin-1 β on spinal cord homogenates 2 weeks after CCI.

Results. Results of the von Frey filament test showed that G-CSF significantly attenuates mechanical allodynia induced by the CCI model. Immunohistochemistry revealed that G-CSF reduced the number of p-p38MAPK–positive cells in the ipsilateral dorsal horn compared with that in the vehicle group rats. Immunofluorescent double staining revealed that p-p38MAPK–expressing cells in the spinal cord dorsal horn are mainly microglia. Western blot analysis indicated that G-CSF decreased the expression levels of both p-p38MAPK and interleukin-1 β in the ipsilateral dorsal horn compared with that in the vehicle group rats.

Conclusion. The present results indicate a beneficial effect of delayed G-CSF treatment in an animal model of peripheral nerve injury-induced neuropathic pain.

Key words: neuropathic pain, G-CSF, animal model.

Level of Evidence: N/A

Spine 2014;39:192–197

Neuropathic pain is caused by damage to or dysfunction of the central or peripheral nervous system. In most cases, it cannot be explained by a single disease process or a locus of damage. It may be associated with dysesthesia or allodynia, spontaneously occurring sensations characterized by abnormal or hypersensitive responses to external stimuli, often limiting a patient's quality of life. Currently, neuropathic pain is difficult to treat, and patients frequently experience poor clinical outcomes, in large part because the precise pathophysiology of neuropathic pain still remains unclear. The search for novel therapeutic agents for the treatment of neuropathic pain is an area of intense laboratory and clinical research.[1]

Granulocyte colony-stimulating factor (G-CSF) is a 19.6-kDa glycoprotein initially identified as a serum factor that induces differentiation of a murine myelomonocytic leukemic cell line.[2] It is widely known as a hematopoietic cytokine that promotes survival, proliferation, and differentiation of cells

From *Department of Orthopedic Surgery, Chiba Medical Center, Chiba, Japan; †Graduate School of Medicine, Chiba University, Chiba Medical Center, Chiba, Japan; ‡Chiba Aoba Municipal Hospital, Chiba Medical Center, Chiba, Japan; and §Department of Orthopedic Surgery, University of Tsukuba, Ibaraki, Japan.

Acknowledgment date: May 16, 2013. Revision date: September 2, 2013. Acceptance date: October 14, 2013.

The manuscript submitted does not contain information about medical device(s)/drug(s).

Grants-in-Aid for Scientific Research from the Ministry of Education, Science and Culture of Japan (16591473-00) funds were received in support of this work.

No relevant financial activities outside the submitted work.

Address correspondence and reprint requests to Masao Koda, MD, PhD, Department of Orthopedic Surgery, Graduate School of Medicine, Chiba University, 1-8-1 Inohana, Chuo-Ku, Chiba 260-8670, Japan; E-mail: masaokod@gmail.com

DOI: 10.1097/BRS.0000000000000108

of neutrophilic lineage.[2,3] G-CSF is used clinically for patients with leukocytopenia and for donors of peripheral blood-derived hematopoietic progenitor cells prior to their collection for transplantation.[3] Recently, nonhematopoietic effects of G-CSF have been reported, including effects on the central nervous system. G-CSF was found to protect neurons from ischemia-induced cell death and to promote neurogenesis in a rat model of brain ischemia model.[4,5] It was also reported that G-CSF protects neurons and oligodendrocytes from apoptosis in mouse and rat spinal cord injury models.[6,7] We recently conducted early-phase clinical trials of G-CSF for spinal cord injury and acute aggravation of compressive myelopathy.[8,9] In those trials, we unexpectedly observed pain relief in several patients.[10] As a result, we hypothesized that G-CSF can attenuate neuropathic pain and tested this hypothesis in a phase 1/2a clinical trial for compression myelopathy-related neuropathic pain.[10] As for its effects in cases of peripheral nerve injury, it has been reported that the immediate administration of G-CSF attenuates neuropathic pain in the Bennett model *via* suppression of inflammatory cytokines, including tumor necrosis factor-α and interleukin-6, and upregulation of endorphins.[11] However, the acute administration of any treatment for neuropathic pain prior to accurate diagnosis of the condition is not realistic in clinical settings.

In this study, we have designed a protocol to better reflect the clinical need to treat neuropathic pain sometime after the initial nerve injury. To elucidate the effects of delayed G-CSF treatment, we administered G-CSF 1 week after the induction of neuropathic pain by sciatic nerve constriction, a time when neuropathic pain characterized by allodynia is obvious and measurable.

MATERIALS AND METHODS

Animals

All animals were treated and cared for in accordance with the Chiba University School of Medicine guidelines pertaining to the treatment of experimental animals. The study was approved by the Animal Care and Use Committee of Chiba University Graduate School of Medicine (approval number 24-276). We used 44 adult female Sprague-Dawley rats (10–12 wk, 200–240 g; Japan SLC, Inc., Hamamatsu, Japan), which were housed in individual cages and given food and water *ad libitum*.

Rats were anesthetized with 1.5% of halothane in oxygen, delivered at 0.5 L/min. Sciatic nerve injury was induced using the Bennett chronic constriction injury (CCI) model,[12] with slight modification. The left side biceps femoris and the gluteus muscles were divided to expose the sciatic nerve, around which 4 loose ligatures (6-0 nylon suture) were placed at 1-mm intervals. This model induces mechanical allodynia on the ipsilateral hind paw within the first week after the injury. Upon awakening, rats were evaluated neurologically, and their food and water consumption and urine output were monitored.

One week after CCI, the majority of rats showed mechanical allodynia as revealed by hypersensitivity to von Frey hair stimulation. Eight rats exhibited no mechanical allodynia and were excluded from further experiments. The remaining rats were assigned randomly to 1 of the 2 groups. Those in the G-CSF group received intraperitoneal recombinant human G-CSF (15.0 μg/kg; Kyowa Kirin Pharma, Tokyo, Japan) dissolved in normal saline for 5 consecutive days. Rats in the vehicle group received an equivalent volume of normal saline at the same time points. We followed the drug administration regimen described in our previous report on the rat spinal cord injury model.[13] On the day following the final administration of G-CSF, peripheral blood samples were collected for leukocyte counts. Blood leukocyte counts for rats in the control and G-CSF groups were 3800 ± 500/μL and 9700 ± 700/μL, respectively.

Mechanical allodynia in rats from the vehicle and G-CSF groups (n = 10 each) was assessed using the von Frey hair, according to a previously described protocol.[14] The von Frey hair were applied in ascending order of force (0.7, 1.2, 1.5, 2.0, 3.6, 5.5, 8.5, 11.7, 15.1, and 29 g) to the central plantar surface of the ipsilateral hind paw. Contralateral hind paw was served as control. Each filament was applied 5 times. When a rat showed a single withdrawal response to a given filament, the bending force for that filament was defined as the paw withdrawal threshold intensity. The median threshold intensity was calculated from the values following 1 descending and 2 ascending trials. The experimental conditions were identical for both groups of rats. Behavioral testing commenced 1 day after the operations and continued for 6 consecutive weeks.

Tissue Preparation

Tissues from a subset of rats (n = 4/group) were prepared for histological evaluation 2 weeks after surgery. Animals were anesthetized with pentobarbital and perfused transcardially with 4% paraformaldehyde in phosphate-buffered saline (PBS, 7.4 pH). Tissue blocks of the spinal lumbar enlargement were removed, postfixed overnight in 4% paraformaldehyde, stored for time at 4°C in 20% sucrose in PBS, and then embedded in OCT compound (Sakura Finetechnical, Tokyo, Japan). The cryoprotected samples were frozen and stored at −80°C until use. The samples were cut into serial 20-μm transverse sections with a cryostat and mounted on aminosilane-coated slides (Matsunami, Tokyo, Japan).

Immunofluorescent Labeling

For immunofluorescent labeling, sections were permeated with 0.3% Triton X in PBS and treated for 1 hour in blocking solution containing 1% bovine serum albumin and Block Ace (Dainippon Pharma, Japan). Sections were then incubated with the following primary antibodies: rabbit polyclonal anti-phosphorylated p38 mitogen-activated kinase antibody (p-p38MAPK, 1:400; Cell Signaling Technology, Beverly, MA); mouse monoclonal anti-Neu-N antibody (1:400; Chemicon Inc., Temecula, CA) for neurons; mouse monoclonal anti-glial fibrillary acidic protein antibody (GFAP, 1:400; Sigma, St Louis, MO) for astrocytes; or anti-CD11b mouse monoclonal antibody (clone OX-42; AbD Serotec, Oxford,

United Kingdom) for microglia. The sections were incubated with primary antibodies overnight at 4°C, after which they were washed in PBS and then incubated for 1 hour at room temperature with secondary antibodies: Alexa 488- labeled anti-rabbit IgG (1:800; Invitrogen, Eugene, OR) and Alexa 594–labeled anti-mouse IgG (1:800; Invitrogen). Finally, the sections were washed twice in PBS and protected with coverslips. Positive labeling was observed using fluorescence microscopy (ECLIPSE E600; Nikon, Tokyo, Japan), or, in the case of double staining for p-p38MAPK/cell markers, positive signals were detected using confocal laser scanning microscopy (LSM5 PASCAL; Carl Zeiss, Jena, Germany). To determine the specificity of staining, procedures were performed on control sections with the omission of primary or secondary antibodies. Positive immunofluorescent signals were counted for every fifth 20-μm transverse section (*i.e.*, at intervals of 100 μm) from the spinal lumbar enlargement using Scion Image computer analysis software (version beta 4.0.3; Scion Corporation, Frederick, MA). At least 10 sections from each animal were counted, covering a 1-mm length of spinal cord.

Western Blot Analysis

Two weeks after CCI, 10-mm sections of the spinal lumbar enlargement ipsilateral and contralateral to the injury were removed from rats in the control and G-CSF groups (n = 4/group). The tissues were homogenized in 50 mM Tris-HCl (7.4 pH), 150 mM NaCl, and 1% Triton X-100 (homogenization buffer) containing a protease inhibitor cocktail (cOmplete; Roche Diagnostics, Basel, Switzerland). The homogenates were centrifuged at 100,000*g* for 10 minutes at 4°C to remove cellular debris. Protein concentrations of the supernatants were measured using the Bradford method (Bio-Rad Dc Protein Assay Reagents; Bio-Rad Laboratories, Hercules, CA) and were adjusted to 1 mg/mL by dilution with homogenization buffer. Protein samples were mixed with an equal volume of concentrated (2×) sample buffer: 250 mM of Tris-HCl, 4% sodium dodecyl sulfate, 20% glycerol, 0.02% bromophenol blue, and 10% β-mercaptoethanol. After boiling for 5 minutes, equal volumes of samples were subjected to 10% sodium dodecyl sulfate-polyacrylamide gel electrophoresis under reducing conditions, and the proteins were transferred to a polyvinylidene difluoride membrane (Immobilon-P; Millipore Corporation, Billerica, MA). After blocking the membrane with PBS containing 0.3% skim milk and 0.05% Tween 20, the membrane was reacted with an anti- IL-1β (BD Biosciences, Franklin Lakes, NJ), anti-p-p38MAPK (Cell Signaling Technology), and an anti-β-actin antibody as a loading control (Santa Cruz Biotechnology, Santa Cruz, CA). For detection, a horseradish peroxidase-conjugated secondary antibody (Cell Signaling Technology) and an ECL chemiluminescence system (GE Healthcare, Piscataway, NJ) were used. Western blot analysis was performed in triplicate for each sample. Protein bands were quantified using ImageJ software (National Institutes of Health, Bethesda, MD).

Statistical Analysis

Mechanical allodynia data from the von Frey hair test were analyzed using repeated measures ANOVA followed by a *post hoc* Fisher protected least significant difference test. Immunohistochemical results were analyzed using the Student *t* test. Results are presented as mean values ± standard error values of $P < 0.05$ were considered statistically significant.

RESULTS

Results of the von Frey filament test showed that G-CSF attenuates mechanical allodynia induced by sciatic nerve injury in the CCI model. One week after the injury, there were no significant differences between the average paw withdrawal threshold for rats in the control and G-CSF groups (controls: 7.2 ± 3.9 g; G-CSF: 9.0 ± 3.9 g, Figure 1). The administration of G-CSF caused a marked attenuation of mechanical allodynia (*i.e.*, increase in paw-withdrawal threshold) relative to that seen in the control group (Figure 1). *Post hoc* analysis with Fisher protected least significant difference (PSLD) revealed a significant increase in the paw withdrawal threshold in the G-CSF group compared with the threshold in the control group 2 weeks after injury (G-CSF 14.3 ± 3.9 g; control 6.3 ± 3.7 g), 3 weeks after injury (G-CSF 12.1 ± 2.9 g, control 6.3 ± 3.7 g), and 4 weeks after injury (G-CSF 12.7 ± 3.1 g, control 8.0 ± 6.4 g). The average paw withdrawal threshold slightly decreased in the nonaffected hind paw in both the groups; however, there were no statistical differences between both groups (Figure 1).

Immunohistochemistry for OX-42 (a marker for activated microglia) in rats from the control group revealed that the number of OX-42–positive cells was larger in the dorsal horn from the ipsilateral spinal cord lumbar enlargement than the contralateral dorsal horn (Figure 2A, B, E). In the ipsilateral dorsal horn of rats from the G-CSF group, the number of OX-42–positive cells was significantly smaller than that in control rats (Figure 2A, C, E). However, for rats in the G-CSF group, the number of OX-42–positive cells in the ipsilateral dorsal horn was larger than that in the contralateral dorsal horn (Figure 2C–E).

Immunohistochemistry for phosphorylated p38 MAPK (p-p38MAPK) showed a greater number of p-p38MAPK–

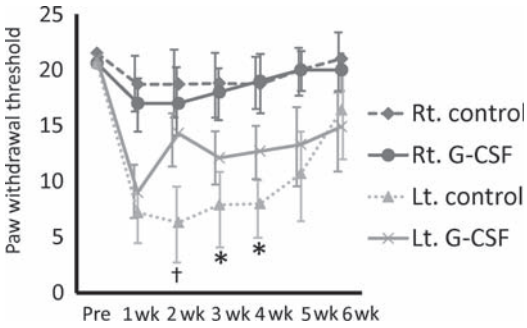

Figure 1. Mechanical allodynia data from the von Frey hair test. One week after the surgery, both groups showed decreased paw withdrawal threshold indicating mechanical allodynia. G-CSF-treated rats (circle) showed significant attenuation of paw withdrawal threshold compared with that of the control rats (square, dotted line) at 2, 3, and 4 weeks after the surgery (1, 2, and 3 weeks after G-CSF treatment). *$P < 0.05$. †$P < 0.01$. Error bar denotes standard error. G-CSF indicates granulocyte colony-stimulating factor; Rt, right; Lt, left.

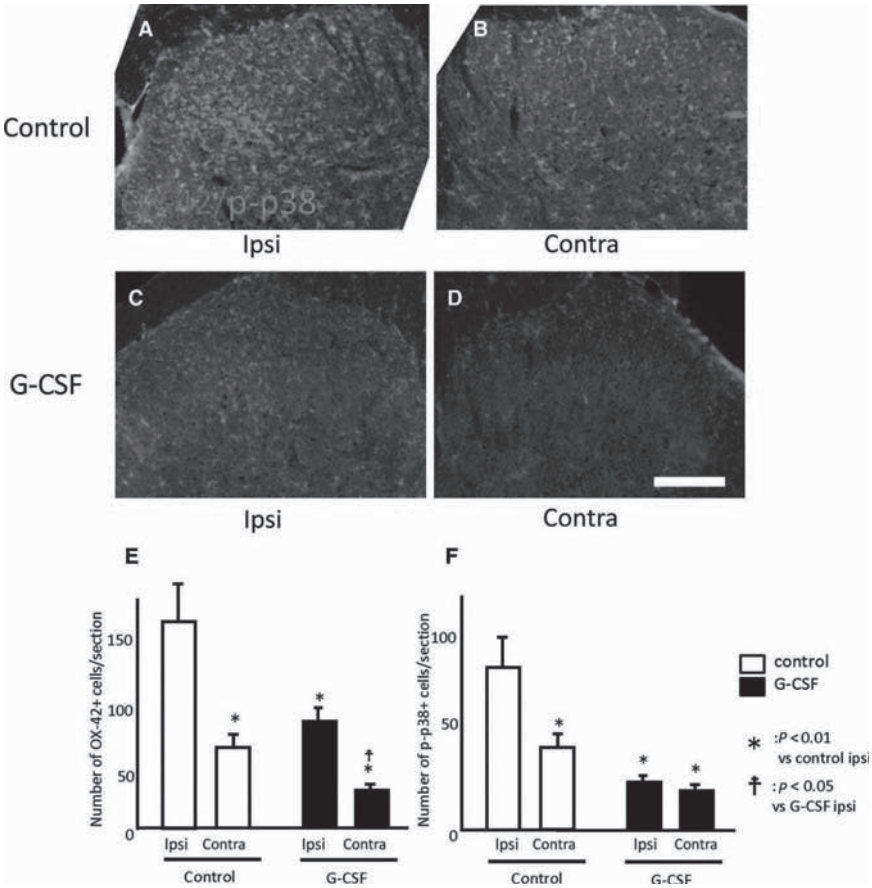

Figure 2. Immunohistochemistry for OX-42 (a marker for microglia) and p-p38MAPK. The number of OX-42–positive microglia decreased in the G-CSF group compared with that in the control group (**E**). A greater number of p-p38MAPK–positive cells in the ipsilateral dorsal horn of the spinal lumbar enlargement compared with the contralateral dorsal horn of control rats was observed (**A**, **B**, **F**). In the G-CSF group, the number of p-p38MAPK–positive cells in the ipsilateral dorsal horn was significantly smaller than that seen in sections from control rats (**A**, **C**, **F**). The number of p-p38MAPK–positive cells was larger in the ipsilateral dorsal horn than that in the contralateral dorsal horn in the G-CSF group (**C**, **D**, **F**). Scale bar = 200 μm. G-CSF indicates granulocyte colony-stimulating factor; p-p38MAPK, phosphorylated p38 mitogen-activated kinase; ipsi, ipsilateral; contra, contralateral.

positive cells in the ipsilateral dorsal horn of the spinal lumbar enlargement than the contralateral dorsal horn of control rats (Figure 2A, B, F). In the G-CSF group, the number of p-p38MAPK–positive cells in the ipsilateral dorsal horn was significantly smaller than that seen in sections from control rats (Figure 2A, C, F). The number of p-p38MAPK–positive cells was larger in the ipsilateral dorsal horn than that in the contralateral dorsal horn in the G-CSF group (Figure 2C, D, F). Immunofluorescent double staining for OX-42 and p-p38MAPK revealed that p-p38MAPK–positive cells were also positive for OX-42, indicating that a large part of p-p38MAPK–expressing cells in the spinal cord dorsal horn are microglia (Figure 3A–D). However, there were several p-p38MAPK–positive/OX-42–negative cells, indicating that p-p38MAPK was also expressed in nonmicroglial cells. Immunofluorescent double staining showed several double positive cells for GFAP and p-p38MAPK, whereas there were no double-positive cells for Neu-N and p-p38MAPK.

Western blot analysis indicated that the expression of p-p38MAPK and IL-1β protein was higher in the ipsilateral dorsal horn than in the contralateral dorsal horn (Figure 4A–D). G-CSF decreased the expression levels of both proteins in the ipsilateral dorsal horn compared with that in the control group.

DISCUSSION

The present results indicate a beneficial effect of delayed G-CSF treatment in an animal model of peripheral nerve injury-induced neuropathic pain. When administered 1 week after peripheral nerve injury, G-CSF significantly suppressed injury-induced phosphorylation of p38MAPK and upregulation of IL-1β expression, reduced the number of activated microglia, and significantly attenuated subsequent mechanical allodynia.

Our results show that CCI injury to the sciatic nerve induces allodynia and causes an increase in the number of microglia in the dorsal horn of the spinal cord on the injured side. This suggests that CCI nerve injury induces microglial activation and that the activation of spinal microglia is highly correlated with pain hypersensitivity. Many authors have reported microglia in response to nerve injury and inflammatory neuropathy in both the central and peripheral nervous systems, and it is thought that microglia may be responsible for the initiation of pain hypersensitivity induced by peripheral nerve injury.[15,16]

p38MAPK is widely known as a key signal mediator that serves as a "hub" in intracellular molecular networks related to inflammatory cytokines. Activation of p38MAPK leads to the upregulation of several inflammatory cytokines, including IL-1β.[17] Our results show that G-CSF suppresses the phosphorylation of p38MAPK and the upregulation of IL-1β. G-CSF also decreased the number of activated microglia, which are a main source of p38 in the spinal cord dorsal horn. Whether G-CSF-mediated suppression of p-p38MAPK and IL-1β results from the suppression of microglial activation, itself, or from a reduction in the number of activated

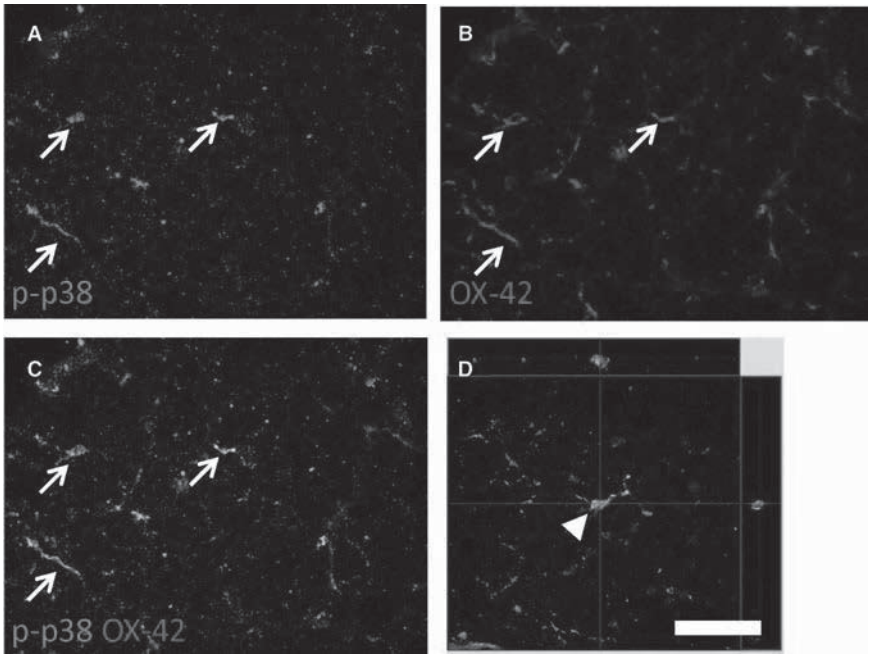

Figure 3. Immunofluorescent double staining for OX-42 and p-p38MAPK confocal laser scanning microscope was used to obtain the images. p-p38MAPK–positive cells (**A**) were also positive for OX-42 (**B**), indicating that p-p38MAPK–expressing cells in the spinal cord dorsal horn are mainly microglia. Scale bar = 100 μm. p-p38MAPK indicates phosphorylated p38 mitogen-activated kinase.

microglia remains unclear. It is also possible that an overall suppression of IL-1β upregulation might attenuate neuropathic pain, and several previous reports have indicated that IL-1β can exacerbate neuropathic pain in various animal models.[18,19] Thus, the suppression of IL-1β protein expression by G-CSF may be directly related to the alleviation of neuropathic pain.

IL-1β is known to modulate neuronal excitability by affecting neuronal receptors such as TRPV1, sodium channels, GABA receptors, and NMDA receptors. In various animal models of neuropathic pain, IL-1β expression is increased in the injured sciatic nerve, dorsal root ganglion, and spinal cord.[20,21,22,23]

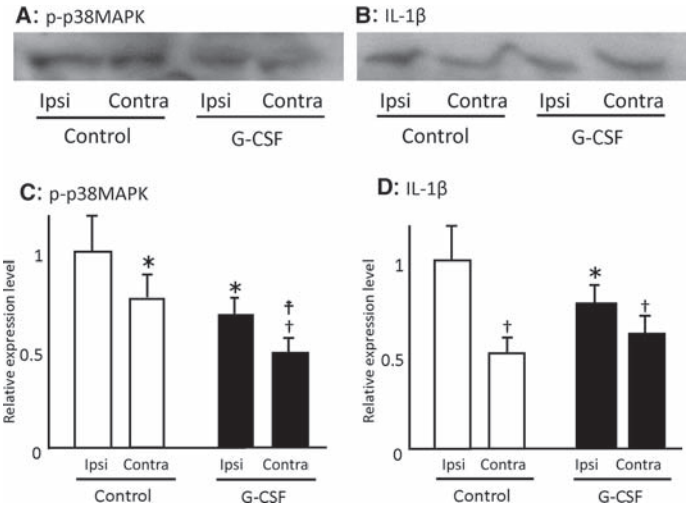

Figure 4. Western blot analysis for p-p38MAPK and IL-1β. G-CSF reduced the protein expression level of p-p38MAPK compared with that in the control group (**A**, **C**). G-CSF also reduced protein expression level of IL-1β (**B**, **D**). G-CSF indicates granulocyte colony-stimulating factor; IL-1β, interleukin-1β; p-p38MAPK, phosphorylated p38 mitogen-activated kinase; ipsi, ipsilateral; contra, contralateral.

In the CCI model in mice, sciatic nerve epineural injections of IL-1R1 neutralizing antibodies have been shown to reduce both thermal hyperalgesia and mechanical allodynia, suggesting a role for the upregulated IL-1β in the induction of neuropathic pain.[24,25] Additionally, in the same CCI model, mechanical allodynia was reduced by intrathecally administered IL-1β neutralizing antibody.[26]

The most important finding of this study is that delayed treatment with G-CSF effectively attenuated CCI-induced mechanical allodynia, extending previous reports showing that immediate G-CSF administration can suppress the onset of allodynia. We are not able to conclude which treatment is more effective, because we did not directly compare the therapeutic effects of immediate and delayed G-CSF treatments. In addition, not all of the animals that experience CCI surgery developed allodynia (82% in our laboratory). Thus, there is a potential to overestimate the beneficial effects of immediate treatment in experimental settings using the CCI model. In most clinical cases involving neuropathic pain, it is not realistic to treat the patient immediately after a nerve injury is sustained. By using a delayed-treatment paradigm, we have more closely approximated a clinical application and reduced the potential for measurement errors.

There were several major limitations of this study in clinical relevance. First, we used intraperitoneal injection for G-CSF administration, of which method cannot be applied for human subjects. There is significant difference in pharmacokynetics between intraperitoneal injection and intravenous injection.[27] Therefore, there might be a difference in antineuropathic effects between both methods of G-CSF administration. Next, we assessed mechanical allodynia as an indicator for neuropathic pain status. Spontaneous pain called dysesthesia, which is one of the characteristics of neuropathic pain

in clinical settings, cannot be evaluated by assessment of allodynia. Therefore, we cannot show the effects of G-CSF for dysesthesia, resulting in limited clinical relevance of the present result. In near future, we better use the assessment tool for dysesthesia.[28] Finally, there was discrepancy between limited period of effectiveness of G-CSF for CCI-induced mechanical allodynia and histological changes. As we previously showed by preliminary human clinical trial of G-CSF for neuropathic pain related to spinal cord lesions,[10] the duration of G-CSF effect was approximately 3 to 4 months in average. The reason why the effects of G-CSF for neuropathic pain is transient although the histological change is obvious because precise mechanism of action of G-CSF for spinal cord lesion-related neuropathic pain is still unclear as same as that for CCI-induced mechanical allodynia. Further exploration is needed to clarify this issue.

CONCLUSION

The present results demonstrate a therapeutic effect of delayed G-CSF treatment for CCI-induced neuropathic pain. The data are relevant to the clinical treatment of neuropathic pain, because, in most cases, patients must be treated not in the acute stage but in the subacute/chronic stage. The elucidation of the therapeutic time window is especially important to guide the future clinical application of G-CSF treatment for peripheral nerve injury-induced neuropathic pain.

➢ Key Points

- ❑ Delayed G-CSF significantly attenuates mechanical allodynia induced by CCI of sciatic nerve.
- ❑ G-CSF reduced the number of activated microglia in the affected dorsal horn of the spinal cord lumbar enlargement.
- ❑ G-CSF reduced the expression level of p-p38MAPK and IL-1β.

References

1. Backonja MM. Neuropathic pain therapy: from bench to bedside. *Semin Neurol* 2012;32:264–8.
2. Nicola NA, Metcalf D, Matsumoto M, et al. Purification of a factor inducing differentiation in murine myelomonocytic leukemia cells. Identification as granulocyte colony-stimulating factor. *J Biol Chem* 1983;258:9017–23.
3. Roberts AW. G-CSF: a key regulator of neutrophil production, but that's not all! *Growth Factors* 2005;23:33–41.
4. Shäbitz WR, Kollmar R, Schwaninger M, et al. Neuroprotective effect of granulocyte colony-stimulating factor after focal cerebral ischemia. *Stroke* 2003;4:745–51.
5. Schneider A, Krüger C, Steigleder T, et al. The hematopoietic factor G-CSF is a neuronal ligand that counteracts programmed cell death and drives neurogenesis. *J Clin Invest* 2005;115:2083–98.
6. Nishio Y, Koda M, Kamada T, et al. Granulocyte colony-stimulating factor (G-CSF) attenuates neuronal death and promotes functional recovery after spinal cord injury in mice. *J Neuropathol Exp Neurol* 2007;66:724–31.
7. Kawabe J, Koda M, Hashimoto M, et al. Neuroprotective effects of granulocyte colony-stimulating factor and relationship to promotion of angiogenesis after spinal cord injury in rats. *J Neurosurg Spine* 2011;15:414–21.
8. Takahashi H, Yamazaki M, Okawa A, et al. Neuroprotective therapy using granulocyte colony-stimulating factor for acute spinal cord injury: a phase I/IIa clinical trial. *Eur Spine J* 2012;21:2580–7.
9. Sakuma T, Yamazaki M, Okawa A, et al. Neuroprotective therapy using granulocyte colony-stimulating factor for patients with worsening symptoms of thoracic myelopathy: a multicenter prospective controlled trial. *Spine* 2012;37:1475–8.
10. Kato K, Yamazaki M, Okawa A, et al. Intravenous administration of granulocyte colony-stimulating factor for treating neuropathic pain associated with compression myelopathy: a phase I and IIa clinical trial. *Eur Spine J* 2013;22:197–204.
11. Chao PK, Lu KT, Lee YL, et al. Early systemic granulocyte-colony stimulating factor treatment attenuates neuropathic pain after peripheral nerve injury. *PLoS One* 2012;7:e43680.
12. Bennett GJ, Chung JM, Honore M, et al. Models of neuropathic pain in the rat. *Curr Protoc Pharmacol* 2003;chap 5:unit 5.32.
13. Kadota R, Koda M, Kawabe J, et al. Granulocyte colony-stimulating factor (G-CSF) protects oligodendrocyte and promotes hind limb functional recovery after spinal cord injury in rats. *PLoS One* 2012;7:e50391.
14. Zhang YQ, Guo N, Peng G, et al. Role of SIP30 in the development and maintenance of peripheral nerve injury-induced neuropathic pain. *Pain* 2009;146:130–40.
15. Cao H, Zhang YQ. Spinal glial activation contributes to pathological pain states. *Neurosci Biobehav Rev* 2008;32:972–83.
16. Gwak YS, Kang J, Unabia GC, et al. Spatial and temporal activation of spinal glial cells: role of gliopathy in central neuropathic pain following spinal cord injury in rats. *Exp Neurol* 2012;234:362–72.
17. Ji RR, Suter MR. p38 MAPK, microglial signaling, and neuropathic pain. *Molecular Pain* 2007;3:33.
18. Zelenka M, Schafers M, Sommer C. Intraneural injection of interleukin-1 beta and tumor necrosis factor-alpha into rat sciatic nerve at physiological doses induces signs of neuropathic pain. *Pain* 2005;116:257–63.
19. Ren K, Torres R. Role of interleukin-1β during pain and inflammation. *Brain Res Rev* 2009;60:57.64.
20. Rotshenker S, Aamar S, Barak V. Interleukin-1 activity in lesioned nerve. *J Neuroimmunol* 1992;39:75–80.
21. Hashizume H, DeLeo JA, Colburn RW, et al. Spinal glial activation and cytokine expression after lumbar root injury in the rat. *Spine* 2000;25:1206–17.
22. Uceyler N, Sommer C. Cytokine regulation in animal models of neuropathic pain and human diseases. *Neurosci Lett* 2008;437:194–8.
23. Kawasaki Y, Zhang L, Cheng JK, et al. Cytokine mechanisms of central sensitization: distinct and overlapping role of interleukin-1beta, interleukin-6, and tumor necrosis factor-alpha in regulating synaptic and neuronal activity in the superficial spinal cord. *J Neurosci* 2008;28:5189–94.
24. Schäfers M, Sorkin L. Effect of cytokines on neuronal excitability. *Neurosci Lett* 2008;437:188–93.
25. Sommer C, Petrausch S, Lindenlaub T, et al. Neutralizing antibodies to interleukin-1 receptor reduce pain associated behavior in mice with experimental neuropathy. *Neurosci Lett* 1999;270:25–8.
26. Schafers M, Brinkhoff J, Neukirchen S, et al. Combined epineural therapy with neutralizing antibodies to tumor necrosis factor-alpha and interleukin-1 receptor has an additive effect in reducing neuropathic pain in mice. *Neurosci Lett* 2001;310:113–6.
27. Tanaka H, Kaneko T. Pharmacokinetics of recombinant human granulocyte colony-stimulating factor in the rat. Single and multiple dosing studies. *Drug Metab Dispos* 1991;19:200–4.
28. Olmarker K, Størkson R, Berge OG. Pathogenesis of sciatic pain: a study of spontaneous behavior in rats exposed to experimental disc herniation. *Spine (Phila Pa 1976)* 2002;27:1312–7.

Spine

SPINE Volume 39, Number 3, pp 213-219

CERVICAL SPINE

Multicenter Prospective Nonrandomized Controlled Clinical Trial to Prove Neurotherapeutic Effects of Granulocyte Colony-Stimulating Factor for Acute Spinal Cord Injury

Analyses of Follow-up Cases After at Least 1 Year

Taigo Inada, MD,* Hiroshi Takahashi, MD, PhD,* Masashi Yamazaki, MD, PhD,* Akihiko Okawa, MD, PhD,* Tsuyoshi Sakuma, MD, PhD,* Kei Kato, MD,* Mitsuhiro Hashimoto, MD,* Koichi Hayashi, MD, PhD,* Takeo Furuya, MD, PhD,* Takayuki Fujiyoshi, MD, PhD,* Junko Kawabe, MD, PhD,* Chikato Mannoji, MD, PhD,* Tomohiro Miyashita, MD, PhD,* Ryo Kadota, MD, PhD,* Yukio Someya, MD, PhD,* Osamu Ikeda, MD, PhD,* Masayuki Hashimoto, MD, PhD,* Kota Suda, MD, PhD,† Tomomichi Kajino, MD, PhD,† Haruki Ueda, MD,† Yasuo Ito, MD, PhD,‡ Takayoshi Ueta, MD, PhD,§ Hideki Hanaoka, MD, PhD,¶ Kazuhisa Takahashi, MD, PhD,* and Masao Koda, MD, PhD*

Study Design. An open-labeled multicenter prospective nonrandomized controlled clinical trial.

Objective. To confirm the feasibility of using granulocyte colony-stimulating factor (G-CSF) for treatment of acute spinal cord injury (SCI).

Summary of Background Data. We previously reported that G-CSF promotes functional recovery after compression-induced SCI in mice. On the basis of these findings, we conducted a multicenter prospective controlled clinical trial to assess the feasibility of G-CSF therapy for patients with acute SCI.

Methods. The trial ran from August 2009 to March 2011, and included 41 patients with SCI treated within 48 hours of onset. Informed consent was obtained from all patients. After providing consent, patients were divided into 2 groups. In the G-CSF group (17 patients), G-CSF (10 μg/kg/d) was intravenously administered for 5 consecutive days, and in the control group (24 patients), patients were similarly treated except for the G-CSF administration. We evaluated motor and sensory functions using the American Spinal Cord Injury Association score and American Spinal Cord Injury Association impairment scale at 1 week, 3 months, 6 months, and 1 year after onset.

Results. Only 2 patients did not experience American Spinal Cord Injury Association impairment scale improvement in the G-CSF group. In contrast, 15 patients in the control group did not experience American Spinal Cord Injury Association impairment scale improvement. In the analysis of increased American Spinal Cord Injury Association motor score, a significant increase in G-CSF group was detected from 1 week after the administration compared with the control group. After that, some spontaneous increase of motor score was detected in control group, but the significant increase in G-CSF group was maintained until 1 year of follow-up.

Conclusion. Despite the limitation that patient selection was not randomized, the present results suggest the possibility that G-CSF administration has beneficial effects on neurological recovery in patients with acute SCI.

Key words: spinal cord injury, secondary injury, G-CSF, clinical trial.

Level of Evidence: 3

Spine 2014;39:213–219

There are currently more than 200,000 people with spinal cord injuries (SCI) in Japan, and about 5000 new cases are diagnosed every year.[1] Thus far, however, there has been no curative treatment of SCI, and the degree of neurological recovery has been dependent on the magnitude of

From the *Spine Section, Department of Orthopaedic Surgery, Chiba University Graduate School of Medicine, Chiba, Japan; †Spinal Cord Injury Center, Hokkaido Chuo Rosai Hospital, Hokkaido, Japan; ‡Department of Orthopaedic Surgery, Kobe Red Cross Hospital, Kobe, Japan; §Department of Orthopaedic Surgery, Japan LHWO Spinal Injuries Center, Iizuka, Japan; and ¶Department of Clinical Research, Chiba University Hospital, Chiba, Japan.

Acknowledgment date: July 10, 2013. First revision date: August 11, 2013. Second revision date: October 21, 2013. Acceptance date: October 28, 2013.

The device(s)/drug(s) that is/are the subject of this manuscript is/are not FDA-approved for this indication and is/are not commercially available in the United States.

Health Labour Science Research Grant of Japan funds were received to support this work. No relevant financial activities outside the submitted work.

Address correspondence and reprint requests to Masao Koda, MD, PhD, Spine Section, Department of Orthopaedic Surgery, Chiba University Graduate School of Medicine, 1-8-1 Inohana, Chuo-ku, Chiba 260-8677, Japan; E-mail: masaokod@gmail.com

DOI: 10.1097/BRS.0000000000000121

the initial injury. SCI is generally divided into 2 consecutive stages: the primary injury and the secondary inflammatory response. The primary injury is caused by a mechanical stress to the spinal cord. Subsequently, the secondary injury occurs, consisting of an inflammatory reaction caused by the release of proinflammatory cytokines.[2] The secondary injury is a potential target for pharmacological interventions. It has been suggested that methylprednisolone sodium succinate (MPSS) can relieve secondary injury to the spinal cord.[3,4] In recent years, however, questions regarding the efficacy of MPSS,[5–8] and its side effects on the respiratory system and digestive systems have arisen.[9] Hence, new pharmacological agents to replace MPSS would be desirable.

Granulocyte colony-stimulating factor (G-CSF) is a 19.6-kDa glycoprotein. It has been well characterized as a growth factor for hematopoietic progenitor cells and is commonly used to treat neutropenia and to mobilize bone marrow hematopoietic stem cells for transplantation.[9,10] Several recent reports have indicated that G-CSF also has nonhematopoietic functions and can potentially be used to treat neuronal injury in stroke and neurodegenerative diseases.[12–16] Thus, we hypothesized that administration of G-CSF might have neurotherapeutic effect on acute SCI. We initially examined this hypothesis in a rodent model of SCI. We previously reported that G-CSF promotes functional recovery after SCI in rodents by mobilizing bone marrow-derived cells to the injured spinal cord, suppressing neuronal apoptosis and oligodendrocyte death, protecting myelin, decreasing the expression of inflammatory cytokines such as TNF-α and IL-1β, and facilitating arterialization.[17–20]

On the basis of those findings, we initiated phase I and IIa clinical trials to confirm the safety and feasibility of neurotherapeutic G-CSF administration for patients with acute SCI. We observed no severe adverse events either during or after G-CSF administration. We determined that a dose of 10 μg/kg/d for 5 days could be safely administered, and that this dose improved the neurological American Spinal Cord Injury Association (ASIA) motor score in patients with SCI.[21] However, the long term effects of G-CSF therapy and the degree of neurological recovery after G-CSF administration remain unclear, in part because some neurological improvement is observed in untreated patients with incomplete SCI. We thus conducted a multicenter prospective nonrandomized controlled clinical trial to assess the neurotherapeutic effects of G-CSF in patients with acute SCI.

MATERIALS AND METHODS

Study Design and Exclusion Criteria

The clinical trial was designed as an open-label, multicenter, prospective, nonrandomized controlled study, and was performed with the approval of the institutional review board of each participating institute. This trial was performed in 4 centers in Japan; Chiba University Hospital, Hokkaido Chuo Rosai Hospital Spinal Cord Injury Center, Kobe Red Cross Hospital, and Japan LHWO Spinal Injuries Center. Starting in August 2009, patients with SCI were recruited within 48 hours of the primary injury. Patients younger than 16 or older than 85 years were excluded, as were patients with intracranial pathologies (*e.g.*, tumors, infection, or ischemia); patients with a history of major bleeding requiring blood transfusion or a history of leukopenia, thrombocytopenia, or hepatic or renal dysfunction, severe heart failure, or splenomegaly; patients diagnosed with a malignant disease within the previous 5 years; and patients who were pregnant or nursing. Written informed consent was obtained from each patient included in the study.

Patients were assigned to either the G-CSF group or the control group according to the institute in which the patients were treated without randomization. Both groups were treated similarly, but the G-CSF group was given a dosage of 10 μg/kg/d of G-CSF (Gran; Kyowa Hakko Kirin, Tokyo) intravenously for 5 consecutive days. The dosage of G-CSF was determined by preliminary open-label, nonrandomized, 1-arm dose-finding trial as we previously reported.[21] G-CSF therapy was performed only at the institute of corresponding author (M.K.). At this institution, all patients with SCI who were treated during the study period and who fulfilled the inclusion criteria received G-CSF treatment. At the other participating institutes, patients were treated similarly but did not receive G-CSF treatment. No patient in either the G-CSF or control group was given MPSS in the follow-up period. Patients received surgery for spinal decompression and stabilization according to each institute's criteria regardless of the patient's treatment group.

Evaluation of Feasibility

Motor and sensory functions were evaluated by the ASIA score (motor scores range from 0 to 100, pinprick scores range from 0 to 112)[22] and the ASIA impairment scale (AIS grade; range A–E). The increase in motor score over time was calculated as previously reported.[23] At least 2 orthopedic spine surgeons in each institute independently evaluated and the data were averaged in each patient's neurological status 1 week, 3 months, and 1 year after the primary injury.

Statistical Analysis

Results are presented as mean ± standard deviation. The Mann-Whitney *U* test was used to evaluate ASIA score improvement, Fisher exact probability test was used to evaluate AIS grade improvement, and Student *t* test was used to analyze hematological data. A *P* value less than 0.05 was considered statistically significant. The biostatistician in the corresponding author's institute reviewed the analysis and verified the statistical results.

RESULTS

Patient Characteristics

A total of 56 patients were enrolled between August 2009 and March 2011. Twenty-six patients were initially assigned to the G-CSF group. Among them, 9 patients did not complete the study; 1 patient developed a fever the day after initiation of G-CSF treatment, 6 patients dropped out during

TABLE 1. Patient Data of G-CSF and Control Groups

	G-CSF	Control	*P*
Number of cases (cases)	17	24	
Sex (cases)			
Male	11	19	
Female	6	5	
Age (yr)	57.1 ± 9.68 (38–68)	56.6 ± 17.9 (23–85)	0.925
Cause of injury (cases)			
Fall	9	13	
Road trauma	6	9	
Sports	1	1	
Falling object	1	0	
Others	0	1	
Level of injury (cases)			
C2–C3	0	2	
C3–C4	4	6	
C4–C5	8	7	
C5–C6	3	7	
C6–C7	2	2	
ASIA impairment scale (cases)			
A	1	7	
B	2	2	
C	5	5	
D	11	12	
Time of first examination after injury (hr)	3.76 ± 2.70 (1–12)	7.73 ± 10.8 (1–48)	0.127
Time of G-CSF administration after injury (hr)	32.7 ± 16.4 (6–48)		

G-CSF indicates granulocyte colony-stimulating factor; ASIA, American Spinal Cord Injury Association.

the follow-up period, 1 patient demonstrated postoperative paralysis and 1 patient died because of heart failure unrelated to the SCI or G-CSF administration. Hence, 17 patients in the G-CSF group completed the study (Table 1). Thirty patients were initially assigned to the control group. Among them, 4 patients dropped out during the follow-up period, 1 patient initially showed paralysis followed by rapid spontaneous recovery during transportation to the hospital, and 1 patient died because of pneumonia. Hence, 24 patients in the control group completed the study (Table 1). There was no significant difference in age, cause of injury, or level of injury between the 2 groups. The groups did, however, differ in the AIS grade because the control group tended to contain more AIS A patients with complete paralysis than the G-CSF group ($P = 0.061$). There was no statistical difference in the number of patient undergone surgery in both groups.

American Spinal Cord Injury Association Impairment Scale

The change in AIS grade between the initial examination and the examination 1 year after treatment is shown in Table 2. The AIS grade improved at least 1 step in 15 patients (88.2%) in the G-CSF group and in 8 patients (33.3%) in the control group, showing significant difference ($P = 0.0002$; Table 3). In patients with incomplete paralysis (AIS grade of B, C, or D at the initial examination; 16 patients in the G-CSF group, and 19 patients in the control group), the AIS grade improved at least 1 step in 15 patients (93.8%) in the G-CSF group and in 6 patients (31.6%) in the control group, still showing significant difference ($P = 0.0002$; Table 2).

ASIA Motor Score

The mean ASIA motor scores at the initial examination were 59.3 ± 28.0 in the G-CSF group and 57.2 ± 34.9 in the control group ($P = 0.979$; Table 3). One week later, the change in motor score was significantly greater in the G-CSF group (14.4 ± 11.6) than in the control group (2.58 ± 8.12) ($P = 0.0002$). Thereafter, patients in both groups continued to increase their motor scores, but the significant difference between the 2 groups was maintained at 1 year after treatment. The change in motor score at 1 year after treatment was significantly higher in the G-CSF group (30.5 ± 20.8) than in the control group (15.7 ± 16.4, $P = 0.013$, power = 0.77; Table 4).

The control group included more patients with AIS A complete paralysis, which might have influenced the results of the study. To exclude this possible bias, we narrowed our analysis to include only patients with incomplete paralysis (AIS grade at first examination: B, C, or D). In these patients, the ASIA motor score at the first examination was 61.3 ± 27.6 in the G-CSF group and 67.6 ± 30.9 in the control group, a difference that was not statistically significant ($P = 0.336$; Table 3). One week later, we found greater improvement in motor scores in the G-CSF group (14.8 ± 11.9) than in the control group (3.26 ± 8.94) ($P = 0.002$). Although motor scores improved in both groups during the next year, the difference in the degree of improvement between the G-CSF and control groups remained significant (31.8 ± 20.7 *vs.* 18.4 ± 17.3, respectively) ($P = 0.050$, power = 0.61; Table 4).

ASIA Pinprick Score

Patients in both the G-CSF and control group demonstrated improvement in their ASIA pinprick scores 1 year after treatment (increased points: 17.8 ± 23.2 and 10.6 ± 24.0, respectively). The difference was not statistically significant ($P = 0.486$; Table 5).

In those patients with incomplete paralysis, improvement was noted in both the G-CSF and control groups 1 year after

TABLE 2. ASIA Impairment Scale

G-CSF Group (17 Cases)						Control Group (24 Cases)					
	Grade at 1 yr After Onset (Cases)						Grade at 1 yr After Onset (Cases)				
First Examination (Cases)	A	B	C	D	E	First Examination (Cases)	A	B	C	D	E
A	1					A	3	2			
B			1	1		B		1	1		
C				4	1	C			2	3	
D				1	8	D				10	2

AIS grades: A, complete paralysis; B, sensory incomplete paralysis, motor complete paralysis; C, motor incomplete paralysis (muscle grading <3/5); D, motor incomplete paralysis (muscle grading >3/5).

G-CSF indicates granulocyte colony-stimulating factor; AIS, ASIA impairment scale; ASIA, American Spinal Cord Injury Association.

treatment (increased points: 20.5 ± 23.0 and 13.8 ± 23.7, respectively). Again, the difference was not statistically significant ($P = 0.254$; Table 5).

Adverse Events

One patient in the G-CSF group developed a fever more than 40°C the day after initiation of G-CSF treatment, and the treatment was thus discontinued. The cause of the fever proved to be a urinary tract infection, which was successfully treated with antibiotics. No relationship was found between the infection and G-CSF administration. One patient developed mild hepatic dysfunction (glutamate oxaloacetate transaminase: 91 U/L [normal range: 13–33 U/L], glutamate-pyruvic transaminase: 99 U/L [normal range: 8–42 U/L]) 5 days after initiation of G-CSF treatment. The patient recovered without intervention. No other severe adverse events occurred during or after G-CSF administration.

DISCUSSION

Nonhematopoietic Effects of G-CSF

Experimental studies on acute myocardial infarction (AMI) have shown that G-CSF mobilizes stem cells into the myocardium, thereby protecting cardiac tissue from injury.[24] In models of ischemic stroke, G-CSF has been shown to protect the brain by suppressing neuronal apoptosis and the expression of inflammatory cytokines.[12–16] We previously made similar observations in preclinical rodent models of acute SCI.[17–20] On the basis of these results, clinical trials have been initiated for the treatment of AMI[25–30] and neurological disorders

TABLE 3. ASIA Motor Score

	G-CSF	Control	*P*
Total cases (G-CSF: n = 17, control: n = 24)			
At first examination	59.3 ± 28.0 (14–98)	57.2 ± 34.9 (4–97)	0.979
1 wk after onset	73.6 ± 24.2 (27–100)	59.8 ± 35.5 (4–100)	0.249
3 mo after onset	86.8 ± 18.6 (35–100)	69.8 ± 34.6 (6–100)	0.154
6 mo after onset	88.9 ± 18.7 (36–100)	71.3 ± 33.6 (6–100)	0.042*
1 yr after onset	89.8 ± 18.5 (36–100)	71.6 ± 14.7 (6–100)	0.025*
Incomplete paralysis cases (AIS: B, C, D) (G-CSF: n = 16, control: n = 19)			
At first examination	61.3 ± 27.6 (14–98)	67.6 ± 30.9 (7–97)	0.336
1 wk after onset	76.1 ± 22.8 (27–100)	70.8 ± 30.5 (6–100)	0.752
3 mo after onset	90.1 ± 13.4 (51–100)	82.8 ± 24.6 (19–100)	0.504
6 mo after onset	92.3 ± 13.2 (51–100)	84.3 ± 23.1 (19–100)	0.137
1 yr after onset	93.1 ± 12.7 (51–100)	84.4 ± 23.1 (19–100)	0.085

AIS grades: B, sensory incomplete paralysis, motor complete paralysis; C, motor incomplete paralysis (muscle grading <3/5); D, motor incomplete paralysis (muscle grading >3/5).

G-CSF indicates granulocyte colony-stimulating factor; AIS, ASIA impairment scale; ASIA, American Spinal Cord Injury Association.

**P < 0.05.*

TABLE 4. Increased Motor Score

	G-CSF	Control	*P*
Total cases (G-CSF: n = 17, control: n = 24)			
1 wk	14.4 ± 11.6 (1–50)	2.58 ± 8.12 (−11 to 24)	0.0002*
3 mo	27.5 ± 18.9 (1–73)	12.6 ± 14.9 (−7 to 48)	0.0005*
6 mo	29.6 ± 19.8 (2–77)	15.4 ± 17.2 (−5 to 64)	0.015†
1 yr	30.5 ± 20.8 (2–81)	15.7 ± 16.4 (−5 to 63)	0.013†
Incomplete paralysis cases (AIS: B, C, D) (G-CSF: n = 16, control: n = 19)			
1 wk	14.8 ± 11.9 (1–50)	3.26 ± 8.94 (−11 to 24)	0.002*
3 mo	28.8 ± 18.8 (1–73)	15.2 ± 15.7 (−7 to 48)	0.029†
6 mo	30.9 ± 19.7 (2–77)	18.3 ± 18.2 (−4 to 64)	0.063
1 yr	31.8 ± 20.7 (2–81)	18.4 ± 17.3 (0–63)	0.050†

AIS grades: B, sensory incomplete paralysis, motor complete paralysis; C, motor incomplete paralysis (muscle grading <3/5); D, motor incomplete paralysis (muscle grading >3/5).

G-CSF indicates granulocyte colony-stimulating factor; AIS, ASIA impairment scale; ASIA, American Spinal Cord Injury Association.

**P < 0.01.*

†P < 0.05.

such as cerebral infarction[31] and amyotrophic lateral sclerosis.[32,33] Many clinical trials in AMI have already reported the safety and feasibility of G-CSF administration.[25–30] A clinical trial in patients with cerebral infarction found that G-CSF administration improved neurological symptoms, although the sample size was small.[31] Furthermore, G-CSF has been shown to attenuate neuronal injury in patients with amyotrophic lateral sclerosis, delaying disease progression and improving quality of life.[33] Ours is the first clinical trial of G-CSF in patients with acute SCI.

Neurotherapeutic Effects of G-CSF for Acute SCI

In our preliminary study, we determined that 10 μg/kg/d dosage of G-CSF, administered by intravenous injection during 5 consecutive days, is the highest dose of G-CSF that can be safely administered to patients.[21,34] On the basis of those results, we conducted this multicenter prospective controlled clinical trial to verify the neurotherapeutic effect of G-CSF in patients with acute SCI. The pathophysiology and symptoms of acute SCI vary depending on the spinal level of injury (cervical, thoracic, or thoracolumbar) and the severity of the trauma. This variability can make data interpretation difficult. Thus, to increase the reliability of our data, we restricted our inclusion criteria to patients with cervical injury and excluded patients with thoracic or thoracolumbar injury.

We analyzed whether G-CSF administration improved muscle power in the upper and lower extremities using the ASIA motor score. One week after the primary injury, the motor score significantly increased in the G-CSF group compared with the control group, and this difference was maintained 1 year later. This result suggests that G-CSF administration may have a neurotherapeutic effect on the descending tracts of the white matter and on the gray matter within the injured spinal segments, resulting in earlier and more pronounced improvement in motor function.

Side Effects of G-CSF

Previous reports have described the side effects of G-CSF administration. Mild symptoms include low back and pelvic pain, fever, headache, nausea, and vomiting.[35–37] Symptoms were transient and disappeared 2 or 3 days after cessation of the drug. In this trial, 1 patient developed a fever 1 day after starting G-CSF treatment, but this was found to be due to a urinary tract infection and resolved with antibiotic treatment. One patient developed mild hepatic dysfunction that resolved spontaneously. Reported severe side effects of G-CSF include cerebral infarction, AMI, and splenic rupture.[38,39] The risk of severe side effects increases with high doses of G-CSF (*e.g.*, 20 μg/kg/d) and the risk of splenic rupture increases with white blood cell counts above $50 \times 10^3/mm^3$.[38] In this study, moderate doses of G-CSF were

TABLE 5. ASIA Pinprick Score

	G-CSF	Control	*P*
Total cases (G-CSF: n = 17, control: n = 24)			
At first examination	71.1 ± 30.0 (21–106)	66.1 ± 39.4 (12–112)	0.874
1 yr after onset	88.9 ± 24.9 (29–112)	77.7 ± 37.5 (16–112)	0.558
Increased points	17.8 ± 23.2 (−12 to 72)	11.6 ± 24.0 (−36 to 81)	0.486
Incomplete paralysis cases (AIS: B, C, D) (G-CSF: n = 16, control: n = 19)			
At first examination	73.6 ± 28.5 (21–106)	81.8 ± 34.6 (20–112)	0.251
1 yr after onset	92.2 ± 20.8 (62–112)	95.6 ± 27.7 (36–112)	0.354
Increased points	20.5 ± 23.0 (−12 to 72)	13.8 ± 23.7 (0–81)	0.254

AIS grades: B, sensory incomplete paralysis, motor complete paralysis; C, motor incomplete paralysis (muscle grading <3/5); D, motor incomplete paralysis (muscle grading >3/5).

G-CSF indicates granulocyte colony-stimulating factor; AIS, ASIA impairment scale; ASIA, American Spinal Cord Injury Association.

administered (10 μg/kg/d) and no severe side effects were observed. Hence, the dosage of 10 μg/kg/d is likely to be safe in patients with acute SCI.

MPSS has been used to treat secondary spinal cord injury (SCI) in patients with acute SCI.[3,4] However, the side effects of MPSS treatment, including pneumonia and gastric ulcer, are harmful to most patients.[5–9] This study suggests that G-CSF as a neurotherapeutic agent might be safer than MPSS in patients with acute SCI.

Future Investigation

This study has several limitations. First, the G-CSF group was treated at 1 institution and the control group was treated at the other institutions. Hence, treatment consistency between the 2 groups have been compromised because we could not control the difference among centers with respect to surgical indication, method of rehabilitation and nursing care, *etc*. As for surgical intervention, surgery itself was no apparent confounding factor shown by univariate analysis, of which result was confirmed by biostatistician. Second, the number of patients enrolled in the study was relatively small to obtain sufficient statistical power. Third, the initial AIS grade differed between the groups, possibly affecting the results. Fourth, this was an open-label study and assignment of patients to the 2 treatment groups was not randomized, resulting in selection bias. Finally, it is possible that evaluators were biased by their knowledge of which patients received the drug because of lacking of the blinding in this study design.

The next phase of the evaluation of G-CSF in acute SCI should be a randomized, double-blind placebo-controlled clinical trial. We are currently designing a phase IIb clinical trial that will include a relatively large number of patients. The results of this trial will provide a better understanding of the effectiveness of neurotherapeutic G-CSF in patients with acute SCI.

CONCLUSION

Despite its limitations, this study suggests that G-CSF administration may have beneficial effects on neurological recovery in patients with acute SCI and encourages the development of additional clinical trials.

➢ Key Points

- ❑ A multicenter prospective controlled clinical trial was performed to confirm the feasibility of G-CSF administration for acute SCI.
- ❑ In 17 acute patients with SCI, within 48 hours of onset, G-CSF (10 μg/kg/d) was intravenously administered for 5 consecutive days.
- ❑ The administration of G-CSF enhanced neurological recovery in 15 of 17 patients with acute SCI.
- ❑ Neurotherapeutic effects of G-CSF could be useful strategy for the treatment of SCI.

Acknowledgment

The authors thank Dr. Yasunori Sato, a biostatistician in Chiba University Hospital Clinical Research Center, for his great assistance in statistical review.

References

1. Shibasaki K. National spinal cord injury registry data 2002.1–12. *J Jpn Med Soc Spinal Cord Lesion* 2005;18: 271–4.
2. Pannu R, Barbosa E, Singh AK, et al. Attenuation of acute inflammatory response by atorvastatin after spinal cord injury in rats. *J Neurosci Res* 2005;79:340–50.
3. Bracken MB, Shepard MJ, Collins WF, et al. A randomized controlled trial of methylprednisolone or naloxone in the treatment of acute spinal cord injury: results of the second national acute spinal cord injury study. *N Engl J Med* 1990;322:1405–11.
4. Bracken MB, Shepard MF, Holford TR, et al. Administration of methylprednisolone for 24 or 48 hours or tirilazad mesylate for 48 hours in the treatment of acute spinal cord injury: results of the third national acute spinal injury randomized controlled trial. *JAMA* 1997;277:1597–604.
5. Hurlbert RJ. Methylprednisolone for acute spinal cord injury: an inappropriate standard of care. *J Neurosurg* 2000;93:1–7.
6. Pointillart V, Petitjean ME, Wiart L, et al. Pharmacological therapy of spinal cord injury during the acute phase. *Spinal Cord* 2000;38:71–6.
7. Polland ME, Apple DF. Factors associated with improved neurologic outcomes in patients with incomplete tetraplegia. *Spine* 2003;28:33–9.
8. Ito Y, Sugimoto Y, Tomioka M, et al. Does high dose methylprednisolone sodium succinate really improve neurological status in patient with acute cervical cord injury?: a prospective study about neurological recovery and early complications. *Spine* 2009;34:2121–4.
9. Matsumoto T, Tamaki T, Kawakami M, et al. Early complications of high-dose methyl-prednisolone sodium succinate treatment in the follow-up of acute cervical spinal cord injury. *Spine* 2001;26: 426–30.
10. Nicola NA, Metcalf D, Matsumoto M, et al. Purification of a factor inducing differentiation in murine myelomonocytic leukemia cells. Identification as granulocyte colony-stimulating factor. *J Biol Chem* 1983;258:9017–23.
11. Roberts AW. G-CSF: a key regulator of neutrophil production, but that's not all! *Growth Factors* 2005;23:33–41.
12. Gibson CL, Jones NC, Prior MJ, et al. G-CSF suppresses edema formation and reduces interleukin-1β expression after cerebral ischemia in mice. *J Cereb Blood Flow Metab* 2005;25:431–9.
13. Kawada H, Takizawa S, Takanashi T, et al. Administration of hematopoietic cytokines in the subacute phase after cerebral infarction is effective for functional recovery facilitating proliferation of intrinsic neural stem/progenitor cells and transition of bone marrow-derived neuronal cells. *Circulation* 2006;113:701–10.
14. Komine-Kobayashi M, Zhang N, Liu M, et al. Neuroprotective effect of recombinant human granulocyte colony-stimulating factor in transient focal ischemia of mice. *J Cereb Blood Flow Metab* 2006;26:402–13.
15. Schäbitz WR, Kollmar R, Schwaninger M, et al. Neuroprotective effect of granulocyte colony-stimulating factor after focal cerebral ischemia. *Stroke* 2003;34:745–51.
16. Schneider A, Kuhn HG, Schäbitz WR. A role for G-CSF (granulocyte colony-stimulating factor) in the central nervous system. *Cell Cycle* 2005;4:1753–7.
17. Koda M, Nishio Y, Kamada T, et al. Granulocyte colony-stimulating factor (G-CSF) mobilizes bone marrow-derived cells into injured spinal cord and promotes functional recovery after compression-induced spinal cord injury in mice. *Brain Res* 2007;1149:223–31.
18. Nishio Y, Koda M, Kamada T, et al. Granulocyte colony-stimulating factor attenuates neuronal death and promotes functional recovery after spinal cord injury in mice. *J Neuropathol Exp Neurol* 2007;66:724–31.
19. Kawabe J, Koda M, Hashimoto M, et al. Granulocyte colony-stimulating factor (G-CSF) exerts neuroprotective effects via

promoting angiogenesis after spinal cord injury in rats. *J Neurosurg Spine* 2011;15:414–21.
20. Kadota R, Koda M, Kawabe J, et al. Granulocyte colony-stimulating factor (G-CSF) protects oligodendrocyte and promotes hind limb functional recovery after spinal cord injury in rats. *PLoS One* 2012;7:e50391.
21. Takahashi H, Yamazaki M, Okawa A, et al. Neuroprotective therapy using granulocyte colony-stimulating factor for acute spinal cord injury: a phase I/IIa clinical trial. *Eur Spine J* 2012;21:2580–7.
22. Maynard FM, Jr, Bracken MB, Creasey G, et al. International standards for neurological and functional classification of spinal cord injury. American Spinal Injury Association. *Spinal Cord* 1997;35:266–74.
23. Tsutsumi S, Ueta T, Shiba K, et al. Effects of the second national acute spinal cord injury study of high-dose methylprednisolone therapy on acute cervical spinal cord injury – results in spinal injuries center. *Spine* 2006;31:2992–6.
24. Iwasaki H, Kawamoto A, Ishikawa M, et al. Dose-dependent contribution of CD34-positive cell transplantation to concurrent vasculogenesis and cardiomyogenesis for functional regenerative recovery after myocardial infarction. *Circulation* 2006;113:1311–25.
25. Engelmann MG, Theiss HD, Hennig-Theiss C, et al. Autologous bone marrow stem cell mobilization induced by granulocyte colony-stimulating factor after subacute ST-segment elevation myocardial infarction undergoing late revascularization: final results from the G-CSF-STMI (granulocyte colony-stimulating factor ST-segment elevation myocardial infarction) trial. *J Am Coll Cardiol* 2006;48:1712–21.
26. Ince H, Petzsch M, Kleine HD, et al. Prevention of left ventricular remodeling with granulocyte colony-stimulating factor after acute myocardial infarction: final 1-year results of the front-integrated revascularization and stem cell liberation in evolving acute myocardial infarction by granulocyte colony-stimulating factor (FIRST-LINE-AMI) trial. *Circulation* 2005;112:173–80.
27. Ripa RS, Jorgensen E, Wang Y, et al. Stem cell mobilization induced by subcutaneous granulocyte colony-stimulating factor to improve cardiac regeneration after acute ST-elevation myocardial infarction: result of the double-blind, randomized, placebo-controlled stem cells in myocardial infarction (STEMMI) trial. *Circulation* 2006;113:1983–92.
28. Takano H, Hasegawa H, Kuwabara Y, et al. Feasibility and safety of granulocyte colony-stimulating factor treatment in patients with acute myocardial infarction. *Int J Cardiol* 2007;122:41–7.
29. Valgimigli M, Rigolin GM, Cittanti C, et al. Use of granulocyte colony-stimulating factor during acute myocardial infarction to enhance bone marrow stem cell mobilization in humans: clinical and angiographic safety profile. *Eur Heart J* 2005;26:1838–45.
30. Zohlnhofer D, Ott I, Mehilli J, et al. REVIVAL-2 Investigators. Stem cell mobilization by granulocyte colony-stimulating factor in patients with acute myocardial infarction: a randomized controlled trial. *JAMA* 2006;295:1003–10.
31. Shyu WC, Lin SZ, Lee CC, et al. Granulocyte colony-stimulating factor for acute ischemic stroke: a randomized controlled trial. *CMAJ* 2006;174:927–33.
32. Nefussy B, Artamonov I, Deutsch V, et al. Recombinant human granulocyte colony-stimulating factor administration for treating amyotrophic lateral sclerosis: a pilot study. *Amyotroph Lateral Scler* 2010;11:187–93.
33. Zhang Y, Wang L, Fu Y, et al. Preliminary investigation of effect of granulocyte colony-stimulating factor on amyotrophic lateral sclerosis. *Amyotroph Lateral Scler* 2009;10:430–1.
34. Sakuma T, Yamazaki M, Okawa A, et al. Neuroprotective therapy using granulocyte colony-stimulating factor for patients with worsening symptoms of compression myelopathy, part 1: a phase I and IIa clinical trial. *Eur Spine J* 2012;21:482–9.
35. Anderlini P, Przepiorka D, Seong D, et al. Clinical toxicity and laboratory effects of granulocyte colony-stimulating factor (filgrastim) mobilization and blood stem cell apheresis from normal donors and analysis of charge for procedures. *Transfusion* 1996;36:590–5.
36. Bensinger WI, Clift TA, Anasetti C, et al. Transplantation of allogeneic peripheral blood stem cells mobilized by recombinant human granulocyte colony-stimulating factor. *Stem Cells* 1996;14:90–105.
37. Murata M, Harada M, Kato S, et al. Peripheral blood stem cell mobilization and apheresis: analysis of adverse events in 94 normal donors. *Bone Marrow Transplant* 1999;24:1065–71.
38. Becker PS, Wagle M, Matous S, et al. Spontaneous splenic rupture following administration of granulocyte colony-stimulating factor (G-CSF) occurrence in an allogeneic donor of peripheral blood stem cells. *Biol Blood Marrow Transplant* 1997;3:45–9.
39. Falzetti F, Aversa F, Minelli O, et al. Spontaneous rupture of spleen during peripheral blood stem cell mobilization in a healthy donor. *Lancet* 1999;353:555.

J. Spine Res. 5 : 162-165, 2014

原著 第42回日本脊椎脊髄病学会優秀論文 Original Article

頚髄症に対する頚椎長範囲前方除圧固定術の10年以上の長期成績

Clinical Results of Anterior Cervical Corpectomy and Arthrodesis for Cervical Myelopathy with more than Ten Years of Follow-up

橋本光宏[*1] 山崎正志[*2] 望月眞人[*3] 山縣正庸[*1]
池田義和[*1] 中島文毅[*1] 高橋和久[*4]

Mitsuhiro Hashimoto[*1], Masashi Yamazaki[*2], Macondo Mochizuki[*3], Masatsune Yamagata[*1], Yoshikazu Ikeda[*1], Fumitake Nakajima[*1], Kazuhisa Takahashi[*4]

要 旨

頚椎長範囲前方除圧固定術を行った頚髄症25例の10年以上の長期成績について検討した．JOAスコアは術前平均9.4点であったが，術後2年で平均13.7点と最大値となり，その後緩やかに低下し，術後10年で平均11.4点となった．固定隣接椎間障害による脊髄症再燃は1例もなかった．経年的な緩やかな成績悪化の原因として，脳や胸腰椎などの加齢性変性疾患の影響や障害された頚髄自体の変性進行が考えられた．

Abstract

In cervical myelopathy cases, it is crucial to know both long-term and short-term results, in order to give patients therapeutic alternatives. We studied the long-term surgical outcomes of anterior cervical corpectomy and arthrodesis.

Twenty-five cervical myelopathy patients treated by anterior cervical corpectomy and arthrodesis, who were followed up more than 10 years were investigated. Average age at surgery was 51.1 years old. Diagnoses included cervical spondylotic myelopathy (11 cases), cervical ossification of the posterior longitudinal ligament (11 cases), and cervical spondylotic amyotrophy (3 cases). We performed anterior cervical corpectomy and strut bone grafting harvested from autologous fibula or iliac bone with halo vest fixation. The corpectomy involved two levels in 10 cases and three levels in 15 cases. We used JOA score to assess the severity of myelopathy and evaluated the following measures : early and late complications, bony union, adjacent disc disease, and detrimental factors affecting the JOA score.

Average JOA score was 9.4 points preoperatively, 12.8 points at 6 months after surgery, 13.1 points at one year, 13.7 points at two years, 13.4 points at three years, and 12.8 points at five years, 11.4 points at ten years. Early complications included graft dislodgement or fracture (3 cases), C5 palsy (3 cases), meningitis (2 cases), recurrent laryngeal nerve palsy (1 case). Late complications included lumbar spinal stenosis (5 cases), thoracic myelopathy (3 cases), Alzheimer disease, cerebral infarction, carpal tunnel syndrome, and cubital tunnel syndrome (1 case each). Bony union

[*1]千葉労災病院整形外科〔〒290-0003 市原市辰巳台東2-16〕Department of Orthopaedic Surgery, Chiba Rosai Hospital
[*2]筑波大学医学医療系整形外科
[*3]沼津市立病院整形外科
[*4]千葉大学大学院医学研究院整形外科学
（2013.7.11受稿，2013.12.23受理）

rate was 88%. There were no recurrences of myelopathy due to adjacent segment disease.

Our study demonstrated that JOA score gradually improved for the first two years after surgery and thereafter slowly decreased. The key factors affecting long-term results were not adjacent disc disease but rather other age-related changes such as cerebrovascular diseases, thoracic and lumbar spinal degenerative diseases, and aging of spinal cord itself. The fact that C3-4 and C4-5 disc levels were included in the fusion levels could decrease the risk of adjacent segment disease after surgery. The damaged spinal cord in cervical myelopathy cases appeared to deteriorate even after surgery, which also might affect the long-term results.

In conclusion, the long-term results after anterior cervical corpectomy and arthrodesis for cervical myelopathy were favorable. Factors related to aging, not adjacent segment disease, appeared to be the major determinants of deterioration.

Key words：頚髄症(cervical myelopathy)，頚椎長範囲前方除圧固定術(anterior cervical corpectomy and arthrodesis)，長期成績(long-term results)

はじめに

頚髄症の手術治療法選択に当たっては短期，中期成績のみならず，長期成績の吟味が重要となる．これまでに頚髄症に対する頚椎椎弓形成術後の長期成績の報告はいくつか散見されるが，頚椎前方除圧固定術の，特に多椎間前方除圧固定術に関する長期成績の報告は多くない．

本報告の目的は頚椎多椎間前方除圧固定術後の長期成績を調査し，長期成績に関与する因子について明らかにすることである．

対象と方法

3椎間以上の頚椎多椎間前方除圧固定術を行い，10年以上の経過観察が可能であった25例について検討した．手術時年齢は16歳から64歳まで，平均年齢は51歳であった．性別は男性19例，女性6例であった．疾患の内訳は頚椎症性脊髄症11例，頚椎後縦靭帯骨化症11例，頚椎症性筋萎縮症3例であった．除圧固定範囲は2椎体亜全摘3椎間固定が10例，3椎体亜全摘4椎間固定が15例であった(表1)．

術式はGotoら[1]，Emeryら[2]の報告に準じて椎体を亜全摘し，前方除圧を行った後に自家腓骨または自家腸骨を移植し，外固定にはハローベストを使用し，プレートによる内固定は行わなかった．

これらの症例について日整会頚部脊髄症治療成績判定基準(JOAスコア)，早期合併症および晩期併発症，骨癒合率，固定隣接椎間障害による脊髄症再燃の有無，JOAスコアの推移に影響を与える因子について検討した．

結　果

術前JOAスコアは平均で9.4点であった．術後2年で13.7点と最高値を示し，その後は緩やかに低下し，術後3年で13.4点，術後5年で12.8点，術後10年で11.4点，最終観察時10.5点であった(図1)．

早期合併症は移植骨脱転2例，移植母床骨折1例，C5麻痺3例，髄膜炎2例，反回神経麻痺1例であった．C5麻痺と反回神経麻痺は一過性であり，自然に回復した．

晩期併発症は腰部脊柱管狭窄症5例，胸椎部脊髄症3例，アルツハイマー病1例，脳梗塞1例，手根管症候群1例，肘部管症候群1例であった(表2)．

晩期併発症によりJOAスコアが低下したのは10例であった．晩期併発症がみられなかった15例のうち，最終観察時までJOAスコアを維持していたのは4例，3点未満の低下は3例，3点以上の低下は8例であった(表3)．

骨癒合は25例中22例に認め，骨癒合率は88%であった．3例の偽関節症例のうち2例に後方手術を追加した．固定隣接椎間障害により脊髄症が再

表1　手術患者背景

手術時年齢	平均51.1歳(16～64歳)
性別	男性19例 女性6例
疾患	頚椎症性脊髄症11例 頚椎後縦靭帯骨化症11例 頚椎症性筋萎縮症3例
除圧固定椎体および椎間数	2椎体亜全摘3椎間10例 C3-6　7例，C4-7　3例 3椎体亜全摘4椎間15例 C2-6　1例，C3-7　13例，C4-T1　1例
経過観察期間	平均13年7か月(10年2か月～19年10か月)

表2　術後合併症

早期合併症	
移植骨脱転	2例
移植母床骨折	1例
C5麻痺	3例
髄膜炎	2例
反回神経麻痺	1例
晩期併発症	
腰部脊柱管狭窄症	5例
胸椎部脊髄症	3例
アルツハイマー病	1例
脳梗塞	1例
手根管症候群	1例
肘部管症候群	1例

燃し，再手術を要した症例は1例もなかった．

考　察

過去の頚髄症に対する長期の手術成績に関する報告では経時的に成績が悪化すると報告されている．椎弓形成術に関するものでは，Kawaguchi ら[3]は24%の患者に神経学的悪化が見られたと報告した．Chiba ら[4]は平均JOAスコアは3年までは著明に改善し，5年以降はわずかに悪化し，特に頚椎後縦靭帯骨化症患者において悪化が見られ，晩期の悪化は下肢機能低下を主症状とし，特に高齢患者では30%に見られたと述べている．一方，頚椎多椎間前方除圧固定術に関するものとして，Ikenaga ら[5]は頚椎多椎間前方法術後10年の経過観察の報告において術後5年で10%の症例において手指の痺れを訴え，JOAスコアが1点悪化したと報告した．本研究においても過去の報告例と同様に術後経時的に成績悪化が認められた．

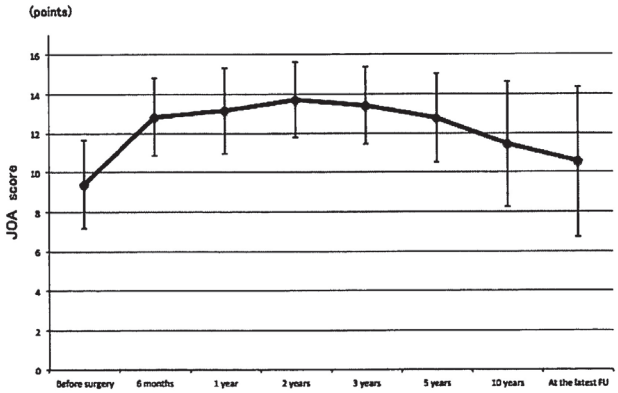

図1　JOAスコアの推移

表3　晩期併発症と術後JOAスコアとの関連

晩期併発症により術後JOAスコア低下	10例
晩期併発症なし	15例
術後JOAスコア維持	4例
術後JOAスコア低下3点未満	3例
術後JOAスコア低下3点以上	8例

頚髄症術後の長期経過観察におけるJOAスコア低下の原因について，Chiba ら[4]は高齢者においては脊椎変性疾患，下肢関節疾患，心血管疾患，脳血管疾患などの併発症の影響があることを挙げ，これには神経，骨格機能の正常な加齢変化が含まれるがゆえに，JOAスコアによる評価ではその影響を除外できないことを指摘した．自験例においては脳や胸腰椎などに新たな変性疾患が出現した患者もいたが，その一方で新たな併発疾患の出現なしに頚髄症が経時的に徐々に悪化した患者がみられた．障害を受けた脊髄は手術により機能改善が見られるが，その機能は完全に回復することはなく，長期経過においてはその遺残した脊髄障害部位において加齢変性変化が進行するのではないか，そのことが長期成績に少なからず影響するのではないかと推察した．近年の脊髄の基礎研究により明らかとなった脊髄障害後の炎症反応に年齢による違いが見られること[6][7]や慢性の圧迫性脊髄症において神経細胞の細胞死が重要な役割を果たすこと[8][9]は上記を裏付けうるものと考える．

頚椎前方除圧固定術の術後成績に影響を及ぼす因子として固定隣接椎間障害が知られている．Hilibrand ら[10]は術後５年で13.6%，術後10年で25.6%の患者に固定隣接椎間障害を生じうると述べ，固定隣接椎間障害による脊髄症発現の原因は加齢による頚椎症性変化の進行によるものであり，固定隣接椎間障害そのものによるのではないと述べている．一方，Matsumoto ら[11]は頚椎前方除圧固定術により固定隣接椎間の椎間板変性は進行すると述べている．ただし，Hilibrand ら[10]，Matsumoto ら[11]はともに固定隣接椎間の椎間板変性が必ずしも症状出現に繋がるとは限らないとも述べている．望月ら[12]は固有脊柱管前後径13mm未満の症例ではC3-4あるいはC4-5椎間での動的脊柱管狭窄により術後10年前後にて成績低下をきたしやすく，10年以上の長期経過での安定した成績維持を期待するならば，C3-4，C4-5椎間の予防的固定を行うことが必要であると述べた．

頚椎多椎間前方除圧固定術術後の固定隣接椎間障害については，Hilibrand ら[10]は多椎間固定例の方が単椎間固定例よりもむしろ頻度が低いと述べ，Ikenaga ら[5]は頚椎の長範囲前方固定においては固定隣接椎間へ及ぼす影響はきわめて少ないと述べた．本研究においても固定隣接椎間障害による再手術症例はなく，Hilibrand ら[10]，Ikenaga[5]らの報告と同様の結果であった．望月ら[12]が述べたように術後に固定隣接椎間障害を起こす危険があるC3-4椎間，C4-5椎間を除圧固定範囲に含めることで，術後固定隣接椎間障害の危険を軽減できると考えた．ゆえに，固定隣接椎間障害による脊髄症再燃は頚椎前方除圧固定術において起こりうる合併症ではあるが，除圧固定範囲を適正に設定することで頻度を減らすことは可能であると考える．固定隣接椎間障害を理由に前方法を回避し，敢えて後方法を選択する根拠は乏しく，頚髄症に対する頚椎長範囲前方除圧固定術は有用な治療選択肢の一つであると考える．

結　論

頚椎多椎間除圧固定術後の長期成績は良好であった．長期成績に影響を及ぼすのは固定隣接椎間障害ではなく，脳，胸腰椎などの変性疾患，障害された頚髄自体の変性進行などの加齢に伴う諸因子であった．

文献

1）Goto S, Mochizuki M, Kita T, et al.：Anterior surgery in four consecutive technical phases for cervical spondylotic myelopathy. Spine 1993；18：1968-1973
2）Emery SE, Bohlman HH, Bolesta MJ, et al.：Anterior cervical decompression and arthrodesis for the treatment of cervical spondylotic myelopathy. Two to seventeen-year follow-up. J Bone Joint Surg Am. 1998；80：941-951
3）Kawaguchi Y, Kanamori M, Ishihara H, et al.：Minimum 10-year followup after en bloc cervical laminoplasty. Clin Orthop Relat Res. 2003；411：129-139
4）Chiba K, Ogawa Y, Ishii K, et al.：Long-term results of expansive open-door laminoplasty for cervical myelopathy-average 14-year follow-up study. Spine. 2006；31：2998-3005：
5）Ikenaga M, Shikata J, Tanaka C.：Long-term results over 10 years of anterior corpectomy and fusion for multilevel cervical myelopathy. Spine. 2006；31：1568-1574
6）Kumamaru H, Saiwai H, Ohkawa Y, et al.：Age-related differences in cellular and molecular profiles of inflammatory responses after spinal cord injury. J cell Physiol. 2012；227：1335-1346
7）Lee DH, Ahn JH, Park JH, et al.：Comparison of expression of inflammatory cytokines in the spinal cord between young adult and aged beagle dogs. Cell Mol Neurobiol. 2013；33：615-624
8）Inukai T, Uchida K, Nakajima H, et al.：Tumor necrosis factor-alpha and its receptors contribute to apoptosis of oligodendrocytes in the spinal cord of spinal hyperostotic mouse (twy/twy) sustaining chronic mechanical compression. Spine. 2009；34：2848-2857
9）Tanabe F, Yone K, Kawabata N, et al.：Accumulation of p62 in degenerated spinal cord under chronic mechanical compression：functional analysis of p62 and autophagy in hypoxic neuronal cells. Autophagy. 2011；7：1462-1471
10）Hilibrand AS, Carlson GD, Palumbo MA, et al.：Radiculopathy and myelopathy at segments adjacent to the site of a previous anterior cervical arthrodesis. J Bone Joint Surg Am. 1999；81：519-528
11）Matsumoto M, Okada E, Ichihara D, et al.：Anterior cervical decompression and fusion accelerates adjacent segment degeneration：comparison with asymptomatic volunteers in a ten-year magnetic resonance imaging follow-up study. Spine. 2010；35：36-43
12）望月眞人，後藤澄雄．頚椎症性脊髄症に対する前方除圧固定術の長期成績．脊椎脊髄．1997；10：803-807

Original Contribution

Myoblast-Mediated Gene Therapy Improves Functional Collateralization in Chronic Cerebral Hypoperfusion

Nils Hecht, MD; Aiki Marushima, MD; Melina Nieminen, MSc; Irina Kremenetskaia, MSc; Georges von Degenfeld, MD; Johannes Woitzik, MD; Peter Vajkoczy, MD

Background and Purpose—Direct extracranial–intracranial bypass surgery for treatment of cerebral hemodynamic compromise remains hindered by complications but alternative simple and safe indirect revascularization procedures, such as an encephalomyosynangiosis (EMS), lack hemodynamic efficiency. Here, the myoblast-mediated transfer of angiogenic genes presents an approach for induction of therapeutic collateralization. In this study, we tested the effect of myoblast-mediated delivery of vascular endothelial growth factor-A (VEGF) to the muscle/brain interface of an EMS in a model of chronic cerebral hypoperfusion.

Methods—Permanent unilateral internal carotid artery-occlusion was performed in adult C57/BL6 mice with or without (no EMS) surgical grafting of an EMS followed by implantation of monoclonal mouse myoblasts expressing either $VEGF_{164}$ or an empty vector (EV). Cerebral hemodynamic impairment, transpial collateralization, angiogenesis, mural cell investment, microvascular permeability, and cortical infarction after ipsilateral stroke were assessed by real-time laser speckle blood flow imaging, 2- and 3-dimensional immunofluorescence and MRI.

Results—VEGF-expressing myoblasts improved hemodynamic rescue by day 14 (no EMS 37±21%, EV 42±9%, VEGF 48±12%; $P<0.05$ for VEGF versus no EMS and versus EV), together with the EMS take rate (VEGF 60%, EV 18.2%; $P<0.05$) and angiogenesis of mature cortical microvessels below the EMS ($P<0.05$ for VEGF versus EV). Importantly, functional and morphological results were paralleled by a 25% reduction of cortical infarction after experimental stroke on the side of the EMS.

Conclusions—Myoblast-mediated VEGF supplementation at the target site of an EMS could help overcome the clinical dilemma of poor surgical revascularization results and provide protection from ischemic stroke. **(*Stroke*. 2015;46:00-00.)**

Key Words: cerebral revascularization ■ cerebrovascular disease ■ gene therapy

The results of the recently published Carotid Occlusion Surgery Study put the benefit of direct surgical flow augmentation for treatment of atherosclerotic hemodynamic compromise into question and show that extra- to intracranial bypass grafting remains technically challenging and carries a perioperative stroke risk of up to 15%.[1,2] Despite this development, however, there still remain clear indications for treatment of cerebral hemodynamic compromise through surgical revascularization, such as multiple vessel disease or Moyamoya disease, in particular.

To reduce the risk of perioperative morbidity, a technically simple and safe solution for extracranial–intracranial flow augmentation is needed. For this purpose, a variety of indirect revascularization techniques have been developed. One of the most commonly applied procedures for indirect revascularization is termed encephalomyosynangiosis (EMS), which describes the placement of a vascularized temporal muscle graft onto the hypoperfused cortical surface and results in spontaneous transpial collateralization of distal intramuscular branches of the external carotid artery (ECA) with the cortical vasculature of the brain.[3–5] Importantly, an EMS has the advantage of being less complex and safer than direct bypass surgery with proven benefit in patients with Moyamoya disease.[6–8] Although indirect revascularization seems attractive, it unfortunately lacks hemodynamic effectiveness compared with direct procedures.[9,10] For this reason, we hypothesized that a continuous and local boosting of proangiogenic activity at the muscle/brain interface of an EMS may present a novel approach to facilitate indirect revascularization as a technically simple and safe procedure.

The key factor for compensation of hemodynamic compromise is endogenous flow augmentation through outgrowth of

Received July 8, 2014; final revision received October 3, 2014; accepted October 10, 2014.

From the Department of Neurosurgery and Center for Stroke Research Berlin (CSB), Charité—Universitätsmedizin Berlin, Germany (N.H., A.M., M.N., I.K., J.W., P.V.); and Baxter Laboratory for Stem Cell Biology, Stanford University, CA (G.v.D.).

Current address for G.v.D.: Common Mechanism Research, Bayer Healthcare AG, Wuppertal, Germany and Institute for Operative Medicine, University of Witten/Herdecke, Cologne, Germany.

The online-only Data Supplement is available with this article at http://stroke.ahajournals.org/lookup/suppl/doi:10.1161/STROKEAHA.114.006712/-/DC1.

Correspondence to Peter Vajkoczy, MD, Department of Neurosurgery, Charité—Universitätsmedizin Berlin, Augustenburger Platz 1, 13353 Berlin, Germany. E-mail peter.vajkoczy@charite.de

Stroke **is available at http://stroke.ahajournals.org** **DOI: 10.1161/STROKEAHA.114.006712**

pre-existing collaterals.[11] This requires an active proliferation of endothelial and perivascular cells, which is naturally limited in the brain. Effective collateralization through an EMS requires the outgrowth and remodeling of pre-existing vessels (arteriogenesis) to form patent collaterals between the extracranial and intracranial vascular beds. In this regard, recent evidence convincingly demonstrated that vascular endothelial growth factor-A (VEGF) acts as a key factor in formation, postnatal maturation, and establishment of adult collateral density in the brain.[12,13] However, VEGF delivery for the purpose of therapeutic neovascularization is often hampered by the formation of aberrant blood vessels and hemangiomas.[14–17] In this regard, experimental studies in nonischemic and ischemic tissue have evidenced that an appropriate microenvironmental VEGF concentration is paramount for induction and maintenance of functional neovascularization at a desired target site.[18,19] Hence, the DNA transfer to myogenic precursor cells seems to be an ideal drug delivery strategy to ensure a consistent, long-term and regionally circumscribed overexpression of VEGF for effective induction of neovascularization at the muscle/brain interface of an EMS. Recently, we demonstrated the general feasibility of this approach by successful implantation and fusion of primary monoclonal mouse myoblasts in the nonischemic temporal muscle of an experimental EMS.[20] We now tested whether a myoblast-mediated local delivery of murine $VEGF_{164}$ to the muscle/brain interface of an EMS may improve morphological revascularization and functional outcome in a model of cerebral hypoperfusion.

Methods

Ethics Statement

Experiments were permitted by the local ethics committee on animal research (LaGeSo No. G 0262/07, Berlin, Germany) and in conformity with the German Law for Animal Protection and the National Institute of Health Guidelines for Care and Use of Laboratory Animals.

Mouse Myoblast Purification, Retroviral Infection, and Selection

The isolation, culture, and retroviral infection of primary myoblasts is described elsewhere in detail.[21–23] Briefly, primary mouse myoblasts were transduced with a constitutive LacZ-encoding retrovirus alone (Empty Vector [EV]) or together with a murine $VEGF_{164}$-encoding retrovirus (VEGF). For this purpose, flow cytometry-isolated single cells of the $VEGF_{164}$-expressing population were expanded into monoclonal populations and $VEGF_{164}$ secretion was monitored periodically by enzyme-linked immunosorbent assay (R&D Systems, Minneapolis, MN). On the basis of previous functional and morphological results,[18,19] a monoclonal VEGF population expressing ≈70 ng VEGF/10^6 cells/day (defined as the 100% clone in relation to the average VEGF expression level of the polyclonal VEGF parent population) was selected for implantation.

Animals and Experimental Design

Seventy-three male C57/BL6 mice (Charles River WIGA GmbH, Sulzfeld, Germany), aged 12 weeks (28–31 g) were randomized and the following procedures were performed in a blinded fashion:

1. VEGF (n=24): Unilateral (right) internal carotid artery-occlusion (ICA-O) with ipsilateral EMS and implantation of $VEGF_{164}$-expressing myoblasts into the temporal muscle of the EMS (4×10^5 cells).
2. EV (n=25): ICA-O with EMS and implantation of EV myoblasts as biological control (4×10^5 cells).
3. No EMS (n=16): ICA-O and no EMS.
4. Sham (n=8): Sham ICA-O and no EMS.

For all procedures, mice were anesthetized with 70 mg/kg ketamine and 16 mg/kg xylazine and body temperature was maintained at 37°C. Before and after all procedures, mice had free access to food and water. All data about transpial collateralization, cortical perfusion, histology, and stroke volume were obtained and analyzed in a blinded fashion.

EMS and Ipsilateral ICA-O

The ICA-O was performed immediately before the EMS procedure at a time point defined as day 0 and is described elsewhere in detail.[20,24] Briefly, the animal was positioned supine and the right-sided ICA was permanently ligated with an 8/0 silk suture. Next, the animal was turned to prone position and a right-sided craniectomy was performed along the superior temporal line to the temporal scull base, extending from the bregma to the lambdoid suture using a diamond-tip micro drill (Proxxon GmbH, Wartberg/Aist, Austria). The dura was completely excised along the margin of the craniectomy. To secure the temporal muscle above the cortical surface after myoblast implantation (see below), the overlying muscle fascia was sutured to the contralateral aponeurosis and the skin was readapted with 6/0 Nylon.

Myoblast Implantation

For implantation, cultured myoblasts were trypsinized and resuspended in phosphate-buffered saline with 0.5% bovine serum albumine. On the basis of previous results,[20] we implanted either 4×10^5 EV or VEGF myoblasts per animal in two 5-µL cell suspensions (each containing 2×10^5 cells) by injection into the temporal muscle using a Hamilton microsyringe with a 26-gauge needle (Hamilton Co., Reno, NV) immediately before completing the EMS procedure on day 0.

Laser Speckle Imaging and Cerebrovascular Reserve Capacity

Baseline (resting) perfusion and hemodynamic impairment was quantified on days 3, 7, 14, and 21 by assessment of the acetazolamide-specific cerebrovascular reserve capacity (CVRC) with laser speckle imaging as described previously[24] in Sham- (n=8), no EMS- (n=10), EV- (n=15), and VEGF (n=14)-treated animals (please see the online-only Data Supplement).

FITC-Lectin Perfusion and Assessment of Transpial Collateralization

On day 21, transpial collaterals in the muscle/brain border region of the EMS were determined by 3-dimensional confocal microscopy after an in vivo fluorescein isothiocyanate (FITC)-lectin perfusion in a random subset of animals (no EMS n=6; EV n=11; VEGF n=10). To determine the blood delivery via the muscle graft and the transpial collaterals, we injected FITC-lectin via the ECA ipsilateral to the side of the EMS (please see the online-only Data Supplement). For analysis, 60-µm coronal cryosections were obtained from the bregma level ±0.0 to −4.5 mm in 0.5 mm intervals and observed under a laser-scanning microscope (LSM710, Zeiss, Oberkochem, Germany). To better characterize the positive or negative development of transpial collaterals, we defined the EMS take rate parameter: In each section, transpial collateralization was determined positive only after direct visual confirmation of (1) continuous FITC-lectin positive vessels crossing from the muscle into the cortex and (2) a distinct association of these vessels with the resident vasculature of the cortical region below the EMS. The total number of sections with positive transpial collaterals was counted in each animal and the individual EMS was only rated positive if collaterals were noted in ≥50% (≥5/10) of all

section levels. The EMS take rate was calculated as the percentage of positive EMS and compared between animals with no EMS, EV, or VEGF treatment.

Immunohistochemistry

In the remaining subset of animals (no EMS n=4, EV n=4, VEGF n=4), vessel density and pericyte coverage in the muscle/brain border region of the EMS on day 21 were determined by immunohistochemistry. Coronal cryosections (6 μm) of nonperfused, snap-frozen, whole-head specimens were obtained from the anterior, middle, and posterior region of the EMS (Bregma −0.5, −1.5, and −3.0 mm, respectively) and a combined CD31/Desmin stain was performed. Vessel density within the cortical area below the EMS and the associated temporal muscle was calculated as CD31-positive vessels per mm^2. Pericyte coverage was expressed as the percentage of CD31-positive vessels with Desmin colocalization. In 3 VEGF-treated animals that underwent FITC-lectin perfusion, cell proliferation at the muscle brain interface and in the cortical region below the EMS was visualized with a combined CD31/Ki67 staining. In a second series of animals (EV n=4, VEGF n=4), half of which underwent middle cerebral artery filament-occlusion (MCA-O) on day 21, the effect of VEGF on vascular permeability in the ischemic/nonischemic cortex below the muscle/brain interface was assessed after in vivo Evans Blue perfusion and CD31 staining. Sections were mounted and observed under a fluorescence-enhanced microscope (Axio Imager 2; Zeiss; please see the online-only Data Supplement).

Middle Cerebral Artery Occlusion and Cortical Stroke Volume Assessment

In a third series of animals (no EMS n=6; EV n=6; VEGF n=6), cortical stroke volume was assessed by MRI after 60-minute MCA-O and 23-hour reperfusion on day 21 (please see the online-only Data Supplement). Laser Speckle Imaging was used to visualize the effect of VEGF on the cortical perfusion pattern over the affected hemisphere during the 60-minute occlusion in the second series of mice used for assessment of vascular permeability (EV n=2; VEGF n=2; see above). The timeline of the experiments is depicted in Figure 1.

Statistical Analysis

Data are presented as mean±SD or percentage. Statistics were performed with GraphPad Prism for Mac (Version 5.0f, GraphPad Software, San Diego, CA). Statistical significance was set at $P<0.05$. For a comprehensive description, please see the online-only Data Supplement.

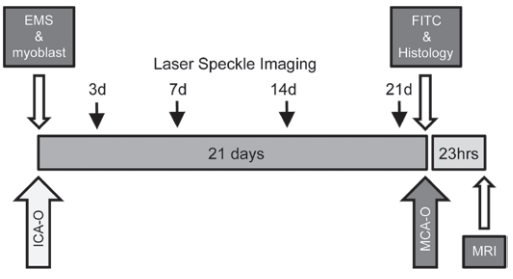

Figure 1. Schematic timeline of the experiments. C57/BL6 mice underwent internal carotid artery-occlusion (ICA-O) with or without subsequent encephalomyosynangiosis (EMS) and implantation of empty vector or vascular endothelial growth factor-A $(VEGF)_{164}$-expressing myoblasts. Cortical perfusion and cerebrovascular reactivity were assessed repeatedly until day 21. At this time point, whole-head specimens were either harvested for histological examination or animals underwent 60-minute middle cerebral artery filament-occlusion (MCA-O) with 23-hour reperfusion for determination of cortical infarct volume. FITC indicates fluorescein isothiocyanate.

Results

Transpial Collateralization at the Muscle/Brain Interface

On day 21 after ICA-O, animals with no EMS did not show signs of spontaneous extracranial–intracranial collateralization across the interface of the temporal muscle and the brain after FITC-lectin perfusion through the ECA on the side of ICA-O (Figure 2A). In contrast, grafting of an EMS with implantation of EV myoblasts yielded patent FITC-positive vessel bridges crossing from the temporal muscle into the brain as a sign of spontaneous EMS collateralization with an 18% EMS take rate among the EV-treated animals. This 18% EMS take rate improved significantly to 60% in animals that received an EMS with implantation of $VEGF_{164}$-expressing myoblasts (*$P<0.05$ versus EV) with distinct signs of pro-angiogenic outgrowth, such as a more tortuous morphology of

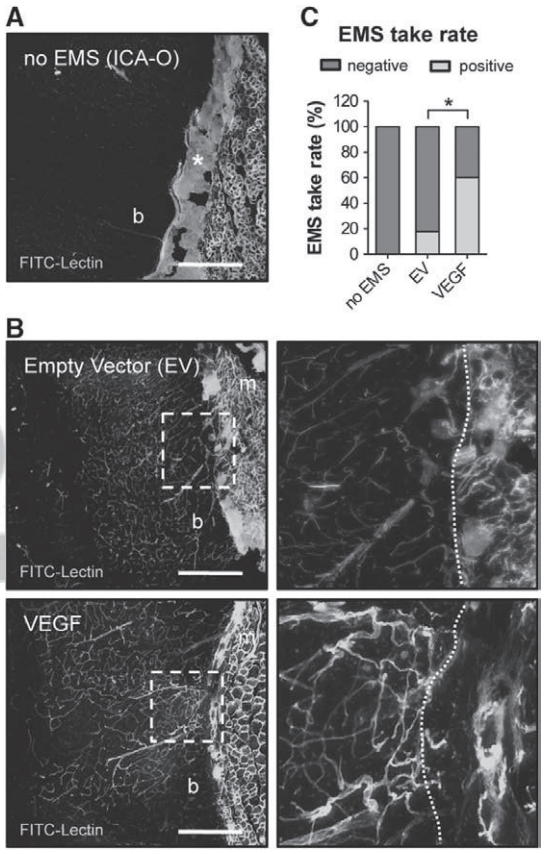

Figure 2. Vascular endothelial growth factor-A $(VEGF)_{164}$-expressing myoblasts improve encephalomyosynangiosis (EMS) take rate. **A**, Fluorescein isothiocyanate (FITC)-lectin injection in an animal without EMS and only internal carotid artery-occlusion (ICA-O; no EMS) fails to show FITC-lectin positive fluorescence within the cortical vasculature. **B**, Vasculature at the muscle/brain interface and within the cortical parenchyma below the EMS shows positive FITC-lectin fluorescence and tortuous transpial vessel sprouts transgressing from the temporal muscle into the cortex after implantation of both empty vector (EV) myoblasts (upper panels) and $VEGF_{164}$-expressing myoblasts (VEGF; lower panels). The dashed rectangle indicates the area of detail enlargement on the right. **C**, Bar graph illustrating the significantly higher EMS take rate after treatment with VEGF myoblasts compared with EV myoblasts (*$P<0.05$). b indicates brain; m, muscle; asterisk, bone; dashed line, muscle/brain interface; bar=1000 μm.

the transpial vessel bridges connecting the vasculature of the EMS interface to the underlying cortical vessels (Figure 2B and 2C).

Hemodynamic Effect of Increased Transpial Collateralization After Treatment With $VEGF_{164}$ Myoblasts

Laser Speckle Images of typical cortical blood flow responses to acetazolamide on day 21 are illustrated in Figure 3A. To get an idea of the physiological cortical perfusion and blood flow response after acetazolamide, we first performed a series of laser speckle measurements in sham-operated animals that did not undergo ICA-O or an EMS procedure. The total mean baseline perfusion in these animals was determined at 565±89 Flux with a mean 49±11% increase in blood flow after acetazolamide stimulation, which is illustrated as the dashed gray line in Figure 3B.

Next, we compared baseline perfusion among treatment groups: In line with previous results,[24] ICA-O alone (no EMS) did not relevantly influence baseline perfusion compared with sham-treated animals at each individual observation time point (data not shown). Furthermore, baseline perfusion did not differ between animals with no EMS, EV, or VEGF (Figure 3B, upper graph).

We then focused on the cortical perfusion response after acetazolamide: Over the untreated hemisphere, acetazolamide led to a marked perfusion increase in all groups (Figure 3A). Over the treated (right) hemisphere, CVRC did at first not differ among groups but remained 24% to 39% below the physiological blood flow response of sham-treated animals. By day 7, we observed a first sign of hemodynamic recovery in EV-treated animals with a significantly higher CVRC compared with animals with no EMS (no EMS 26±14%, EV 41±9%; **P*<0.05). Later, however, animals with no EMS also showed signs of spontaneous CVRC recovery, whereas EV-treated animals showed no further improvement of CVRC (Figure 3B, lower graph).

In contrast, animals that received an EMS with VEGF myoblasts showed a significant 21% to 25% better CVRC recovery beginning at day 14 (no EMS 37±21%, EV 42±9%, VEGF 48±12%; **P*<0.05 for VEGF versus no EMS and #*P*<0.05 for VEGF versus EV) until day 21 (no EMS 36±22%, EV 38±11%, VEGF 48±9%; **P*<0.05 for VEGF versus no EMS and #*P*<0.05 for VEGF versus EV). Importantly, hemodynamic improvement after VEGF did not result in an overshooting CVRC response or cortical hyperperfusion but reached the physiological parameters of sham-treated animals (Figure 3A and 3B).

Vessel Density and Pericyte Coverage

Next, we searched for signs of proangiogenic activity and vessel maturation at the muscle/brain interface. Because, we wanted to distinguish between capillaries—mainly responsible for nutritive perfusion—and the larger pre- and postcapillary vessels, CD31-positive vessels were grouped according to their diameter. As a sign of positive proangiogenic activity in the cortex below the EMS, treatment with VEGF resulted in a significant 21% increase in the parenchymal microvascular density compared with animals that only received EV myoblasts (no EMS 194±32 1/mm^2, EV 174±14 1/mm^2, VEGF 220±50 1/mm^2; **P*<0.05 for VEGF versus EV; Figure 4A and 4B). This proangiogenic activity in the cortex and around FITC-lectin perfused transpial collaterals was confirmed by Ki67/CD31 colocalization at the muscle/brain interface of the EMS, indicating a marked increase in endothelial cell proliferation in the VEGF myoblast group (Figure 4D).

Functionality of blood vessels is not only determined by vessel density and diameter but also by pericyte coverage, which

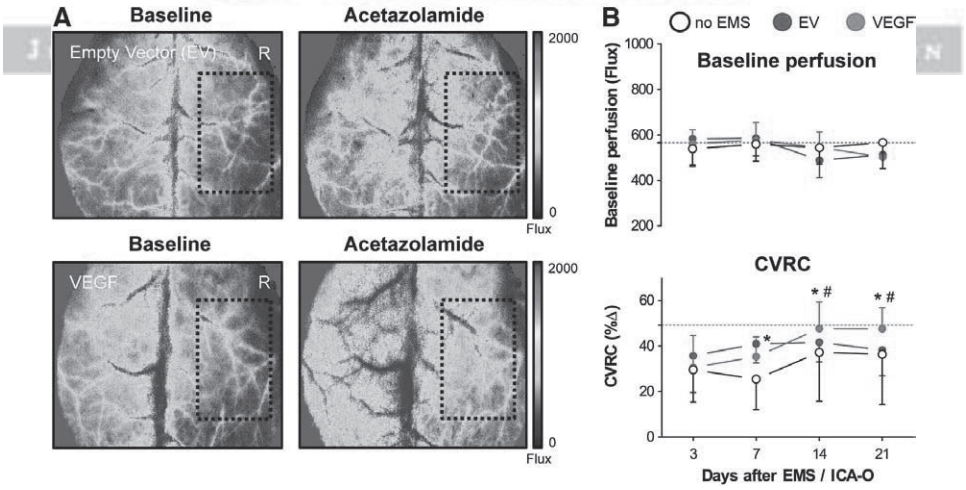

Figure 3. Encephalomyosynangiosis (EMS) and vascular endothelial growth factor-A $(VEGF)_{164}$-expressing myoblasts improve cerebral hemodynamic rescue. **A**, Real-time laser speckle images of cortical perfusion before (left) and after (right) acetazolamide challenge on day 21 after EMS and implantation of empty vector (EV) myoblasts or $VEGF_{164}$-expressing myoblasts (VEGF). Relative perfusion in the arbitrary perfusion unit CBF-Flux (Flux) is mapped as a color-coded image of cortical cerebral blood flow. The higher relative perfusion increase after acetazolamide after EMS and VEGF can be noted on the right. The dashed rectangle shows the area of perfusion assessment. R indicates right. **B**, Line graphs illustrating the mean resting (baseline) perfusion (CBF-Flux; upper panel) and mean cerebrovascular reserve capacity (CVRC; percent change in CBF-Flux; lower panel) in animals with internal carotid artery-occlusion (no EMS) and no EMS and in animals treated with EMS and EV or VEGF myoblasts over the 21-day monitoring period (day 7: **P*<0.05 EV vs no EMS; day 14 and 21: **P*<0.05 VEGF vs no EMS and #*P*<0.05 VEGF vs EV). The dashed horizontal lines show the mean resting perfusion and CVRC of sham animals without ICA-O or EMS.

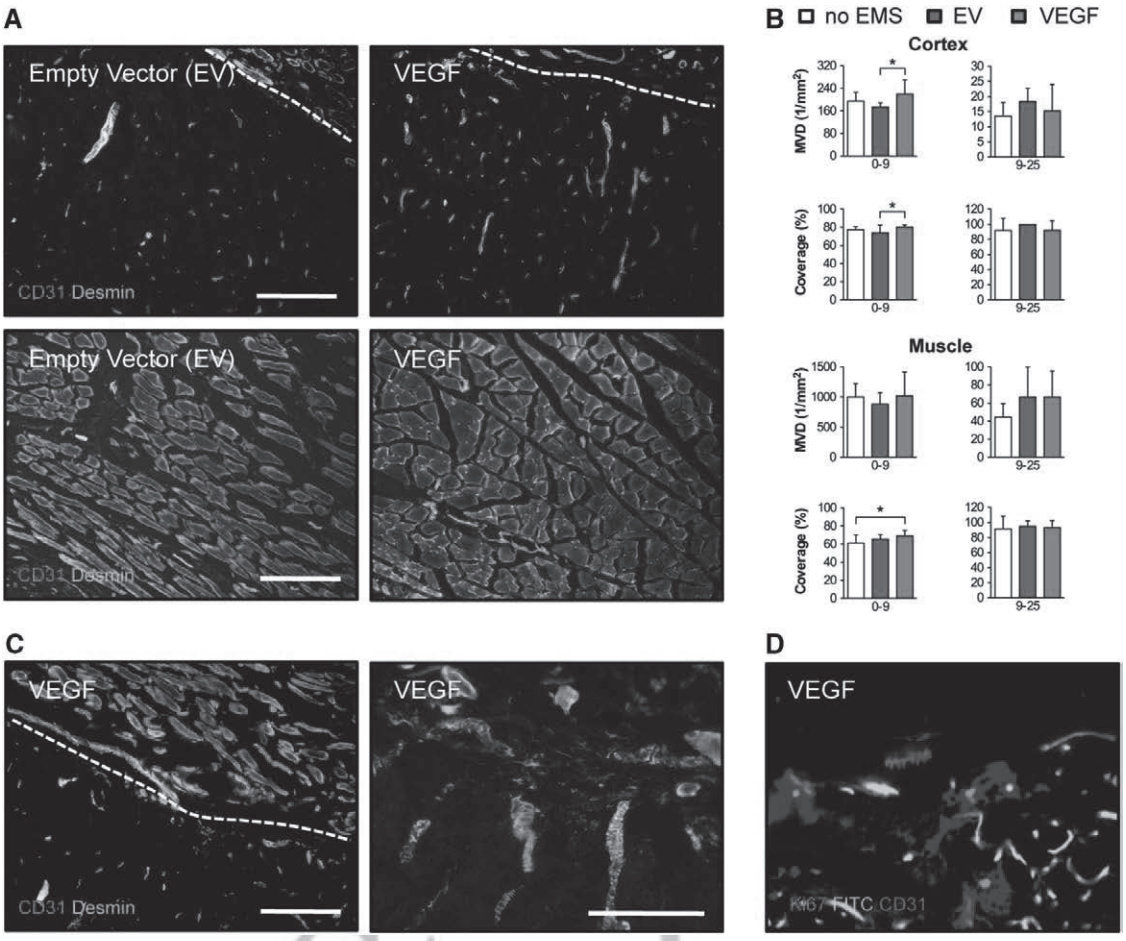

Figure 4. Vascular endothelial growth factor-A $(VEGF)_{164}$-mediated microvascular remodeling after encephalomyosynangiosis (EMS). **A**, Photomicrographs of the cortex (upper panels) and temporal muscle (lower panels) at the muscle/brain interface (dashed line) after internal carotid artery-occlusion (ICA-O) and EMS with empty vector (EV; left) or $VEGF_{164}$-expressing (VEGF; right) myoblasts show a combined CD31 (red) and Desmin (green) staining on day 21 and illustrate the increased microvascular density and pericyte coverage of nutrient vessels in the cortical parenchyma after EMS and VEGF. **B**, Bar graphs of the cortical and muscular vessel density (1/mm^2) and vascular pericyte coverage (%) in vessels <9 mm (left) and >9 mm (right) in diameter in animals with no EMS and in animals treated with EMS and EV or VEGF myoblasts (*P<0.05). **C**, Positive CD31/Desmin colocalization at the muscle/brain interface of the EMS after VEGF-myoblast implantation confirms localized pericyte coverage as a sign of vessel maturity (left). The image on the right shows a 3-dimensional confocal microscope reconstruction of a 60 μm section at high magnification to confirm the intimate cell–cell interaction between green-stained pericytes wrapping around red-stained endothelial tubes**. D**, Angiogenic remodeling of the cortical vasculature at the muscle/brain interface of an EMS after VEGF-myoblast treatment is confirmed by Ki67 (red)/CD31 (blue) colocalization in an animal that underwent fluorescein isothiocyanate (FITC)-lectin perfusion (green) to visualize the patent vasculature at the muscle/brain interface of the EMS. Bar in **A**, **C** (left)=100 μm; bar in **C** (right)=50 μm.

determines the vascular maturity and stability. In addition, pericytes are involved in cerebrovascular flow regulation. Thus, it is noteworthy that cortical angiogenesis was accompanied by a significant 8% increase in the pericyte coverage of these vessels (no EMS 77±3%, EV 74±8%, VEGF 80±2%; *P<0.05 for VEGF versus EV; Figure 4A and 4B). Moreover, animals treated with EMS and VEGF showed a dense mural Desmin coverage of the vasculature bordering the muscle/brain interface, which we confirmed by a confocal microscope-generated reconstruction of the cortical vasculature at the muscle/brain interface adjacent to the myoblast implantation site (Figure 4C).

Cortical T2 Signal Hyperintensity and Regional Perfusion After MCA-O on Day 21

Having shown that local VEGF expression improved transpial collateralization, hemodynamic recovery and cortical angiogenesis, we next sought to determine whether these findings also translated into protection from ischemic stroke after temporary vessel occlusion. Thus, we applied a protocol with 60-minute occlusion of the ipsilateral MCA on day 21 followed by a 23-hour reperfusion period before determining the cortical stroke volume by MRI. All animals subject to MCA-O survived the 23-hour reperfusion period and underwent MRI. In all cases, apparent signs of intracerebral hemorrhage were not observed. The mean volume of the total right-hemispheric cortex did not differ among groups (no EMS 79±10.3 mm^3, EV 76±10.3 mm^3, VEGF 75±9.7 mm^3). In animals that received an EMS with EV myoblast implantation, cortical T2 signal hyperintensity was comparable with animals with no EMS. Animals treated with VEGF, however, showed a significant 25% reduction in cortical T2 signal hyperintensity compared with animals with no EMS (no EMS

74.4±9%, VEGF 56.2±16%; *P<0.001; Figure 5). Moreover, VEGF-treated animals also showed areas of sustained cortical perfusion during the MCA-O period compared with animals that only received EV myoblasts (Figure 6A).

Microvascular Permeability Under Regional VEGF Supplementation

Finally, we assessed the effect of regional VEGF supplementation on microvascular permeability in ischemic and nonischemic cortex at the muscle/brain interface. Most importantly, VEGF supplementation for 21 days in nonischemic animals without MCA-O did not result in perivascular Evans Blue extravasation, supporting our finding of functional but also nonleaky microvessels. In ischemic animals with MCA-O, however, VEGF treatment was associated with notable Evans Blue extravasation around the cortical microvasculature compared with EV-treated mice (Figure 6B).

Discussion

In this proof-of-concept study, we explored the potential of $VEGF_{164}$-expressing myoblasts as a novel proangiogenic gene therapy for treatment of chronic cerebral hypoperfusion in combination with indirect vasoreconstructive surgery. Implantation of $VEGF_{164}$-expressing myoblasts into the temporal muscle of an EMS significantly improved extracranial–intracranial collateralization at the muscle/brain interface, as well as parenchymal angiogenesis in the cortical region below the EMS. Morphological findings were in line with functional results showing better hemodynamic rescue and an attenuated cortical stroke volume in living mice. Together, this demonstrates that the myoblast-mediated delivery of recombinant angiogenic growth factor to the target site of an EMS may be harvested as a novel translational approach to facilitate indirect revascularization in patients at risk of ischemic stroke because of chronic cerebral hypoperfusion.

Myoblast-Mediated Gene Delivery

Myoblast-mediated gene delivery offers a several advantages over other gene delivery approaches: On intramuscular injection, myoblasts fuse stably with pre-existing muscle fibers, providing long-term, possibly lifelong, highly localized gene product expression without the need for immune suppression or the propensity to proliferate in an uncontrolled manner.[18–20,22,25] Furthermore, myoblasts can be characterized in vitro before implantation, allowing, for example, the quantification of gene expression. In view of the potentially high complication rate after direct bypass grafting (ie, in patients with atherosclerotic cerebrovascular disease), myoblast-mediated gene delivery in combination with an EMS represents a novel approach to improve functional and morphological collateralization after indirect revascularization, which remains to lack hemodynamic effectiveness compared with direct bypass procedures.

Spontaneous Extracranial–Intracranial Collateralization After Indirect Revascularization

First, we investigated whether an EMS results in spontaneous transpial collateralization in a mouse model of chronic cerebral hypoperfusion. We sought to assess transpial vessel sprouts at the muscle/brain interface because a functional EMS is characterized by development of patent extracranial–intracranial anastomoses in form of transpial collaterals crossing from the temporal muscle into the brain.[3,4,7] To assess the patency of these collaterals and ensure an exclusive staining of the vasculature connected to the EMS, we established an in vivo FITC-lectin perfusion through the ipsilateral ECA feeding the temporal muscle. As a first interesting finding, patent extracranial–intracranial collaterals were also detected after EMS without VEGF supplementation, which is in line with a previous report[4] and confirms the hypothesis that cortical hypoperfusion alone may act as an inductor of extracranial–intracranial collateralization. The fact that the FITC-lectin positive vasculature in the brain was only noted in circumscribed cortical areas associated with the EMS and not in the brain of animals with no EMS excluded an incidental filling of intracranial vessel segments through more proximal preformed collaterals of the ECA and ICA.

Stimulated Neovascularization Through VEGF

Collateral outgrowth is initially governed by physical forces (ie, fluid shear-stress) that activate the endothelium of preexisting arterioles. One recently suggested pathway lies in the activation of the transcription factor nuclear factor kappa-light-chain-enhancer of activated B cells (NF-κB), which leads to stabilization of hypoxia-inducible factor-1α expression with a

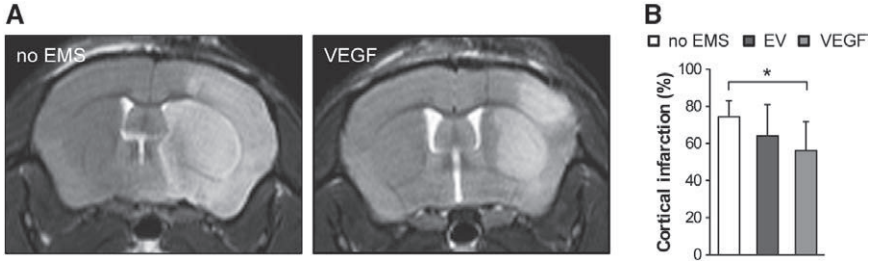

Figure 5. Encephalomyosynangiosis (EMS) and vascular endothelial growth factor-A (VEGF)$_{164}$-expressing myoblasts attenuate cortical stroke after middle cerebral artery filament-occlusion (MCA-O). **A**, In animals with internal carotid artery-occlusion (ICA-O) and no EMS (left), T2-weighted coronal MRI at the bregma level show a widespread T2 signal hyperintensity after ipsilateral MCA-O on day 21. In comparison, animals that received an EMS with VEGF$_{164}$-expressing myoblasts (right) showed marked attenuation of the T2 signal hyperintensity in the cortical area below the muscle/brain interface of the EMS. **B**, Bar graph illustrating the 25% lower cortical infarct volume after treatment with EMS and VEGF compared with animals with no EMS (*P<0.001). EV indicates empty vector.

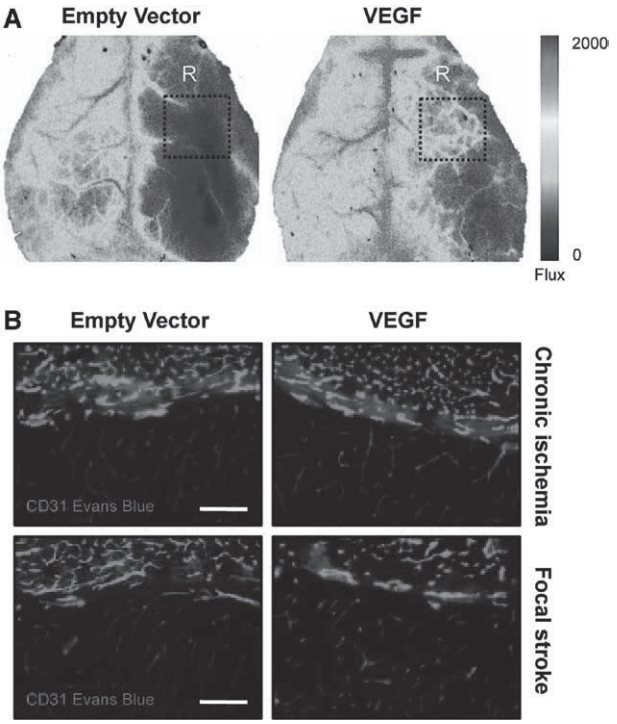

Figure 6. Regional cortical perfusion and vascular permeability after middle cerebral artery filament-occlusion (MCA-O). **A**, Laser Speckle Imaging during 60-minute MCA-O revealed sustained perfusion within the cortical region next to the muscle/brain interface (dashed rectangle) on day 21 after vascular endothelial growth factor-A (VEGF)-myoblast implantation. **B**, Photomicrographs of the muscle/brain interface after in vivo Evans Blue perfusion and CD31 staining demonstrate Evans Blue extravasation around the cortical microvasculature in the ischemic cortex below the encephalomyosynangiosis (EMS) in VEGF-treated mice (lower panels) but not in nonischemic animals without MCA-O (upper panels); bar=100 μm.

subsequent induction of VEGF-A and platelet-derived growth factor-BB, required for capillary arterialization and maturation of the new arterial collateral network.[26] To date, previous studies have only reported on the proangiogenic activity after localized VEGF supplementation through a plasmid VEGF vector in an EMS rat model.[27,28] However, these studies did not address transpial collateralization or cerebral hemodynamics, which serve as the main markers of effective collateral flow augmentation. Therefore, we specifically designed our animal model to simulate cerebral hemodynamic impairment with preservation of blood flow through the ipsilateral ECA and temporal muscle. In our study, treatment with $VEGF_{164}$ significantly improved the degree of collateralization and confocal microscopy revealed a clearly distinct and more tortuous morphology of transpial collaterals and the connected parenchymal vasculature below the EMS as a sign of vascular remodeling and collateral outgrowth at the target site of the EMS. Importantly, leaky vessels or hemangiomas were not detected, which is in line with previous results[18,19] and confirmed the safety and feasibility of our approach. Possibly, the observed VEGF effect on collateralization between 2 separate arteriolar beds could be mediated through mobilization and recruitment of leukocytes to the pericollateral space after interaction between VEGF and VEGF-Receptor-1.[13] Despite VEGF being a key factor, however, functional collateralization relies on a complex interaction of several growth factors (ie, fibroblast growth factor and colony-stimulating factors), cytokines (ie, monocyte chemoattractant protein-1), cell types (ie, monocytes and endothelial progenitor cells), as well as a multitude of proteolytic enzymes (ie, matrix-metalloproteinases).

Although previous reports suggest that implantation of the $VEGF_{164}$-expressing myoblasts mainly results in proangiogenic activity at the target site of implantation,[18,25] at this point, we can only speculate on a more distant effect of our treatment, for example, on the native collateral vasculature. Possibly, the localized VEGF supplementation could stimulate outward remodeling of the preformed leptomeningeal or pial collaterals[12,13] but it remains unclear, whether our localized VEGF delivery might also have influenced the more proximal collateral vasculature, such as the Circle of Willis, particularly in the setting of chronic cerebral hypoperfusion.

Hemodynamic Improvement After Myoblast-Mediated VEGF Therapy

Previous experimental VEGF gene-therapy studies for cerebral ischemia have mainly focused on the treatment of acute focal stroke[29–31] and VEGF-induced angiogenesis has been shown to result in structural neuroprotection and functional recovery.[29,30] However, whether the beneficial effects of VEGF were a consequence of improved hemodynamics because of neovascularization remains unknown since proangiogenic strategies aimed at increasing the global vascular density may worsen rather than improve cerebral hemodynamics.[30] Therefore, we next addressed whether VEGF-mediated neovascularization at the muscle/brain interface also translated into improved cerebral hemodynamics. Typically, nonischemic cerebral hypoperfusion is characterized by a normal or at best mild reduction of baseline (resting) cerebral blood flow.[32,33] In this study, semiquantitative baseline perfusion (CBF-Flux) between animals with no EMS, EV, or VEGF treatment did not differ and remained within the physiological range of sham-treated animals. Most importantly, the improved morphological and functional results that we observed after VEGF delivery were not accompanied by an overshooting increase of regional cortical blood flow compared with the physiological blood flow response of sham-treated animals, which is essential for our translational approach to avoid the dilemma of postoperative hyperperfusion syndrome in hemodynamically compromised patients undergoing surgical revascularization.[34]

In clinical practice, the degree of cerebrovascular reactivity remains one of the most important parameters to assess the patients' risk of hemodynamic ischemic stroke, as well as to determine hemodynamic improvement after a surgical intervention. In adult C57/BL6 mice, we previously demonstrated that assessment of the acetazolamide-specific CVRC is practical for quantification of hemodynamic impairment after unilateral ICA-O.[24] In this study, the acetazolamide-associated blood flow increase within the macro- and microcirculation of the untreated hemisphere most likely represents an intact CVRC due to the dilation of precapillary resistance vessels in response to acetazolamide with a resulting blood flow increase in the draining veins and sagittal sinus. Over

the affected hemisphere, however, CVRC in animals with ICA-O and no EMS was markedly reduced and within the same range as reported previously,[24] tending toward spontaneous hemodynamic recovery but still remaining 27% below the physiological CVRC response of sham-treated animals. Although this CVRC recovery was somewhat better in animals that received an EMS and EV myoblasts, only VEGF supplementation resulted in complete functional recovery. Importantly, the time frame of this better hemodynamic rescue also seemed to be in line with the previously reported time required for stable host integration of the myoblasts, as well as the first reported observation time point of positive vascular remodeling between days 7 and 14 after $VEGF_{164}$-myoblast implantation.[18,19]

Parenchymal Angiogenesis After Myoblast-Mediated VEGF Therapy

Compared with animals that only underwent ICA-O, an EMS with EV myoblast implantation did not result in a higher proangiogenic activity. Implantation of $VEGF_{164}$-expressing myoblasts, however, resulted in cortical angiogenesis of the nutritive vasculature, which supports the idea of a direct and regionally localized VEGF effect at the muscle/brain interface of the EMS and may be beneficial for protection from ischemic stroke. Next to the mere de novo formation of a vascular network, however, a functional vasculature also requires pericyte recruitment for regulation of vessel diameters and blood flow. In this regard, implantation of $VEGF_{164}$-myoblasts resulted in a significant increase in the pericyte coverage of the resident and newly formed microvasculature. This indicates that high-dose local delivery of VEGF did not simply result in immature and nonfunctional blood vessels but may in fact regulate the formation of mature vessels in the brain.[31] However, a previous report demonstrated that VEGF alone may also act as a negative regulator of pericyte function and vessel maturation,[35] which underlines that blood vessel stability depends on the co-ordinated and balanced interaction of multiple signaling pathways in the endothelial and perivascular cells. A key factor that mediates pericyte recruitment and vessel maturation is platelet-derived growth factor-BB.[36] Therefore, future studies could address whether a balanced codelivery of VEGF and platelet-derived growth factor-BB might further improve the positive effects that we observed.

Cortical Stroke and Vascular Permeability After $VEGF_{164}$-Treatment in Combination With EMS

The main goal of an EMS is the reduction of subsequent ischemic events through improvement of collateral flow at the level of the leptomeningeal vasculature because the degree of leptomeningeal collateralization is a major determinant in the severity of stroke.[37] Although the endogenous leptomeningeal collaterals were not directly addressed in this study, the positive VEGF effect on transpial collateralization underlines that VEGF not only increases parenchymal angiogenesis[30] but also act as an important mediator of pial collateral formation and maintenance in the adult mouse brain.[12,13] Interestingly, VEGF seems not to significantly change the time line in which new vessels are formed.[30] Therefore, VEGF probably has negligible effect on brain hemodynamics when applied at the time point of an acute ischemic event but may rather protect the brain against subsequent ischemic episodes. Consequently, we tested whether our morphological findings also translated in regional ischemic protection. The significant 25% reduction of cortical infarct volume next to the circumscribed area of higher cortical perfusion following MCA-O on day 21 after treatment with EMS and $VEGF_{164}$-expressing myoblasts are in line with this hypothesis. Although VEGF increased the microvascular leakiness after MCA-O, no leakiness was noted in animals without focal stroke and the overall effect on blood flow and tissue survival was beneficial, which is in line with previous results.[18,19] Possibly, the increased permeability after MCA-O could be explained by the fact that the supplementation of only VEGF may render the vasculature more fragile and susceptible to hypoxic injury or additional endogenous VEGF, which is known to accumulate in response to focal stroke. Again, this highlights that future studies should address the important question whether a balanced and controlled myoblast-mediated codelivery of multiple exogenous growth factors, such as VEGF and platelet-derived growth factor-BB, may further improve collateralization and hemodynamic rescue, microvascular remodeling and ischemic protection.

Sources of Funding

This work has been supported by the Federal Ministry of Education and Research, Center for Stroke-research Berlin.

Disclosures

None.

References

1. Powers WJ, Clarke WR, Grubb RLJ, Videen TO, Adams HPJ, Derdeyn CP, et al. Extracranial-intracranial bypass surgery for stroke prevention in hemodynamic cerebral ischemia: the Carotid Occlusion Surgery Study randomized trial. *JAMA*. 2011;306:1983–1992.
2. Grubb RLJ, Powers WJ, Clarke WR, Videen TO, Adams HPJ, Derdeyn CP. Surgical results of the Carotid Occlusion Surgery Study. *J Neurosurg*. 2013;118:25–33.
3. Karasawa J, Kikuchi H, Furuse S, Sakaki T, Yoshida Y. A surgical treatment of "moyamoya" disease "encephalo-myo synangiosis". *Neurol Med Chir (Tokyo)*. 1977;17(1 pt 1):29–37.
4. Nakamura M, Imai H, Konno K, Kubota C, Seki K, Puentes S, et al. Experimental investigation of encephalomyosynangiosis using gyrencephalic brain of the miniature pig: histopathological evaluation of dynamic reconstruction of vessels for functional anastomosis. Laboratory investigation. *J Neurosurg Pediatr*. 2009;3:488–495.
5. Czabanka M, Vajkoczy P, Schmiedek P, Horn P. Age-dependent revascularization patterns in the treatment of moyamoya disease in a European patient population. *Neurosurg Focus*. 2009;26:E9.
6. Guzman R, Lee M, Achrol A, Bell-Stephens T, Kelly M, Do HM, et al. Clinical outcome after 450 revascularization procedures for moyamoya disease. Clinical article. *J Neurosurg*. 2009;111:927–935.
7. Scott RM, Smith ER. Moyamoya disease and moyamoya syndrome. *N Engl J Med*. 2009;360:1226–1237.
8. Kim SK, Cho BK, Phi JH, Lee JY, Chae JH, Kim KJ, et al. Pediatric moyamoya disease: an analysis of 410 consecutive cases. *Ann Neurol*. 2010;68:92–101.
9. Komotar RJ, Starke RM, Otten ML, Merkow MB, Garrett MC, Marshall RS, et al. The role of indirect extracranial-intracranial bypass in the treatment of symptomatic intracranial atheroocclusive disease. *J Neurosurg*. 2009;110:896–904.
10. Czabanka M, Peña-Tapia P, Scharf J, Schubert GA, Münch E, Horn P, et al. Characterization of direct and indirect cerebral revascularization for

the treatment of European patients with moyamoya disease. *Cerebrovasc Dis*. 2011;32:361–369.
11. Schaper W. Collateral circulation: past and present. *Basic Res Cardiol*. 2009;104:5–21.
12. Lucitti JL, Mackey JK, Morrison JC, Haigh JJ, Adams RH, Faber JE. Formation of the collateral circulation is regulated by vascular endothelial growth factor-A and a disintegrin and metalloprotease family members 10 and 17. *Circ Res*. 2012;111:1539–1550.
13. Clayton JA, Chalothorn D, Faber JE. Vascular endothelial growth factor-A specifies formation of native collaterals and regulates collateral growth in ischemia. *Circ Res*. 2008;103:1027–1036.
14. Pettersson A, Nagy JA, Brown LF, Sundberg C, Morgan E, Jungles S, et al. Heterogeneity of the angiogenic response induced in different normal adult tissues by vascular permeability factor/vascular endothelial growth factor. *Lab Invest*. 2000;80:99–115.
15. Sundberg C, Nagy JA, Brown LF, Feng D, Eckelhoefer IA, Manseau EJ, et al. Glomeruloid microvascular proliferation follows adenoviral vascular permeability factor/vascular endothelial growth factor-164 gene delivery. *Am J Pathol*. 2001;158:1145–1160.
16. Lee RJ, Springer ML, Blanco-Bose WE, Shaw R, Ursell PC, Blau HM. VEGF gene delivery to myocardium: deleterious effects of unregulated expression. *Circulation*. 2000;102:898–901.
17. Gaál EI, Tammela T, Anisimov A, Marbacher S, Honkanen P, Zarkada G, et al. Comparison of vascular growth factors in the murine brain reveals placenta growth factor as prime candidate for CNS revascularization. *Blood*. 2013;122:658–665.
18. Ozawa CR, Banfi A, Glazer NL, Thurston G, Springer ML, Kraft PE, et al. Microenvironmental VEGF concentration, not total dose, determines a threshold between normal and aberrant angiogenesis. *J Clin Invest*. 2004;113:516–527.
19. von Degenfeld G, Banfi A, Springer ML, Wagner RA, Jacobi J, Ozawa CR, et al. Microenvironmental VEGF distribution is critical for stable and functional vessel growth in ischemia. *FASEB J*. 2006;20:2657–2659.
20. Hecht N, Peña-Tapia P, Vinci M, von Degenfeld G, Woitzik J, Vajkoczy P. Myoblast-mediated gene therapy via encephalomyosynangiosis–a novel strategy for local delivery of gene products to the brain surface. *J Neurosci Methods*. 2011;201:61–66.
21. Banfi A, Springer ML, Blau HM. Myoblast-mediated gene transfer for therapeutic angiogenesis. *Methods Enzymol*. 2002;346:145–157.
22. Rando TA, Blau HM. Primary mouse myoblast purification, characterization, and transplantation for cell-mediated gene therapy. *J Cell Biol*. 1994;125:1275–1287.
23. Springer ML, Blau HM. High-efficiency retroviral infection of primary myoblasts. *Somat Cell Mol Genet*. 1997;23:203–209.
24. Hecht N, He J, Kremenetskaia I, Nieminen M, Vajkoczy P, Woitzik J. Cerebral hemodynamic reserve and vascular remodeling in C57/BL6 mice are influenced by age. *Stroke*. 2012;43:3052–3062.
25. Springer ML, Ozawa CR, Banfi A, Kraft PE, Ip TK, Brazelton TR, et al. Localized arteriole formation directly adjacent to the site of VEGF-induced angiogenesis in muscle. *Mol Ther*. 2003;7:441–449.
26. Tirziu D, Jaba IM, Yu P, Larrivée B, Coon BG, Cristofaro B, et al. Endothelial nuclear factor-κB-dependent regulation of arteriogenesis and branching. *Circulation*. 2012;126:2589–2600.
27. Kusaka N, Sugiu K, Tokunaga K, Katsumata A, Nishida A, Namba K, et al. Enhanced brain angiogenesis in chronic cerebral hypoperfusion after administration of plasmid human vascular endothelial growth factor in combination with indirect vasoreconstructive surgery. *J Neurosurg*. 2005;103:882–890.
28. Katsumata A, Sugiu K, Tokunaga K, Kusaka N, Watanabe K, Nishida A, et al. Optimal dose of plasmid vascular endothelial growth factor for enhancement of angiogenesis in the rat brain ischemia model. *Neurol Med Chir (Tokyo)*. 2010;50:449–455.
29. Zhang ZG, Zhang L, Jiang Q, Zhang R, Davies K, Powers C, et al. VEGF enhances angiogenesis and promotes blood-brain barrier leakage in the ischemic brain. *J Clin Invest*. 2000;106:829–838.
30. Wang Y, Kilic E, Kilic U, Weber B, Bassetti CL, Marti HH, et al. VEGF overexpression induces post-ischaemic neuroprotection, but facilitates haemodynamic steal phenomena. *Brain*. 2005;128(pt 1):52–63.
31. Zechariah A, ElAli A, Doeppner TR, Jin F, Hasan MR, Helfrich I, et al. Vascular endothelial growth factor promotes pericyte coverage of brain capillaries, improves cerebral blood flow during subsequent focal cerebral ischemia, and preserves the metabolic penumbra. *Stroke*. 2013;44:1690–1697.
32. Grubb RL Jr, Derdeyn CP, Fritsch SM, Carpenter DA, Yundt KD, Videen TO, et al. Importance of hemodynamic factors in the prognosis of symptomatic carotid occlusion. *JAMA*. 1998;280:1055–1060.
33. Derdeyn CP, Videen TO, Yundt KD, Fritsch SM, Carpenter DA, Grubb RL, et al. Variability of cerebral blood volume and oxygen extraction: stages of cerebral haemodynamic impairment revisited. *Brain*. 2002;125(pt 3):595–607.
34. Stiver SI, Ogilvy CS. Acute hyperperfusion syndrome complicating EC-IC bypass. *J Neurol Neurosurg Psychiatry*. 2002;73:88–89.
35. Greenberg JI, Shields DJ, Barillas SG, Acevedo LM, Murphy E, Huang J, et al. A role for VEGF as a negative regulator of pericyte function and vessel maturation. *Nature*. 2008;456:809–813.
36. Gaengel K, Genové G, Armulik A, Betsholtz C. Endothelial-mural cell signaling in vascular development and angiogenesis. *Arterioscler Thromb Vasc Biol*. 2009;29:630–638.
37. Brozici M, van der Zwan A, Hillen B. Anatomy and functionality of leptomeningeal anastomoses: a review. *Stroke*. 2003;34:2750–2762.

SUPPLEMENTAL MATERIAL

Myoblast-mediated gene therapy improves functional collateralization in chronic cerebral hypoperfusion

[1]Nils Hecht, MD; [1]Aiki Marushima, MD; [1]Melina Nieminen, MSc; [1]Irina Kremenetskaia, MSc; [2]Georges von Degenfeld, MD; [1]Johannes Woitzik, MD; [1]Peter Vajkoczy, MD

[1]Department of Neurosurgery and Center for Stroke research Berlin (CSB), Charité - Universitätsmedizin Berlin, Berlin, Germany.

[2]Baxter Laboratory for Stem Cell Biology, Stanford University, Stanford, CA, USA. *Current address:* Common Mechanism Research, Bayer Healthcare AG, Wuppertal, Germany and Institute for Operative Medicine, University of Witten/Herdecke, Cologne, Germany.

SUPPLEMENTAL METHODS

Laser Speckle Imaging and cerebrovascular reserve capacity
After positioning of the laser speckle device (MoorFLPI, Moor Instruments, Devon, England), a five-minute baseline measurement of cortical resting perfusion (CBF-Flux measured in arbitrary perfusion units) was recorded within a 6x4 mm region of interest (ROI) over the right middle cerebral artery (MCA) territory, which permitted a combined arterial, venous and parenchymal perfusion and blood flow assessment. A 120-second CBF-Flux plateau was calculated as baseline perfusion. Next, 50mg/kg acetazolamide (Diamox, Goldshield Pharmaceuticals Ltd., Surrey, England) was injected intraperitoneally and the acetazolamide-specific cerebrovascular reserve capacity (CVRC) was calculated as the percent perfusion change between the baseline plateau and a 120-second CBF-Flux plateau after a maximum rise in CBF-Flux.

FITC-lectin perfusion and assessment of transpial collateralization
The external carotid artery was cannulated with a polyethylene catheter (inner diameter 0.28mm; outer diameter 0.61mm) connected to a micro syringe. The ipsilateral common carotid artery was proximally ligated and a solution of 50µl (100µg) FITC-lycopersicon esculentum (tomato) lectin (Vector Laboratories Inc., Burlingame, CA, USA) and 200µl PBS was injected. The mice were decapitated within 2 seconds after the injection and whole-head specimens were snap-frozen at -80°C.

Immunohistochemistry
The cerebral vasculature was detected by a rat anti-mouse CD31 antibody (1:50 dilution in 0.5% Casein; PECAM-1, BD Biosciences, Franklin Lakes, NJ, USA) and a donkey anti-rat IgG conjugated with Cy^{TM}3 (1:200 dilution in 0.5% Casein; Jackson ImmunoResearch Laboratories, West Grove, PA, USA) antibody. Pericytes were detected with a rabbit anti-desmin polyclonal antibody (Dilution 1:100 in 0.5% Casein; Abcam, Cambridge, UK) detected by Cy^{TM}5-conjugated donkey anti-rabbit IgG antibody (Dilution 1:100 in 0.5% Casein; Jackson ImmunoResearch Laboratories, West Grove, Pennsylvania, USA). Proliferating cells were visualized with a monoclonal rabbit anti-mouse Ki67 antibody (Dilution 1:200 in 0.5% Casein; Thermo Scientific, Waltham, MA, USA) detected by Cy^{TM}5-conjugated donkey anti-rabbit IgG (Dilution 1:100 in 0.5% Casein; Jackson ImmunoResearch Laboratories, West Grove, Pennsylvania, USA).

Middle cerebral artery occlusion and cortical stroke volume assessment
For temporary middle cerebral artery occlusion (MCA-O), animals were turned to supine position and the midline neck incision was reopened. The carotid sheath was carefully dissected and the right internal carotid artery (ICA) was incised distal to the site of the previous ICA-occlusion. Next, a 7/0 silicone-rubber coated monofilament (Doccol monofilament, length 20mm, diameter with coating 0.21±0.01mm; Doccol cooperation, Sharon, MA, USA) was smoothly inserted up to the level of the ICA/MCA bifurcation. After 60 minutes, the filament was removed and the ICA was permanently ligated proximal to the incision. Twenty-three hours later, the volume of the ischemic cortical tissue and of the total cortex ipsilateral to the EMS was determined in a 7-tesla animal MRI (Bruker Pharmascan 70/16 with a 20mm radio frequency volume resonator, Bruker Biospin, Ettlingen, Germany) and analyzed with purpose-designed biomedical imaging software (Analyze 10.0, Biomedical Imaging Resource, Mayo Clinic, Rochester, MN, USA) according to signal hyperintensity in serial T2-weighted coronal images.

Evans Blue perfusion

For assessment of vascular permeability in ischemic and non-ischemic cortical microvessels on day 21, an additional series of mice with ICA-O and EMS were randomized to undergo Empty Vector (EV) or VEGF myoblast implantation (n=4 per group) with or without additional MCA-O on day 21 (n=4 per group). For visualization of vascular permeability, a 2% Evans Blue (Sigma #E2129, Sigma-Aldrich, St. Louis, Missouri, USA) stock solution (diluted in 0.9% saline) was prepared. The animals were anesthetized 4 hours prior to their scheduled sacrifice (in the case of MCA-O: 19 hours after the 60-minute filament occlusion) and a solution of 5µl (500µg) per gram bodyweight Evans Blue was injected into the tongue vein with a micro syringe. Four hours after injection (in the case of MCA-O: 23 hours after the 60 minute filament occlusion) the animals were anesthetized again and a lateral skin incision was performed through the abdominal wall to expose the diaphragm and left cardiac ventricle. Next, a 26-gauge needle affixed to a syringe loaded with Phosphate Buffered Saline (PBS) was inserted into the ventricle and the animals were perfused with 20ml PBS after incision of the vena cava to allow venous outflow. Whole-head specimens were snap-frozen at -80°C and coronal cryosections (20µm) of snap-frozen, whole-head specimens were obtained from the anterior, middle and posterior region of the EMS (Bregma -0.5mm, -1.5mm and -3.0mm, respectively). The cerebral vasculature was detected immunohistochemically by a rat anti-mouse CD31 antibody (1:50 dilution in 0.5% Casein; PECAM-1, BD Biosciences, Franklin Lakes, NJ, USA) and a donkey anti-rat IgG conjugated with Cy^{TM}3 (1:200 dilution in 0.5% Casein; Jackson ImmunoResearch Laboratories, West Grove, PA, USA) antibody.

Statistical analysis

Baseline perfusion and CVRC were compared by a two-way ANOVA for repeated measures with subsequent pair-wise comparison of means by Fisher's least projected difference test. The EMS take rate was compared by a non-parametric Kruskal-Wallis test with Dunn's post-test for multiple comparisons. Vessel density, pericyte coverage and cortical stroke volume were compared by a one-way ANOVA with Bonferroni's multiple comparison tests.

SciMedCentral

Journal of Neurological Disorders & Stroke

Research Article

Cerebro-Cardiovascular Risk Factors are Equivalent for Retinal Ischemia and Cerebral Ischemia Patients with Carotid Artery Stenosis

Aiki Marushima[1]*, Yasunobu Nakai[1], Go Ikeda[1], Wataro Tsuruta[1], Hideo Tsurushima[1], Kensuke Suzuki[1,2] and Akira Matsumura[1]

[1]Department of Neurosurgery, Faculty of Medicine, University of Tsukuba, Japan
[2]Department of Neurosurgery, Dokkyo Medical University Koshigaya Hospital, Japan

Special Issue on
Ischemic Stroke: A Cerebrovascular Accident

*Corresponding author
Aiki Marushima, Department of Neurosurgery, Faculty of Medicine, University of Tsukuba, 1-1-1 Tennoudai, Tsukuba, Ibaraki, 305-8575, Japan, Tel: +81-29-853-3220, Fax: +81-29-853-3214; Email: aiki.marushima@md.tsukuba.ac.jp

Submitted: 25 December 2013
Accepted: 27 January 2014
Published: 29 January 2014

Keywords
- Retinal artery occlusion
- Retinal vein occlusion
- Retinal transient ischemic attack
- Carotid artery stenosis
- Cerebro-cardiovascular risk factors

Abstract

Retinal ischemia associated with carotid artery stenosis is an important clinical sign for the prevention of repeated retinal and cerebral ischemic attacks. In this study, we compared the cerebro-cardiovascular risk factors of patients with symptomatic carotid artery stenosis presented with retinal ischemia and with cerebral ischemia. Forty-six patients were diagnosed with symptomatic carotid artery stenosis for five years in our institute. Sixteen patients (34.8%) presented with retinal ischemia, and 30 patients (65.2%) presented with cerebral ischemia. Retinal ischemia was divided into retinal artery occlusion (RAO: n=7, 15.2%), retinal vein occlusion (RVO: n=5, 10.9%) and retinal transient ischemic attack (RTIA: n=4, 8.7%). Stenosis more than 70% in the internal carotid artery was recognized in 62.5% of the patients with retinal ischemia (RAO: n=4, RVO: n=2, AF: n=4) and 73.3% of the patients with cerebral ischemia (p=0.45), and vulnerable plaque evaluated by ultrasonography was recognized in 42.9% of the patients with retinal ischemia (RAO: n=5, RVO: n=2, RTIA: n=2) and 33.3% of patients with cerebral ischemia (p=0.33). No significant difference were seen in the cardiovascular risk factors for hypertension, diabetes mellitus, dyslipidemia, smoking and previous cardiovascular events, and in the cerebrovascular risk factors for stenosis rate, vulnerable plaque, cerebral white matter lesions (WMLs), and impaired cerebrovascular reserve (CVR), between the patients with retinal ischemia and cerebral ischemia. Attentions to the future's stroke should be paid for patients with retinal ischemia of RAO, RVO and RTIA as well as patients with cerebral ischemia, because both patients could possess equivalent cerebro-cardiovascular risk factors.

ABBREVIATIONS

RAO: Retinal Artery Occlusion; **Rvo:** Retinal Vein Occlusion; **Rtia:** Retinal Transient Ischemic Attack; **Ica:** Internal Carotid Artery; **Ht:** Hypertension; **Dm:** Diabetes Mellitus; **Wmls:** White Matter Lesions; **Cvr:** Cerebrovascular Reserve; **Tia:** Transient Ischemic Attack; **Ffa:** Fundus Fluorescein Angiography; **Mr:** Magnetic Resonance; **Flair:** Fluid Attenuated Inversion Recovery; **Dswmh:** Deep Subcortical White Matter Hyperintensity; **Cbf-Spect:** Cerebral Blood Flow – Single Photon Emission Computed Tomography; **Cea:** Carotid Endarterectomy; **Cas:** Carotid Artery Stenting; Or **Pta:** Percutaneous Transluminal Angioplasty

INTRODUCTION

Symptomatic carotid artery stenosis is a major cause of recurrent retinal and cerebral ischemic attack due to artery-to-artery embolism and impaired hemodynamics. Previous population-based studies have revealed that retinal ischemia, including retinal artery occlusion (RAO), retinal vein occlusion (RVO) and retinal transient ischemic attack (RTIA), is associated with carotid artery plaque [1-4]. The evaluation of carotid artery disease in patients with retinal ischemia is important for the prevention of repeated retinal and cerebral ischemic attacks. Retinal ischemia associated with carotid artery stenosis is a sight-threatening retinal vascular condition. It shares common risk factors with cardiovascular disease, including hypertension, diabetes mellitus, dyslipidemia and cigarette smoking, which cause the progression of atherosclerosis in the retinal and carotid arteries [4-7]. Therefore, the associations between retinal artery

ischemia (RAO, RTIA) and carotid artery stenosis can be explained pathophysiologically. However, the association between RVO and carotid artery stenosis has not been established. Recent studies examining the association between the retinal microcirculation and cardiovascular risk factors, including carotid artery disease, revealed that retinal vascular signs, such as retinal arteriovenous nicking and a wider retinal venular caliber, were associated with carotid artery disease [1,6,8-11]. Therefore, retinal ischemic symptoms caused by RVO as well as RAO and RTIA are important clinical signs for the evaluation of occult carotid artery stenosis. In the present study, we analyzed retrospective data in patients with symptomatic carotid artery stenosis who presented with retinal ischemia or cerebral ischemia. We compared the cerebro-cardiovascular risk factors of patients with retinal ischemia to those of patients with cerebral ischemia. The pathophysiology of RVO associated with carotid artery stenosis is discussed based on the anatomical structure of retinal vessels and cerebro-cardiovascular risk factors.

MATERIALS AND METHODS

Patients

Forty-six patients with symptomatic carotid artery stenosis were diagnosed in our institute for five years. Sixteen patients presented with the onset of retinal ischemia, and 30 patients presented with the onset of cerebral ischemia. Retinal ischemia was divided into RAO, RVO and RTIA. Cerebral ischemia was divided into transient ischemic attack (TIA) and cerebral infarction. Hypertension, diabetes mellitus, dyslipidemia, cigarette smoking and previous cerebro-cardiovascular events were examined as cardiovascular risk factors, and stenosis rate, plaque characteristics, cerebral white matter lesions (WMLs) and cerebrovascular reserve (CVR) were examined as cerebrovascular risk factors. Risk factors in retinal ischemia and cerebral ischemia associated with symptomatic carotid artery stenosis were compared. Patients with more than 30% of carotid artery stenosis were included in this study.

Definition of retinal ischemia and cerebral ischemia

Retinal findings were examined by an ophthalmologist using fundus microscopy and fundus fluorescein angiography (FFA). RAO was defined as occlusion of the central or a branch retinal artery that could be characterized by a whitish, edematous retina and a cherry-red spot. FFA demonstrated delayed filling of the affected retinal artery. RVO was defined as occlusion of the central or a branch retinal vein that could be characterized by retinal and papilla edema, scattered retinal hemorrhage and venous dilation. FFA demonstrated retinal capillary obliteration. RTIA was defined as a transient monocular visual loss associated with retinal ischemia that continued for seconds to a few minutes. Fundus microscopy demonstrated no acute abnormal findings, including occlusion of the retinal artery or vein. Cerebral infarction and TIA were diagnosed by neuroradiologists and neurosurgeons based on clinical symptoms and abnormal findings obtained by magnetic resonance (MR) imaging, MR angiography and ultrasonography.

Cardiovascular risk factors

Hypertension, diabetes mellitus, dyslipidemia, cigarette smoking and previous cerebro-cardiovascular events were examined as cardiovascular risk factors. Hypertension was defined as systolic blood pressure > 140 mmHg, diastolic blood pressure > 90 mmHg, or current use of antihypertensive medication. Diabetes mellitus was defined as > 200 mg/dl of serum glucose, > 6.5% of HbA1C, use of insulin or oral hypoglycemic medication or diagnosis by a physician. Dyslipidemia was defined as low-density lipoprotein cholesterol > 139 mg/dL, triglyceride levels > 150 mg/dL, or use of lipid-lowering medication. Smoking was defined as a Brinkman index > 400.

Cerebrovascular risk factors

Evaluation of stenosis rate and plaque characteristics: Carotid arterial ultrasonographies were examined by a medical technologist and cardiologist. The data obtained by MR angiography and digital subtraction angiography (DSA) were analyzed by a neuroradiologist and a neurosurgeon. The stenosis rate of the origin of the internal carotid artery was measured according to the protocol of the North American Symptomatic Carotid Endarterectomy Trial (NASCET) using ultrasonography, MR angiography or DSA [12]. Stenosis in the cavernous and petrous portion of the internal carotid artery was also measured according to the protocol of NASCET using MRA or DSA. The plaque characteristics of the origin of the internal carotid artery were evaluated using ultrasonography (patients with retinal ischemia: n=14, patients with cerebral ischemia: n=27). Vulnerable plaques were defined as echolucent plaques, intraplaque hemorrhages, or mobile plaques with or without ulcer formation [13,14].

Deep white matter lesions (WMLs): MR imaging of the brain was performed in all patients to evaluate the small-vessel changes of the deep white matter, which have been reported to be associated with retinal microvascular abnormalities [15]. T1 weighted imaging (repetition time: 450 ms, echo time 14 ms), T2 weighted imaging (repetition time: 2500 ms, echo time 90 ms) and fluid attenuated inversion recovery (FLAIR) imaging (repetition time; 6000 ms, echo time; 100 ms) was used to estimate periventricular hyperintensity (PVH) and deep subcortical white matter hyperintensity (DSWMH) [16]. These were graded from 0 to 4 using set standards. PVH exhibits white matter hyperintensities on T2-weighted imaging and FLAIR imaging, and isointensities on T1-weighted imaging in contact with the ventricular wall. PVH were classified as follows. Grade 0: absent or only a "rim"; grade 1: limited lesion-like "caps"; grade 2: irregular "halo"; grade 3: irregular margins and extension into the deep white matter; grade 4: extension into the deep white matter and the subcortical portion. DSWMH exhibits hyperintensities in the deep white matter on T2 weighted imaging and FLAIR imaging, and isointensities on T1 weighted imaging that are separated from the ventricular wall. DSWMH were classified as follows. Grade 0: absent; grade 1: ≤3 mm, small foci and regular margins; grade 2: ≥3 mm, large foci; grade 3: diffusely confluent; grade 4: extensive changes in the white matter. Hyperintensities of greater than grade 2 were defined as deep WMLs.

Cerebral blood flow – single photon emission computed tomography (CBF-SPECT): For CBF-SPECT imaging, 500 MBq/kg of Technetium-99m ethyl cysteinate dimer (Tc-99m ECD; FUJIFILM RI pharma, Japan) was injected intravenously into the

patients, and the basal acquisition was started after 7 minutes. Ten minutes before the end of basal SPECT acquisition, 15 mg/kg of acetazolamide was injected intravenously. Seven minutes after the end of the basal study acquisition, 500 MBq/kg of Tc-99m ECD was injected, and the acquisition of the stress study began after 7 minutes. A multi-detector SPECT machine (E. CAM, Siemens Medical, Malvern, PA, USA), and a high-solution collimator (LEHR, Siemens Medical, Malvern, PA, USA) was used for acquisition. Forty five step-and-shoot images per detector were acquired with intervals of 4° for 20 seconds per each step. The Butter-worth pre-correction filter and the Chang method were used for pre-attenuation and post-attenuation corrections. The Ramp filter was used for reconstruction. The image matrixes were 128 × 128, and the pixel sizes 3.3mm. The slice thickness was 6.6 mm. The cut off was 0.61 cycle/cm. SPECT images were generated using the patlack plot method by a nuclear physician. Rest CBF (C rest) and acetazolamide-activated CBF (C acetazolamide) in the region of the middle cerebral artery were calculated using a three-dimensional stereotactic ROI template (3DSRT: FUJIFILM RI pharma, Japan) [17]. CVR was calculated using the following equation:

CVR = C acetazolamide – C rest / C rest × 100.

Impaired CVR was defined as less than 10% CVR in at least one-third of the region of the middle cerebral artery, excluding the cerebral infarct area evaluated by MR imaging.

Treatment

Anti-platelet therapy with or without carotid endarterectomy (CEA), carotid artery stenting (CAS), or percutaneous transluminal angioplasty (PTA) was performed for the prevention of retinal or cerebral ischemic attack recurrence. CEA or CAS was performed in patients with severe stenosis in the origin of the internal carotid artery, considering the stenosis rate, plaque characteristics and operative risk. PTA was performed in patients with stenosis in the petrous or cavernous portion of the internal carotid artery.

Statistics

All values are expressed as the mean ± standard deviation (S. D.). Continuous data between groups were compared using the chi-square test. Differences with a value of $p < 0.05$ were considered as statistically significant.

RESULTS

Incidence of RAO, RTIA, and RVO

Forty-six patients with symptomatic carotid artery stenosis were diagnosed at the onset of retinal ischemia or cerebral ischemia. 16 patients (34.8%) presented with retinal ischemia and 30 patients (65.2%) presented with cerebral ischemia. Patients with retinal ischemia were divided into RAO (n=7, 15.2%), RVO (n=5, 10.9%) or RTIA (n=4, 8.7%). 2 patients with retinal ischemia had a stenosis in the intracranial internal carotid artery (ICA) portion and 14 patients had a stenosis in the cervical ICA portion. The 3 patients with cerebral ischemia had a stenosis in the intracranial ICA portion and 27 patients had a stenosis in the cervical ICA portion. (Table 1)

Cerebro-cardiovascular risk factors

There were no significant differences in cardiovascular risk factors (hypertension, diabetes mellitus, dyslipidemia, cigarette smoking and previous cardiovascular events) between the patients with retinal ischemia and those with cerebral ischemia. Stenosis more than 70% in the internal carotid artery was recognized in 62.5% of the patients with retinal ischemia (RAO: n=4, RVO: n=2, RTIA: n=4) and 73.3% of the patients with cerebral ischemia (p=0.45), and vulnerable plaque evaluated by ultrasonography was recognized in 42.9% of the patients with retinal ischemia (RAO: n=5, RVO: n=2, RTIA: n=2) and 33.3% of patients with cerebral ischemia (p=0.33). Deep WMLs, defined as more than grade 2 PVH or DSWMH, were recognized in 18.8% of patients with retinal ischemia and 16.7% of the patients with cerebral ischemia. Findings of less than 10% CVR, as evaluated by acetazolamide-activated CBF-SPECT, were recognized in 33.3% of the patients with retinal ischemia and 58.6% of the patients with cerebral ischemia. There were no significant differences in these cerebrovascular risk factors between the two groups. (Table 2)

Table 1: Summary of retinal ischemia and cerebral ischemia patients with symptomatic carotid artery stenosis.

	Onset		Total
	Retinal ischemia (RAO, RVO, RTIA)	Cerebral ischemia	
Symptomatic ICA stenosis	16 (34.8 %) (7, 5, 4)	30 (65.2 %)	46 (100 %)
Intracranial ICA stenosis	2 (0, 1, 1)	3	5
Cervical ICA stenosis	14 (7, 4 3)	27	41

RAO: Retinal Artery Occlusion, Rvo: Retinal Vein Occlusion, Rtia: Retinal Transient Ischemic Attack, Ica: Internal Carotid Artery.

Treatment

Eight patients (50%, RAO: n=3, RVO: n=2, AF: n=3) with retinal ischemia and 22 patients (73.3%) with cerebral ischemia were treated by CEA, CAS or PTA (no significant difference).

DISCUSSION

Our retrospective data revealed that 34.8% of patients with symptomatic carotid artery stenosis presented with onset of retinal ischemia. Visual disturbances due to RAO and AF could be caused by an impaired blood supply to the retina associated with an artery-to-artery embolism derived from the vulnerable carotid artery plaque, or by a hemodynamic disorder derived from severe carotid artery stenosis. There are many reports about the association between retinal arterial ischemia and carotid artery disease [1,3,4]. In addition, the association between retinal venous ischemia and carotid artery disease has been controversial. However, Wong, et al. reported that 27.3% of RVO was related to carotid artery plaque and that RVO was significantly related to hypertension, smoking, and arteriovenous nicking in the retina and carotid artery plaque. They explained the atherosclerosis of retinal artery causal might cause stenosis and occlusion in the adjacent retinal veins [4]. In addition, the Rotterdam and MCRS studies revealed that retinal venular widening was strongly associated with ipsilateral severe extracranial carotid artery stenosis [8,11]. These studies indicated that reduced retinal blood flow caused by severe carotid artery stenosis was

Table 2: Comparison of cerebro-cardiovascular risk factors between retinal ischemia and cerebral ischemia patients.

	Retinal ischemia, n=16 (%) (RAO=7, RVO=5, RTIA=4)	Cerebral ischemia, n=30 (%)	P value
Age	65.6±7.3 (67.9±7.3, 66.6±5.4, 60.3±9.9)	66.7±7.3	0.69
Men	13 (81.3) (6, 3, 4)	26 (86.7)	0.39
HT	15 (93.8) (7, 4, 4)	25 (83.3)	0.32
DM	9 (56.3) (5, 3, 1)	11 (36.7)	0.20
Dyslipidemia	9 (56.3) (5, 2, 2)	9 (30)	0.08
Cardiovascular events	6 (37.5) (3, 1, 2)	9 (30)	0.61
Cigarette smoking	6 (37.5) (4, 1, 1)	4 (13.3)	0.06
ICA stenosis > 70%	10 (62.5) (4, 2, 4)	22 (73.3)	0.45
Vulnerable plaque	9/14 (42.9) (5, 2, 2)	9/27 (33.3)	0.33
Cerebral WMLs	3 (18.8) (2, 1, 0)	5 (16.7)	0.86
Impaired CVR	5/15 (33.3) (3, 1, 1)	17/29 (58.6)	0.11

Abbreviations: Rao: Retinal Artery Occlusion, Rvo: Retinal Vein Occlusion, Rtia: Retinal Transient Ischemic Attack, Ht: Hypertension, Dm: Diabetes Mellitus, Wmls: White Matter Lesions, Cvr: Cerebrovascular Reserve.

compensated by the retinal venular widening. Based on those previous reports, it could be considered that impaired retinal circulation hemodynamics induced by carotid artery stenosis caused the occlusion of the retinal vein.

It is known that the retinal artery and vein are affected by cardiovascular risk factors such as hypertension, diabetes mellitus, dyslipidemia, and smoking. These cardiovascular risk factors are also associated with cerebral ischemia. Recent studies have indicated that retinal microvascular abnormalities are significantly related to high-grade cerebral WMLs, and the risk of stroke is higher in patients with both retinopathy and cerebral WMLs [15]. The present study revealed that 18.8% of patients with retinal ischemia presented with cerebral WML. In addition, 33.3% of patients with retinal ischemia had impaired CVR. There was no significant difference in the cerebral small-vessel abnormalities and hemodynamic disorder between the patients with retinal ischemia and cerebral ischemia. Few studies have compared the cerebral hemodynamics between retinal ischemia and cerebral ischemia patients with symptomatic carotid artery stenosis. Our data obtained from patients' profiles, stenosis rates, plaque characteristics, cerebral WMLs and impaired CVRs revealed that patients with retinal ischemia associated with carotid artery stenosis possessed equivalent cerebro-cardiovascular risk factors with the patients with cerebral ischemia associated with carotid artery stenosis.

The number of patients reported herein who presented with retinal ischemia associated with carotid artery ischemia might be relatively high compared to previous studies [18]. Most patients who presented to our hospital were asymptomatic, mildly symptomatic or were admitted for endovascular treatment. Patients with severe symptoms caused by cerebral infarction were rare. However, many patients with retinal ischemia who were admitted to the department of ophthalmology were referred to our department for the management of their carotid artery disease. Collaborations between physicians, ophthalmologists, neurologists and neurosurgeons are important for the diagnosis of retinal ischemia associated with carotid artery stenosis and to prevent future retinal and/or cerebral ischemic attacks.

CONCLUSION

Attentions to the future's stroke should be paid for patients with retinal ischemia of RAO, RVO and RTIA as well as patients with cerebral ischemia, because both patients could possess equivalent cerebro-cardiovascular risk factors.

REFERENCES

1. Doubal FN, Hokke PE, Wardlaw JM. Retinal microvascular abnormalities and stroke: a systematic review. J Neurol Neurosurg Psychiatry. 2009; 80: 158-165.

2. Matsushima C, Wakabayashi Y, Iwamoto T, Yamauchi Y, Usui M, Iwasaki T. Relationship between retinal vein occlusion and carotid artery lesions. Retina. 2007; 27: 1038-1043.

3. [No authors listed] Current management of amaurosis fugax. The Amaurosis Fugax Study Group. Stroke. 1990; 21: 201-208.

4. Wong TY, Larsen EK, Klein R, Mitchell P, Couper DJ, Klein BE, et al. Cardiovascular risk factors for retinal vein occlusion and arteriolar emboli: the Atherosclerosis Risk in Communities & Cardiovascular Health studies. Ophthalmology. 2005; 112: 540-547.

5. Cheung N, Klein R, Wang JJ, Cotch MF, Islam AF, Klein BE, et al. Traditional and novel cardiovascular risk factors for retinal vein occlusion: the multiethnic study of atherosclerosis. Invest Ophthalmol Vis Sci. 2008; 49: 4297-4302.

6. Klein R, Klein BE, Moss SE, Meuer SM. The epidemiology of retinal vein occlusion: the Beaver Dam Eye Study. Trans Am Ophthalmol Soc. 2000; 98: 133-141.

7. Wang JJ, Cugati S, Knudtson MD, Rochtchina E, Klein R, Klein BE, et al. Retinal arteriolar emboli and long-term mortality: pooled data analysis from two older populations. Stroke. 2006; 37: 1833-1836.

8. De Silva DA, Liew G, Wong MC, Chang HM, Chen C, Wang JJ, et al. Retinal vascular caliber and extracranial carotid disease in patients with acute ischemic stroke: the Multi-Centre Retinal Stroke (MCRS) study. Stroke. 2009; 40: 3695-3699.

9. Ikram MK, de Jong FJ, Vingerling JR, Witteman JC, Hofman A, Breteler MM, et al. Are retinal arteriolar or venular diameters associated with markers for cardiovascular disorders? The Rotterdam Study. Invest Ophthalmol Vis Sci. 2004; 45: 2129-2134.

10. Kawasaki R, Wang JJ, Rochtchina E, Taylor B, Wong TY, Tominaga M, et al. Cardiovascular risk factors and retinal microvascular signs in an adult Japanese population: the Funagata Study. Ophthalmology. 2006; 113: 1378-1384.

11. van Leeuwen R, Ikram MK, Vingerling JR, Witteman JC, Hofman A, de Jong PT. Blood pressure, atherosclerosis, and the incidence of age-related maculopathy: the Rotterdam Study. Invest Ophthalmol Vis Sci. 2003; 44: 3771-3777.

12. Wardlaw JM, Lewis S. Carotid stenosis measurement on colour Doppler ultrasound: agreement of ECST, NASCET and CCA methods applied to ultrasound with intra-arterial angiographic stenosis measurement. Eur J Radiol. 2005; 56: 205-211.

13. Nighoghossian N, Derex L, Douek P. The vulnerable carotid artery plaque: current imaging methods and new perspectives. Stroke. 2005; 36: 2764-2772.

14. U-King-Im JM, Young V, Gillard JH. Carotid-artery imaging in the diagnosis and management of patients at risk of stroke. Lancet Neurol. 2009; 8: 569-580.

15. Wong TY, Klein R, Sharrett AR, Couper DJ, Klein BE, Liao DP, et al. Cerebral white matter lesions, retinopathy, and incident clinical stroke. JAMA. 2002; 288: 67-74.

16. Shinohara Y, Tohgi H, Hirai S, Terashi A, Fukuuchi Y, Yamaguchi T, et al. Effect of the Ca antagonist nilvadipine on stroke occurrence or recurrence and extension of asymptomatic cerebral infarction in hypertensive patients with or without history of stroke (PICA Study). 1. Design and results at enrollment. Cerebrovasc Dis. 2007; 24: 202-209.

17. Takeuchi R, Sengoku T, Matsumura K. Usefulness of fully automated constant ROI analysis software for the brain: 3DSRT and FineSRT. Radiat Med. 2006; 24: 538-544.

18. SPACE Collaborative Group, Ringleb PA, Allenberg J, Brückmann H, Eckstein HH, Fraedrich G, et al. 30 day results from the SPACE trial of stent-protected angioplasty versus carotid endarterectomy in symptomatic patients: a randomised non-inferiority trial. Lancet. 2006; 368: 1239-1247.

Cite this article

Marushima A, Nakai Y, Ikeda G, Tsuruta W, Tsurushima H, et al. (2014) Cerebro-Cardiovascular Risk Factors are Equivalent for Retinal Ischemia and Cerebral Ischemia Patients with Carotid Artery Stenosis. J Neurol Disord Stroke 2(2): 1045.

Anatomical Risk Factors for Ischemic Lesions Associated with Carotid Artery Stenting

GO IKEDA[1] , WATARO TSURUTA[1], YASUNOBU NAKAI[1], MASANARI SHIIGAI[2], AIKI MARUSHIMA[1], TOMOHIKO MASUMOTO[2], HIDEO TSURUSHIMA[1], AKIRA MATSUMURA[1]

[1] Department of Neurosurgery, [2] Department of Radiology, Faculty of Medicine, University of Tsukuba; Ibaraki, Japan

Key words: anatomical risk, carotid artery stenting, tortuosity, ischemic lesion, diffusion-weighted imaging

Summary

The purpose of this study was to investigate the anatomical risk factors for ischemic lesions detected by diffusion-weighted imaging (DWI) associated with carotid artery stenting (CAS).

DWI was performed within four days after CAS in 50 stenotic lesions between January 2008 and September 2013. We retrospectively analyzed the correlation between the anatomical factors and ischemic lesions associated with CAS.

Post-procedural DWI revealed new ischemic lesions after 24 (48%) of the 50 CAS procedures. All three patients with common carotid artery tortuosity, defined as the presence of severe angulation (less than 90 degrees) in the common carotid artery, developed new ischemic lesions. However, there were no significant differences between the patients with and without tortuosity, likely due to the small number of cases. Meanwhile, seven of eight patients with internal carotid artery tortuosity, defined as the presence of severe angulation (less than 90 degrees) in the cervical segment of the internal carotid artery, developed new ischemic lesions. A multivariate analysis showed internal carotid artery tortuosity (odds ratio: 11.84, 95% confidence interval: 1.193-117.4, P= 0.035) to be an independent risk factor for the development of ischemic lesions associated with CAS.

Anatomical factors, particularly severe angulation of the internal carotid artery, have an impact on the risk of CAS. The indications for CAS should be carefully evaluated in patients with these factors.

Introduction

Recently, carotid artery stenting (CAS) has been presented as an alternative to carotid endarterectomy (CEA) for the treatment of carotid artery stenosis [1,2]. The data published so far suggest that CAS has the same efficacy as CEA in terms of long-term stroke prevention, but it is associated with a higher periprocedural stroke rate [2,3].

Likewise, new ischemic lesions detected by diffusion-weighted imaging (DWI) occur more frequently after CAS than after CEA [4-7]. Although many new lesions seen on DWI after CAS are asymptomatic, the incidence of new DWI lesions is associated with the clinical outcome [8]. Moreover, the development of ischemic lesions after CAS may be associated with cognitive impairment, as was recently described [9].

To improve the outcome after CAS, the identification of patients likely to be at high-risk for new lesions after CAS is necessary. There is growing evidence that CAS is associated with a higher periprocedural complication rate in octogenarians than in other age groups [2,10,11].

Other authors advocate the importance of anatomical characteristics as predictors of the complications associated with CAS [11-14]. However, it remains unclear and controversial which factor is the most important.

The purpose of this study was to investigate the anatomical risk factors for ischemic lesions detected by DWI associated with CAS.

Materials and Methods

Study design and patient population

Between January 2008 and September 2013, 51 consecutive patients underwent 58 CAS procedures at our institution. Five CAS procedures performed via a trans-brachial or transradial approach, two where the patient could not be examined by post-procedural magnetic resonance imaging (MRI) within four days after the procedure due to systemic complications and one who underwent subclavian artery stenting during the same procedure were excluded. Therefore, 50 CAS procedures (45 patients) were retrospectively enrolled in this study. CAS was indicated by the presence of angiographically documented carotid artery stenosis of more than 50% in symptomatic patients or more than 60% in asymptomatic patients, according to the criteria established by the Stenting and Angioplasty with Protection in Patients at High Risk for Endarterectomy (SAPPHIRE) trial [1] and the Asymptomatic Carotid Atherosclerosis Study (ACAS) [15]. Carotid stenosis was considered to be symptomatic if the patients had experienced an ipsilateral ocular or cerebral (transient or permanent) ischemic event within the past six months. All patients underwent MRI before and after the procedure to detect all ischemic lesions, including new lesions after the procedure. The clinical, anatomical and procedural data were collected for each patient by reviewing their medical records, imaging data and surgical records. This study was approved by the Institutional Review Committee at our institution and all subjects gave informed consent.

Definitions

Ischemic lesions associated with CAS were defined as at least one high intensity signal on the DWI performed after CAS that was not present on the preprocedural MRI. No distinction was made between symptomatic and asymptomatic lesions, and all lesions in the ipsilateral territory and the other vascular territories were included. Contralateral lesions were defined as stenosis of more than 70% and occlusion of the common carotid artery (CCA) or internal carotid artery (ICA).

Imaging procedure

The postprocedural MRI was performed within four days after CAS (average, 1.29 days). No neurological events were found between the preprocedural MRI and the CAS procedure. We used four MRI scanners as follows: the Gyroscan NT 1.5T (Philips Medical Systems, Best, The Netherlands), Achiva 1.5T (Philips Medical Systems), Achiva 3.0T (Philips Medical Systems) and Ingenia 3.0T (Philips Medical Systems). New ischemic lesions were identified by a single neuroradiologist at our institution who did not participate in the procedure using the DWI with echo planar methods, and an MRI report was made at that time. We collected the data on ischemic lesions on the post-procedural MRI from these reports. The protocols used for DWI are summarized in Table 1.

Carotid artery stenting procedure

More than three days before the procedure, all patients received antiplatelet therapy with

Table 1 **Magnetic resonance imaging scanners and protocols used for diffusion-weighted imaging with the echo planar method.**

	TR (ms)	TE (ms)	ST (mm)	Matrix	b value (s/mm²)
Gyroscan NT 1.5T (Philips Medical Systems, Best, The Netherlands)	3768.7	88.0	5.0	256×256	1000
Achieva 1.5T (Philips Medical Systems)	3500	67.1	5.0	256×256	1000
Achieva 3.0T (Philips Medical Systems)	5000	57.5	5.0	288×288	1000
Ingenia 3.0T (Philips Medical Systems)	6250	83.2	5.0	256×256	1000

TR: repetition time, TE: echo time, ST: slice thickness.

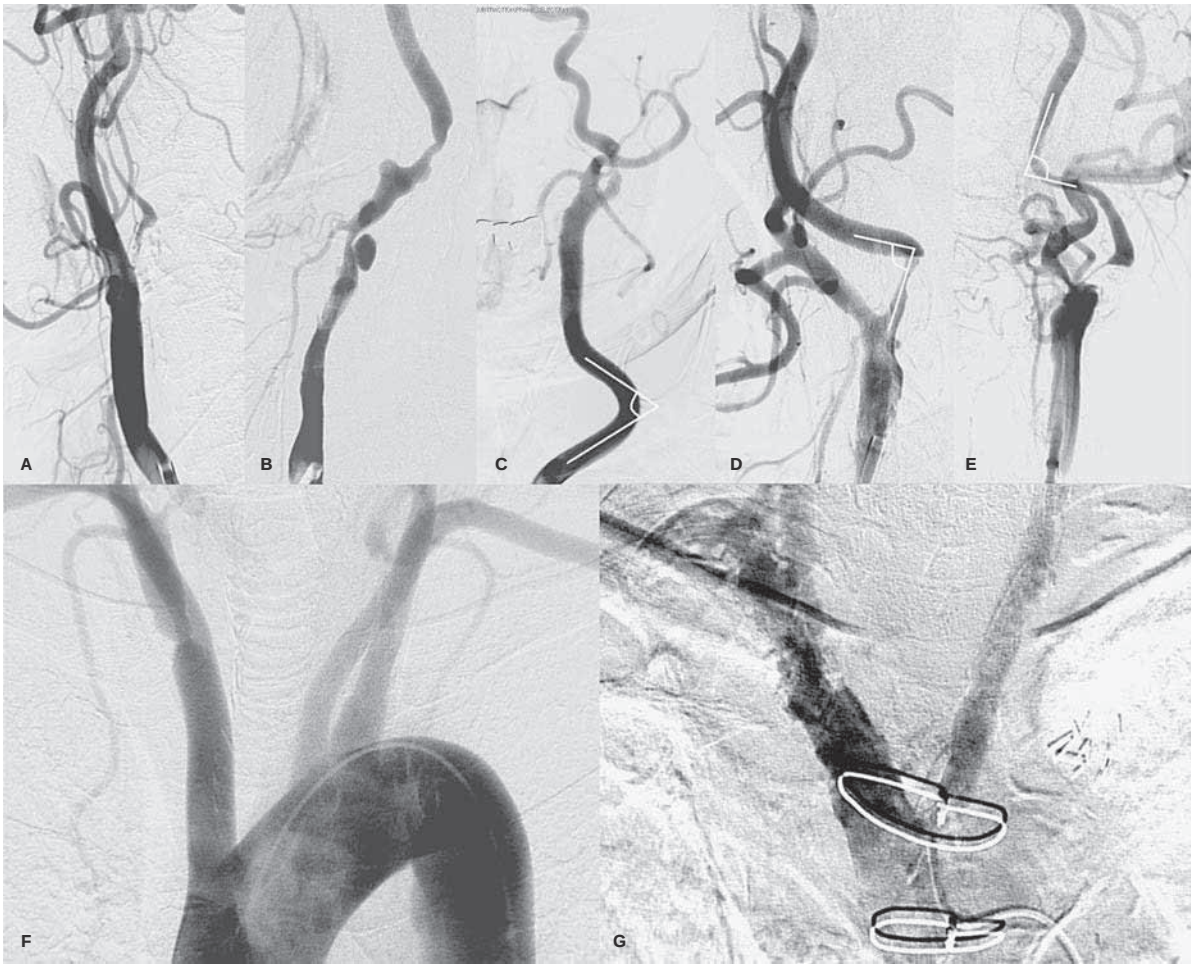

Figure 1 Angiographic images of the anatomical factors. A) Pseudo-occlusion. B) ECA occlusion and CCA stenosis. C-E) Tortuosity of the CCA and ICA (the severe angle is shown between reference lines). F) Type III arch. G) Bovine arch.

two of the following four drugs: aspirin (100 mg/day), ticlopidine (200-300 mg/day), clopidogrel (75 mg/day), or cilostazol (200 mg/day). All but two procedures were performed under local anesthesia, whereas two were performed under general anesthesia to eliminate body motion. Stenting was carried out through the femoral route with the use of stents and embolic protection devices (EPDs). After placement of an 8-9F sheath, each patient received intravenous heparin to achieve an activated coagulation time of 250-300 seconds. An 8-9F guide catheter was then advanced to the CCA. An EPD was used in all patients. We used an ANGIOGUARD XP (Cordis Endovascular, Miami Lakes, FL, USA) in 13 procedures (26.0%), PercuSurge GuardWire (Medtronic, Santa Rossa, CA, USA) in 27 (54.0%), FilterWire EZ (Boston Scientific, Natick, MA, USA) in ten (20.0%) and an Optimo (Tokai Medical Products, Aichi, Japan) in 13 (26.0%) cases with distal protection (PercuSurge GuardWire in 12, ANGIOGUARD XP in one). All lesions were treated with self-expandable stents. In one procedure two stents had to be deployed to cover the lesion. A Precise stent (Cordis Endovascular, Miami Lakes, FL, USA) was used in 19 procedures (38.0%) and a Carotid Wallstent (Boston Scientific, Natick, MA, USA) was used in 31 (62.0%). Angioplasty balloons were used for predilation during 45 (90%) CAS procedures (3.0-4.5 mm in diameter) and post-dilatation in 43 (86%) CAS procedures (3.5-7.0 mm in diameter). When balloon protection was used (distal, or proximal and distal), an adequate amount of blood was aspirated through the catheter to collect debris before the balloon was deflated. Filter occlusion that required blood aspiration occurred in one procedure using the filter protection.

Evaluation of the angiogram

All angiographic images were retrospectively evaluated for the following anatomical properties by a single investigator (GI): the laterality of the lesion; pseudo-occlusion; external carotid artery (ECA) occlusion; CCA stenosis, defined as stenosis of more than 50% of the CCA, including the lesion itself located in the CCA; CCA tortuosity, defined as the presence of severe angulation (less than 90 degrees) in the CCA on the anteroposterior view; ICA tortuosity, defined as the presence of severe angulation (less than 90 degrees) in cervical segment of the ICA (bifurcation, first bend or second bend) on either the anteroposterior or lateral view; unfavorable arch anatomy, defined as a type III arch for right lesions or a bovine arch for left lesions (Figure 1). If an angiographic image of the aortic arch was not available, the preprocedural magnetic resonance angiography findings were investigated.

Statistical analysis

Continuous variables are expressed as mean values ± standard deviation, and comparisons of these variables between groups were performed using the Mann-Whitney U test. Categorical variables are expressed as counts and percentage frequencies, and were compared using the chi-square test and Fisher's exact test. A multivariate logistic regression test was used to identify the independent risk factors for ischemic lesions associated with CAS. The Kruskal-Wallis one-way analysis was used to compare multiple groups. Statistical significance was defined as a P value < 0.05, and all of the analyses were carried out using the IBM SPSS statistics software program, version 22 (IBM, Armonk, New York, USA).

Results

The mean age of the patients who underwent the 50 CAS procedures was 71.6 ± 6.43 years, and the mean degree of stenosis was 80.0 ± 10.4 %. Twenty-two (44.0%) cases showed symptomatic lesions and ten showed contralateral lesions, including seven cases with occlusion of the contralateral ICA. Ten cases had a history of neck radiation, four had a history of CEA and one had a history of CAS. Concomitant disease states were recorded in many cases, including 47 (94.0%) cases with hypertension, 19 (38.0%) with hyperlipidemia, 21 (42.0%) with diabetes mellitus and 14 (28.0%) with coronary artery disease. Twenty-eight (56.0%) cases showed vulnerable plaques and seven (14.0%) cases showed heavily calcified plaques, both of which were diagnosed by MRI, computed tomography and ultrasonography. The anatomical factors investigated by preprocedural angiography were as follows: the left side was affected in 30 (60.0%) cases; pseudo-occlusion in seven (14.0%), ECA occlusion in three (6.0%), CCA stenosis in seven (14.0%), CCA tortuosity in three (6.0%), ICA tortuosity in eight (16.0%) and there was unfavorable arch anatomy in six (12.0%) cases.

CAS was performed successfully for all lesions, although hemodynamic instability due to the carotid sinus reflex occurred in 21 (42.0%) cases. DWI after CAS revealed new ischemic lesions after 24 (48%) of the 50 CAS procedures, including two (4%) symptomatic lesions that led to permanent neurological deficits. There was no mortality associated with the procedure. The correlations between the clinical characteristics of patients and ischemic lesions associated with CAS are shown in Table 2. Only smoking status was significantly different between the two groups (P= 0.049). Age, sex, hypertension, hyperlipidemia, diabetes mellitus, coronary disease, prior neck radiation, prior CEA and prior CAS were not significantly different between the groups. The correlations between the anatomical or non-anatomical factors and ischemic lesions associated with CAS are shown in Table 3. Only ICA tortuosity was significantly (P= 0.021) different among the anatomical factors, whereas symptomatic lesions were significantly (P= 0.050) different among the non-anatomical factors. All cases with CCA tortuosity revealed new ischemic lesions, but there were no significant differences between the cases with and without tortuosity because of the small number of cases. Additionally, a multivariate analysis showed that only ICA tortuosity (odds ratio 11.84, 95% confidence interval 1.193-117.4) was an independent risk factor for ischemic lesions associated with CAS (Table 4). We experienced eight patients with ICA tortuosity, among whom postprocedural MRI showed new ischemic lesions in seven patients. Severe angulation of the ICA was detected at both first and second bends in four cases, the first bend only in three cases and the second bend only in one case;

Table 2 **Correlation between clinical characteristics and ischemic lesions associated with carotid artery stenting.**

	All cases (n = 50)	Ischemic lesions		P value
		Yes (n = 24)	No (n = 26)	
Age, years	71.6 ± 6.43	73.3 ± 6.27	70.0 ± 6.30	0.078
Female	8 (16.0)	4 (16.7)	4 (15.4)	1.000
Hypertension	47 (94.0)	23 (95.8)	24 (92.3)	1.000
Hyperlipidemia	19 (38.0)	8 (33.3)	11 (42.3)	0.514
Diabetes mellitus	21 (42.0)	9 (37.5)	12 (46.2)	0.536
Coronary artery disease	14 (28.0)	8 (33.3)	6 (23.1)	0.420
Smoking	30 (60.0)	11 (45.8)	19 (73.1)	0.049
Prior neck radiation	10 (20.0)	5 (20.8)	5 (19.2)	1.000
Prior CEA	4 (8.0)	0 (0)	4 (15.4)	0.111
Prior CAS	1 (2.0)	0 (0)	1 (3.8)	1.000

Data are presented as the n (%) or means ± SD. CEA: carotid endarterectomy, CAS: carotid artery stenting.

Table 3 **Correlation between anatomical or non-anatomical factors and ischemic lesions associated with carotid artery stenting.**

	All cases (n = 50)	Ischemic lesions		P value
		Yes (n = 24)	No (n = 26)	
Non-anatomical factors:				
Age ≥ 80 years	7 (14.0)	5 (20.8)	2 (7.7)	0.239
Degree of stenosis, %	80.0 ± 10.4	81.2 ± 11.1	78.8 ± 9.86	0.527
Symptomatic lesion	22 (44.0)	14 (58.3)	8 (30.8)	0.050*
Contralateral lesion	10 (20.0)	6 (25.0)	4 (15.4)	0.490
Vulnerable plaque	28 (56.0)	13 (54.2)	15 (57.7)	0.802
Heavily calcified plaque	7 (14.0)	4 (16.7)	3 (11.5)	0.697
Filter type EPD	23 (46.0)	11 (45.8)	12 (46.2)	0.982
Proximal protection	13 (26.0)	4 (16.7)	9 (34.6)	0.148
Precise stent	19 (38.0)	12 (50.0)	7 (26.9)	0.093
Carotid sinus reflex	21 (42.0)	13 (54.2)	8 (30.8)	0.094
Filter occlusion	1 (2.0)	1 (4.2)	0 (0)	0.480
Anatomical factors:				
Left side	30 (60.0)	16 (66.7)	14 (53.8)	0.355
Pseudo occlusion	7 (14.0)	5 (20.8)	2 (7.7)	0.239
ECA occlusion	3 (6.0)	2 (8.3)	1 (3.8)	0.602
CCA stenosis	7 (14.0)	3 (12.5)	4 (15.4)	1.000
CCA tortuosity	3 (6.0)	3 (12.5)	0 (0)	0.103
ICA tortuosity	8 (16.0)	7 (29.2)	1 (3.8)	0.021
Unfavorable arch anatomy	6 (12.0)	3 (12.5)	3 (11.5)	1.000

*Data are presented as the n (%) or means ± SD. EPD: embolic protection device, ECA: external carotid artery, CCA: common carotid artery, ICA: internal carotid artery. * The P value was actually < 0.05.*

Table 4 **Results of the multivariate logistic regression analysis of risk factors for ischemic lesions associated with carotid artery stenting.**

	Odds ratio	95% CI	P value
Smoking	0.505	0.134 - 1.905	0.313
Symptomatic lesion	3.483	0.930 - 13.05	0.064
ICA tortuosity	11.84	1.193 - 117.4	0.035

CI: confidence interval.

there were no cases of severe angulation of the carotid bifurcation. A summary of these cases is shown in Table 5.

The frequency of the detection of new ischemic lesions was not significantly different among the various scanners used (P=0.202) (Gyroscan NT 1.5T, 13 of 20 (65.0%); Achieva 1.5T, four of 14 (28.6%); Achieva 3.0T, six of 13 (46.2%); Ingenia 3.0T, one of three (33.3%)).

Discussion

The present study demonstrated that ICA tortuosity is an independent risk factor for ischemic lesions associated with CAS. Vessel tortuosity increases the technical difficulty of performing CAS. This increase in unfavorable anatomy may be associated with ischemic complications. From this point of view, octogenarians are thought to be at higher risk for complications during CAS than other age groups because elderly patients theoretically have a higher incidence of unfavorable anatomy [16,17]. However, a recent study showed that the incidence of periprocedural complications was increased in patients with unfavorable aortic arch anatomy but not in octogenarians [13]. This suggests that unfavorable anatomical factors may be more important than the age of patients.

Several authors have referred to the risk factors for the ischemic lesions detected by DWI after CAS. A history of coronary artery disease [7], hemodynamic instability due to the carotid

Table 5 **Summary of the patients with ICA tortuosity.**

Case	Age	Sex	Location of lesion	Location of ICA tortuosity	EPD	Stent	Stent-induced kinking	Number of ischemic lesions
1	68	M	ICA proximal	2nd bend	PercuSurge GuardWire	Precise	+	4
2	68	M	ICA proximal	1st + 2nd bend	Angioguard XP	Precise	–	1
3	76	M	ICA proximal	1st bend	Angioguard XP	Precise	–	2
4	72	M	ICA proximal	1st + 2nd bend	Angioguard XP	Precise	+	1
5	73	M	ICA proximal	1st bend	Filterwire EZ	Carotid Wall	–	7
6	71	F	CCA	1st + 2nd bend	PercuSurge GuardWire	Carotid Wall	–	1
7	81	F	ICA proximal	1st bend	PercuSurge GuardWire	Carotid Wall	+	3
8	79	M	ICA proximal	1st + 2nd bend	Filterwire EZ	Carotid Wall	+	0

ICA proximal means the area between the carotid bifurcation and first bend of ICA.

sinus reflex [18,19], performing an arch aortogram prior to CAS [6], advanced age [20], the presence of ulcerated stenosis [20] and a lesion length more than 1 cm [20] were all described as risk factors. However, it remains unclear which factor is the most important, and few clinical studies have addressed the anatomical risk factors for ischemic lesions associated with CAS [21].

A scoring system of anatomical suitability for CAS based on an objective expert consensus was published in 2009 [22]. Twelve anatomical factors were ranked in ascending order from the most straightforward (low bifurcation) to the most difficult (tortuous CCA) with a mean difficulty score chosen by experts. The rankings reported in that article were as follows: low bifurcation, occluded or severely diseased ECA, bovine arch, 99% stenosis (flow beyond), diseased CCA (> 50%), angulated distal ICA, severe arch atheroma, a type III arch, circumferential calcification of the ICA, an angulated ICA origin, severe arch origin disease and a tortuous CCA. After low bifurcation and a tortuous CCA were excluded, the scoring system was developed to categorize the expected difficulty of CAS and to aid in case selection. In a retrospective clinical study using this scoring system reported by Werner et al. [23], the classification correlated well with the periprocedural neurological outcome. We investigated nine of the above factors, although we classified calcification as a non-anatomical factor. We also distinguished plaque morphology from the anatomical factors.

Various anatomical factors associated with periprocedural complications during CAS were described in previous reports. For example, Naggara et al. [12] assessed the relationships between anatomical and technical factors and the 30-day risk of stroke or death after CAS in the Endarterectomy versus Stenting in Patients with Symptomatic Severe Carotid Stenosis (EVA-3S) trial, and performed a systematic review of the literature. The risk of stroke and death was higher in patients with increased ICA-CCA angulation, left-sided CAS and when the target ICA stenosis was >10 mm, whereas the risk was not related to the stent or EPD type. Werner et al. [23] reported that the presence of a bovine arch, tortuous CCA and angulated distal ICA were associated with higher risks of stroke and transit ischemic attack. Faggioli et al. [14] evaluated the impact of arch angulation and proximal and distal tortuosity in a series of CAS procedures. They used a tortuosity index defined as the sum of all angles diverging from the ideal straight axis, and showed that the proximal tortuosity index was an independent predictor of both neurological complications and technical failure. Conversely, Ito et al. [24] demonstrated that the angles at the carotid bifurcation and the first bend of the ICA were significantly associated with the incidence of microembolization. Thus, vascular tortuosity is an important factor for predicting the development of periprocedural ischemic complications after CAS, as we described above.

There may be some reasons why ICA tortuosity is associated with ischemic lesions. When the lesion was located proximally at the ICA and the site of tortuosity was located at the first bend of the ICA, stent deployment directly influenced the severe angulation of the ICA. The extension of the ICA angulation may increase the amount of debris associated with CAS, as described by Sorimachi et al. [26]. To reduce the changes in ICA angulation, they recommended the use of shorter devices (stents or angioplasty balloons) when the ICA angulation is pronounced.

On the other hand, when the site of vessel tortuosity was far from the stenotic lesion, the stent did not cover the tortuous lesion. However, the EPDs were always influenced by the change in angulation of the tortuous vessels during the procedure, despite the distance between the stenotic and tortuous lesions. The instability of the EPDs during the procedure caused by the straightened nature of the ICA may result in inadequate protection, consequently leading to embolic complications. Therefore, we believe that the presence of tortuosity both near and far from the stenotic lesion is a risk factor for ischemic events.

With respect to reducing the incidence of ischemic complications associated with EPDs, the use of proximal protection without insertion of an EPD into the ICA is theoretically useful for treating patients with ICA tortuosity. Although the use of proximal protection was not found to be a significant factor affecting the incidence of ischemic lesions in the present study, Asakura et al. [25] reported the usefulness of protection by reverse carotid arterial flow during CAS. In this article, both the CCA and ECA were continuously occluded using balloons before the insertion of a guidewire through the stenotic lesion until the end of the procedure. The rate of appearance of new ischemic lesions detected by DWI was not sig-

nificantly different between conventional angiography and the CAS procedure using this protection system.

From another point of view, the condition after stent deployment, such as incomplete attachment of the stent and stent-induced kinking, may be associated with the development of ischemic lesions after CAS. Four of the eight patients treated in the present study exhibited stent-induced kinking after stent deployment. Ischemic lesions were detected after CAS in three of these cases. Stent-induced kinking may occur more frequently in cases involving ICA tortuosity, although we were unable to demonstrate an increase in the frequency of ischemic lesions in patients with stent-induced kinking. Onizuka et al.[27] stated that the existence of incomplete stent apposition had no adverse morphological or clinical effects. In addition, although stent-induced kinking was observed in eight of 15 patients in this article, no ischemic lesions were detected in any of the 15 patients. A sufficiently large sample size is necessary to confirm the correlation between the postprocedural condition and the ischemic complications in CAS.

Considering the risk of CAS, the entire access route from the puncture site to the objective lesion should be considered. This is because ICA and/or vessel tortuosity throughout the access route may increase the incidence of thromboembolic complications due to endothelial damage caused by the interventional devices. In such high-risk cases, selecting CEA as an alternative to CAS or changing the access route should be considered. Regarding the periprocedural management of CAS in patients with severe vessel tortuosity, the administration of antiplatelet and anticoagulant therapy should be intensified. Therefore, evaluating the degree of vessel tortuosity associated with the lesion and access route is important to determine the treatment strategy in patients with carotid artery stenosis.

The principal limitations of the present study are its retrospective nature and small sample size. Nevertheless, a statistically significant outcome was observed among patients with ICA tortuosity. The patients with CCA tortuosity represented a similar trend, but the data did not reach statistical significance due to the small number of cases. Another limitation of the present study is that we did not evaluate the risk factors for stroke and death as described in previous reports. We also did not investigate the changes in cognitive function after CAS. Further studies are needed to determine the anatomical risk factors for neurological morbidity, including cognitive impairment, and mortality associated with CAS.

Conclusions

The present study showed that the most important anatomical factor to predict the development of ischemic lesions associated with CAS was ICA tortuosity. This result may aid in a better selection of patients for CAS. We should therefore evaluate preprocedural angiography findings from an anatomical point of view.

Acknowledgment

This work was partly supported by a Grant-in-Aid for Scientific Research (C), No.23592085 and the Ministry of Education, Culture, Sports, Science, and Technology-Japan.

References

1 Yadav JS, Wholey MH, Kuntz RE, et al. Stenting and angioplasty with protection in patients at high risk for endarterectomy investigators. Protected carotid-artery stenting versus endarterectomy in high-risk patients. N Engl J Med. 2004; 351: 1493-1501. doi: 10.1056/NEJMoa040127.

2 Brott TG, Hobson RW 2nd, Howard G, et al. CREST Investigators. Stenting versus endarterectomy for treatment of carotid-artery stenosis. N Engl J Med. 2010; 363: 11-23. doi: 10.1056/NEJMoa0912321.

3 Meier P, Knapp G, Tamhane U, et al. Short term and intermediate term comparison of endarterectomy versus stenting for carotid artery stenosis: systematic review and meta-analysis of randomised controlled clinical trials. BMJ. 2010; 340: c467. doi: 10.1136/bmj.c467.

4. Schnaudigel S, Gröschel K, Pilgram SM, et al. New brain lesions after carotid stenting versus carotid endarterectomy: a systematic review of the literature. Stroke. 2008; 39: 1911-1919. doi: 10.1161/STROKEAHA.107.50 0603.

5 Bonati LH, Jongen LM, Haller S, et al. ICSS-MRI study group. New ischaemic brain lesions on MRI after stenting or endarterectomy for symptomatic carotid stenosis: a substudy of the International Carotid Stenting Study (ICSS). Lancet Neurol. 2010; 9: 353-362. doi: 10.1016/S1474-4422(10)70057-0.

6 Tedesco MM, Lee JT, Dalman RL, et al. Postprocedural microembolic events following carotid surgery and carotid angioplasty and stenting. J Vasc Surg. 2007; 46: 244-250. doi: 10.1016/j.jvs.2007.04.049.

7 Tedesco MM, Coogan SM, Dalman RL, et al. Risk factors for developing postprocedural microemboli following carotid interventions. J Endovasc Ther. 2007; 14: 561-567.

8 Kastrup A, Nägele T, Gröschel K, et al. Incidence of new brain lesions after carotid stenting with and without cerebral protection. Stroke. 2006; 37: 2312-2316. doi: 10.1161/01.STR.0000236492.86303.85.

9 Maggio P, Altamura C, Landi D, et al. Diffusion-weighted lesions after carotid artery stenting are associated with cognitive impairment. J Neurol Sci. 2013; 328: 58-63. doi: 10.1016/j.jns.2013.02.019.

10 Sayeed S, Stanziale SF, Wholey MH, et al. Angiographic lesion characteristics can predict adverse outcomes after carotid artery stenting. J Vasc Surg. 2008; 47: 81-87. doi: 10.1016/j.jvs.2007.09.047.

11 White CJ, Ramee SR, Collins TJ, et al. Carotid artery stenting: patient, lesion, and procedural characteristics that increase procedural complications. Catheter Cardiovasc Interv. 2013; 82: 715-726. doi: 10.1002/ccd.24984.

12 Naggara O, Touzé E, Beyssen B, et al. EVA-3S Investigators. Anatomical and technical factors associated with stroke or death during carotid angioplasty and stenting: results from the endarterectomy versus angioplasty in patients with symptomatic severe carotid stenosis (EVA-3S) trial and systematic review. Stroke. 2011; 42: 380-388. doi: 10.1161/STROKEAHA.110.588 772.

13 Dumont TM, Mokin M, Wach MM, et al. Understanding risk factors for perioperative ischemic events with carotid stenting: is patient age over 80 years or is unfavorable arch anatomy to blame? J Neurointerv Surg. 2014;6 (3):219-24. doi:10.1136/neurintsurg-2013-010721.

14 Faggioli G, Ferri M, Gargiulo M, et al. Measurement and impact of proximal and distal tortuosity in carotid stenting procedures. J Vasc Surg. 2007; 46: 1119-1124. doi: 10.1016/j.jvs.2007.08.027.

15 Executive Committee for the Asymptomatic Carotid Atherosclerosis Study. Endarterectomy for asymptomatic carotid artery stenosis. JAMA. 1995; 273: 1421-1428. doi: 10.1001/jama.1995.03520420037035.

16 Lam RC, Lin SC, DeRubertis B, et al. The impact of increasing age on anatomic factors affecting carotid angioplasty and stenting. J Vasc Surg. 2007; 45: 875-880. doi: 10.1016/j.jvs.2006.12.059.

17 Hofmann R, Niessner A, Kypta A, et al. Risk score for peri-interventional complications of carotid artery stenting. Stroke. 2006; 37: 2557-2561. doi: 10.1161/01.STR.0000240688.81918.32.

18 Ito Y, Kato N, Matsumura A, et al. Hemodynamic instability increases new ischemic brain lesions on diffusion-weighted imaging after carotid artery stenting. Neurol Med Chir (Tokyo). 2013; 53: 375-380. doi: 10.2176/nmc.53.375.

19 Altinbas A, Algra A, Bonati LH, et al. ICSS Investigators. Periprocedural hemodynamic depression is associated with a higher number of new ischemic brain lesions after stenting in the international carotid stenting study-MRI substudy. Stroke. 2014; 45: 146-151. doi: 10.1161/STROKEAHA.113.003397.

20 Gröschel K, Ernemann U, Schnaudigel S, et al. A risk score to predict ischemic lesions after protected carotid artery stenting. J Neurol Sci. 2008; 273: 112-115. doi: 10.1016/j.jns.2008.07.004.

21 Faggioli G, Ferri M, Rapezzi C, et al. Atherosclerotic aortic lesions increase the risk of cerebral embolism during carotid stenting in patients with complex aortic arch anatomy. J Vasc Surg. 2009; 49: 80-85. doi: 10.1016/j.jvs.2008.08.014.

22 Macdonald S, Lee R, Williams R, et al. Delphi Carotid Stenting Consensus Panel. Towards safer carotid artery stenting: a scoring system for anatomic suitability. Stroke. 2009; 40: 1698-1703. doi: 10.1161/STROKEAHA.109.547117.

23. Werner M, Bausback Y, Bräunlich S, et al. Anatomic variables contributing to a higher periprocedural incidence of stroke and TIA in carotid artery stenting: single center experience of 833 consecutive cases. Catheter Cardiovasc Interv. 2012; 80: 321-328. doi: 10.1002/ccd.23483.

24 Ito Y, Kato N, Nakai Y, et al. [The relation between tortuosity of carotid artery and microembolization during carotid artery stenting using a closed-cell stent]. J Neuro Endovasc Ther. 2013; 7: 75-80. Japanese. doi: 10.5797/jnet.7.75.

25 Asakura F, Kawaguchi K, Sakaida H, et al. Diffusion-weighted MR imaging in carotid angioplasty and stenting with protection by the reversed carotid arterial flow. Am J Neuroradiol. 2006; 27: 753-758.

26 Sorimachi T, Kakita A, Morita K, et al. Routine aspiration method during filter-protected carotid stenting: histological evaluation of captured debris and predictors for debris amount. Acta Neurochir (Wien). 2011; 153: 2159-2167. doi: 10.1007/s00701-011-1093-3.

27 Onizuka M, Kazekawa K, Nagata S, et al. The significance of incomplete stent apposition in patients undergoing stenting of internal carotid artery stenosis. Am J Neuroradiol. 2006; 27:1505-1507.

Wataro Tsuruta MD
Department of Neurosurgery
Faculty of Medicine, University of Tsukuba
1-1-1 Tennodai, Tsukuba, Ibaraki 305-8575, Japan
Tel.: +81-29- 853-3220
Fax: +81-29- 853-3214
E-mail: tsuruta.wataro@md.tsukuba.ac.jp